

mailed to DTIC
5/1/03

AFRL-MN-EG-TR-2003-7044

Experiments And Elastic/Viscoplastic Constitutive Modeling Of Concrete And Geomaterials

**C. Allen Ross
N.D. Cristescu
Oana Cazacu**

**The University of Florida
Graduate Engineering and Research Center
1350 North Poquito Road
Shalimar, Florida 32579**

**The University of Florida
Department of Aerospace Engineering,
Mechanics, and Engineering Science
PO Box 116250
Gainesville, Florida 32611-6250**



CONTRACT NO. F08635-98-D-0016

MARCH 2003

FINAL REPORT FOR PERIOD MAY 98 to SEP 02

DISTRIBUTION A – Approved for public release; distribution unlimited.

20030527 124

AIR FORCE RESEARCH LABORATORY, MUNITIONS DIRECTORATE

■ Air Force Materiel Command ■ United States Air Force ■ Eglin Air Force Base

NOTICE

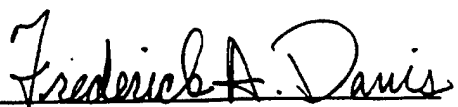
When Government drawings, specifications, or other data are used for any purpose other than in connection with a definitely Government-related procurement, the United States Government incurs no responsibility or any obligation whatsoever. The fact that the Government may have formulated or in any way supplied the said drawings, specifications, or other data, is not to be regarded by implication, or otherwise in any manner construed, as licensing the holder, or any other person or corporation; or as conveying any rights or permission to manufacture, use, or sell any patented invention that may in any way be related thereto.

Contract Number: F08635-98-D-0016

Contractor: The University of Florida

This technical report has been reviewed and is approved for publication.

FOR THE COMMANDER


FREDERICK A. DAVIS
Technical Director
Assessment and Demonstrations Division


MICHAEL E. NIXON
Program Manager

Anyone having need of a copy of this report should first contact the Defense Technical Information Center (DTIC) at the address shown below. If you are a registered DTIC User and qualify as a recipient of this document, DTIC can provide you with a copy. If you are a registered DTIC User and do not qualify as a recipient, DTIC can submit a request for release, on your behalf, to the controlling DoD agency for their review and determination. Please do not request copies from the Air Force Research Laboratory, Munitions Directorate. Requests for additional copies should be directed to:

Defense Technical Information Center (DTIC)
8725 John J. Kingman Road, Ste 0944
Ft Belvoir, VA 22060-6218

This report is published in the interest of the scientific and technical information exchange. Publication of this report does not constitute approval or disapproval of the ideas or findings. Do not return copies of this report unless contractual obligations or notice on a specific document requires its return. If you no longer have a need to retain this document, please refer to the Destruction Notice on the cover page for instruction.

If your address has changed, if you wish to be removed from our mailing list, or if your organization no longer employs the addressee, please notify AFRL/MNAC, 101 W. Eglin Blvd., Ste 135, Eglin AFB FL 32542-6810, to help us maintain a current mailing list.

REPORT DOCUMENTATION PAGEForm Approved
OMB No. 0704-0188

Public reporting burden for this collection of information is estimated to average 1 hour per response, including the time for reviewing instructions, searching existing data sources, gathering and maintaining the data needed, and completing and reviewing the collection of information. Send comments regarding this burden estimate or any other aspect of this collection of information, including suggestions for reducing this burden, to Washington Headquarters Services, Directorate for Information Operations and Reports, 1215 Jefferson Davis Highway, Suite 1204, Arlington, VA 22202-4302, and to the Office of Management and Budget, Paperwork Reduction Project (0704-0188), Washington, DC 20503.

1. AGENCY USE ONLY (Leave blank)

2. REPORT DATE

13 Mar 03

3. REPORT TYPE AND DATES COVERED

Final Report May 98 – Sep 02

4. TITLE AND SUBTITLE

Experiments and Elastic/Viscoplastic Constitutive Modeling of Concrete and Geomaterials

5. FUNDING NUMBERS

Contract #: F08635-98-D-0016

JON: PE: 62602F

PR: 2502

TA: 07

WU: 28

6. AUTHOR(S): C. Allen Ross, N.D. Cristescu, Oana Cazacu

7. PERFORMING ORGANIZATION NAME(S) AND ADDRESS(ES)

The University of Florida
Graduate Engineering and Research Center
1350 North Poquito Road
Shalimar, Florida 32579The University of Florida
Department of Aerospace Engineering,
Mechanics, and Engineering Science
PO Box 116250
Gainesville, Florida 32611 62508. PERFORMING ORGANIZATION REPORT
NUMBER9. SPONSORING/MONITORING AGENCY NAME(S) AND ADDRESS(ES) (Program Mgr Name & Ph #)
Air Force Research Laboratory, Munitions Directorate Michael Nixon
Computational Mechanics Branch (AFRL/MNAC) (850) 882-8302, ext. 3434
101 West Eglin Boulevard, Suite 334
Eglin AFB, Florida 32542-681010. SPONSORING/MONITORING AGENCY
REPORT NUMBER

AFRL-MN-EG-TR-2003-7044

11. SUPPLEMENTARY NOTES

N/A

12a. DISTRIBUTION/AVAILABILITY STATEMENT

DISTRIBUTION A: Approved for public release; distribution unlimited.

12b. DISTRIBUTION CODE

13. ABSTRACT:

Confined, unconfined, dynamic, and quasistatic compressive tests were conducted on strain gage instrumented specimens of concrete, mortar, and granite to produce data for determination of the parameters of an elastic/viscoplastic (EVP) constitutive model of these materials. In addition, concrete grout specimens were tested in dynamic and quasistatic compression to observe columnar fracture and changes in ultrasonic wave speeds. The EVP model captures the basic features of the material behavior such as strain-hardening, confining pressure, rate influence, creep, and relaxation phenomena. The model is applicable to fully 3-D stress conditions, but all parameters can be determined from the results of a few quasistatic and dynamic tests. Reasonable agreements between model and tests were obtained within the natural scatter of the data.

14. SUBJECT TERMS:

mortar, dynamic response, shear, compression, dilatancy, elastic viscolastic,
static response, concrete, granite

15. NUMBER OF PAGES

142

16. PRICE CODE

17. SECURITY CLASSIFICATION OF
REPORT

Unclassified

18. SECURITY CLASSIFICATION
OF THIS PAGE

Unclassified

19. SECURITY CLASSIFICATION
OF ABSTRACT

Unclassified

20. LIMITATION OF ABSTRACT

UL

AQM03-08-2059

PREFACE

This report represents the combination of two tasks under the USAF Task Order Contract F08635-98-D-0016. Task 98-02 with the Test Wing, 460G/OGMTE, was conducted by the University of Florida Graduate Engineering and Research Center (UF/GERC), 1350 N. Poquito Road, Shalimar, FL, 32579. Mr. R. K. Cameron, 460G/OGMTE managed this task for the Test Wing. Task 99-01 with the Munition Directorate, AFRL/MNAC, was conducted by the UF/GERC and the University of Florida Department of Aerospace Engineering, Mechanics and Engineering Science (UF/AMES), P. O. Box 116250, Gainesville, FL, 32611-6250. Mr. M. E. Nixon of AFRL/MNAC, managed this task for the Munitions Directorate.

The authors acknowledge the technical support of Dr. D. M. Jerome and staff of the Advanced Weapons Experimental Facility (AWEF) for their help in many of the tests. Thanks to Mr. Martin Schmidt, AFRL/MNAC and UF Doctoral Candidate, for his help in material tests and assistance in getting work in and out of the AF Machine Shop. Also, a special thanks to the UFGERC staff for their technical and clerical help.

TABLE OF CONTENTS

SECTION	TITLE	PAGE
I	INTRODUCTION	
	1. Background	
	2. Objective	
	3. Approach/Methodology	
	4. Conclusions	
II	EXPERIMENTS	
	1. Introduction	
	2. Mortar Tests	
	3. Concrete Tests	
	4. Granite Tests	
	5. Ultrasonic Grout Tests	
	a. Background	
	b. Quasistatic Tests	
	c. Dynamic Tests	
III	RESULTS AND DISCUSSION	
	1. Experiments	
	a. Mortar, Concrete and Granite Tests	
	b. Grout Tests	
	2. Elastic/Viscoplastic Model for concrete	
	a. Introduction	
	b. Experimental basis	
	c. Structure of the Constitutive Equation	
	d. Comparison Between Model Prediction and Data	
	e. Conclusions	
	REFERENCES	
	APPENDIX A	

LIST OF FIGURES

<i>Figure No.</i>	<i>Title</i>	<i>Page</i>
1	Schematic of a split Hopkinson pressure bar (SHPB) showing an arrangement for the compressive, splitting tensile and shear specimens.	9
2	Schematic of confining pressure cell.	10
3	Schematic showing the strain gage locations on the test specimen.	11
4	Stress-strain curve for mortar.	14
5	Longitudinal, transverse and volumetric strain for mortar.	15
6	Modulus test for mortar.	16
7	Stress-strain curve from modulus test of mortar.	17
8	Stress-strain curve from modulus test of granite.	22
9	Longitudinal, transverse and volumetric strain for granite.	23
10	Stress-strain curve for quasistatic confined test of granite.	24
11	Longitudinal, transverse and volumetric strain for quasistatic confined test of granite.	25
12	Schematic of quasistatic compressive cube test.	29
13	Schematic of a split Hopkinson pressure bar (SHPB) showing the arrangement for the compressive cube specimen.	30
14	Strain pulses for grout Specimen DCU-10.	32
15	Average value of incident stress generated by impactor when driven by a given gas gun pressure.	33
16	Incident, reflected and transmitted pulse for dynamic mortar test.	37
17	Incident, reflected and transmitted pulses for dynamic granite test.	38
18	Incident, reflected and transmitted pulses for dynamic granite test.	39
19	Schematic of fracture planes. (a) Plane approximately parallel to the XZ plane. (b) Two planes approximately parallel to the XZ plane. (c) Plane diagonal across the XZ plane, but approximately parallel to Y axis.	41
20	Ultrasonic grout tests using the SHPB as a loading device.	43
21	Ultrasonic grout tests using SHPB as a loading device.	45
22a	Ultrasonic grout tests comparison of data obtained in dynamic tests with data obtained in quasistatic tests.	46
22b	Ultrasonic grout tests comparison of data obtained in dynamic tests with data obtained from quasistatic tests.	47

23	Axial Stress vs. Volumetric Strain curve obtained in the unconfined compression test QSC-2.	51
24	Comparison of the deviatoric stress vs. axial strain curves obtained in quasi-static confining compression tests QSSC12 (1.8 MPa confining), QSCC1 (3.45 MPa confining), and QSCC6 (6.9 MPa confining).	53
25	Deviatoric stress vs. volumetric strain curves obtained in the quasi-static confined tests QSSC12 (1.8 MPa), QSCC1 (3.46 MPa), QSCC6 (6.9 MPa) showing compressibility for low stress levels and pronounced dilatancy for high stress levels.	54
26	Hydrostatic Pressure vs. Axial Strain curve obtained in WES test 150 MPa -4 th try.	56
27	Deviatoric stress vs. axial strain curve obtained in the WES quasi-static test (150 MPa, 4 th try), confining pressure of 150 MPa.	57
28	Deviatoric stress vs. Radial Strain curve obtained in WES test at 150 MPa confining pressure (150MPa -4 th try); <u>Inset</u> : first 2 cycles show creep compressibility whereas in the next cycles creep dilatancy is observed.	58
29	Deviatoric stress vs. Volumetric Strain curve obtained in WES test at 150 MPa confining pressure (150 MPa -4 th try) showing no dilatancy.	59
30	Hydrostatic Pressure vs. Radial Strain curve obtained in WES test 300 MPa -2 nd try.	61
31	Deviatoric stress vs. Axial Strain curve obtained in the deviatoric part of WES test at 300 MPa confining pressure (300 MPa -2 nd try).	62
32	Deviatoric stress vs. Radial Strain curve obtained in the deviatoric part of WES test at 300 MPa confining pressure (300 MPa -2 nd try); <u>Inset</u> : first 3 cycles, showing creep compressibility.	63
33	Deviatoric stress vs. Volumetric Strain curve obtained in WES test at 300 MPa confining pressure (300 MPa -2 nd try) showing no dilatancy.	64
34	Hydrostatic Pressure vs. Radial Strain curve obtained in WES test 450 MPa -2 nd try.	66
35	Deviatoric stress vs. Axial Strain curve obtained in the deviatoric part of WES test at 450 MPa confining pressure (450 MPa -2 nd try).	67
36	Deviatoric stress vs. Radial Strain curve obtained in the deviatoric part of WES test at 450 MPa confining pressure (450 MPa -2 nd try).	68
37	Deviatoric stress vs. Volumetric Strain curve obtained in the deviatoric part of WES test at 450 MPa confining pressure (450 MPa -2 nd try).	69

38	Comparison between the theoretical $\sigma_1 - \varepsilon_1$ curve, elastic curve, and data in the unconfined quasi-static test QSC-1.	76
39	Comparison between the theoretical $\sigma_1 - \varepsilon_1$ curve, elastic curve, and data in the unconfined dynamic test DCCU3 conducted at a strain rate of 52/s.	77
40	Comparison between the theoretical $\sigma_1 - \varepsilon_3$ curve, elastic curve, and data in the unconfined dynamic test DCCU3 conducted at a strain rate of 52/s.	78
41	Comparison between the theoretical $\sigma_1 - \varepsilon_1$ curve, elastic curve, and data in the unconfined dynamic test DCCU5 conducted at a strain rate of 107/s.	79
42	Comparison between the theoretical $\sigma_1 - \varepsilon_3$ curve, elastic curve, and data in the unconfined dynamic test DCCU5 conducted at a strain rate of 107/s.	80
43	Comparison between the theoretical $\sigma_1 - \varepsilon_1$ curve, elastic curve, and data in the unconfined quasi-static test QSCC-1 ($\sigma_3 = 3.45$ MPa).	82
44	Comparison between the theoretical $\sigma_1 - \varepsilon_3$ curve, elastic curve, and data in the confined quasi-static test QSCC1 ($\sigma_3 = 3.45$ MPa).	83
45	Comparison between the theoretical $\sigma_1 - \varepsilon_1$ curve, elastic curve, and data in the unconfined dynamic test DCCC4 conducted at a strain rate of 53/s, confining pressure 3.57 MPa.	84
46	Comparison between the theoretical $\sigma_1 - \varepsilon_3$ curve, elastic curve, and data in the unconfined dynamic test DCCC4 conducted at a strain rate of 53/s, confining pressure 3.57 MPa.	85
A-1	Stress-strain curve for quasistatic confined mortar test.	91
A-2	Longitudinal, transverse and volumetric strain for quasistatic confined mortar test.	92
A-3	Stress-strain curve for quasistatic confined mortar test.	93
A-4	Longitudinal, transverse and volumetric strain for quasistatic confined mortar test.	94
A-5	Stress-strain curve for quasistatic confined mortar test.	95
A-6	Longitudinal, transverse and volumetric strain for quasistatic confined mortar test.	96
A-7	Stress-strain curve for quasistatic confined mortar test.	97
A-8	Longitudinal, transverse and volumetric strain for quasistatic confined mortar test.	98
A-9	Stress-strain curve and confining pressure for dynamic confined mortar test.	99
A-10	Longitudinal, transverse and volumetric strain for dynamic confined mortar test.	100
A-11	Stress-strain curve and confining pressure for dynamic confined mortar test.	101

A-12	Longitudinal, transverse and volumetric strain for dynamic confined mortar test.	102
A-13	Stress-strain curve and confining pressure for dynamic confined test of mortar.	103
A-14	Longitudinal, transverse and volumetric strain for dynamic confined mortar test.	104
A-15	Stress-strain curve and confining pressure for dynamic confined mortar test.	105
A-16	Longitudinal, transverse and volumetric strain for dynamic confined mortar test.	106
A-17	Stress-strain curve and confining pressure for dynamic confined mortar test.	107
A-18	Longitudinal, transverse and volumetric strain for dynamic confined mortar test.	108
A-19	Stress-strain curve for modulus test of concrete.	109
A-20	Modulus test for quasistatic concrete.	110
A-21	Stress-strain curve and confining pressure for quasistatic confined concrete test.	111
A-22	Longitudinal, transverse and volumetric strain for quasistatic confined concrete test.	112
A-23	Stress-strain curve and confining pressure for quasistatic confined concrete test.	113
A-24	Longitudinal, transverse and volumetric strain for quasistatic confined concrete test.	114
A-25	Stress-strain curve and confining pressure for quasistatic confined concrete test.	115
A-26	Longitudinal, transverse and volumetric strain for quasistatic confined concrete test.	116
A-27	Stress-strain curve for dynamic unconfined concrete test.	117
A-28	Longitudinal, transverse and volumetric strain for dynamic unconfined concrete test.	118
A-29	Stress-strain curve for dynamic unconfined concrete test.	119
A-30	Longitudinal, transverse and volumetric strain for dynamic unconfined concrete test.	120
A-31	Stress-strain curve for dynamic unconfined concrete test.	121
A-32	Longitudinal, transverse and volumetric strain for dynamic unconfined concrete test.	122
A-33	Stress-strain curve and confining pressure for dynamic confined concrete test.	123
A-34	Longitudinal, transverse and volumetric strain for dynamic confined concrete test.	124
A-35	Stress-strain curve and confining pressure for dynamic confined concrete test.	125

A-36	Longitudinal, transverse and volumetric strain for dynamic confined concrete test.	126
A-37	Stress-strain curve for dynamic unconfined granite test.	127
A-38	Longitudinal, transverse and volumetric strain for dynamic unconfined granite test.	128
A-39	Stress-strain curve for dynamic unconfined granite test.	129
A-40	Longitudinal, transverse and volumetric strain for dynamic unconfined granite test.	130

LIST OF TABLES

<i>Figure No.</i>	<i>Title</i>	<i>Page</i>
1	Mix Proportions for Mortar	13
2	Mix Proportions for SAC-5 Concrete	13
3	Compressive Data for Mortar	19
4	Compressive Data for Concrete	21
5	Mix Proportions for Grout	27
6	Dimensions, Transit Times and Weight for Grout Cubes	27
7	Test Data Analysis for Grout	34
8	Elastic Moduli as determined from the Quasistatic GERC Tests	52
9	Bulk Modulus K as determined from the Hydrostatic part of Quasistatic WES test 150 MPa -4 th try.	55
10	Elastic Moduli determined from the Deviatoric phase of the Quasistatic WES test 150 MPa -4 th try.	60
11	Bulk Modulus K as determined from Hydrostatic part of Quasistatic WES test 300 MPa -2 nd try.	65
12	Elastic Moduli determined from the Deviatoric phase of the Quasistatic WES test 300 MPa -2 nd try.	65
13	Bulk Modulus K as determined from the Hydrostatic part of Quasistatic WES test 450 MPa -2 nd try.	70
14	Elastic Moduli determined from the Deviatoric phase of the Quasistatic WES test 300 MPa -2 nd try.	70
15	Average values of the Elastic Moduli as determined from the Deviatoric phase of each WES test.	70

Section I

INTRODUCTION

1. Background

Most materials exhibit strain rate sensitivity giving increases in uniaxial stresses as the strain rate increases. In addition geomaterials are pressure sensitive, the effect of increased hydrostatic pressure being an increase in the quasi-static material strength, especially compressive strength. Also, geomaterials exhibit volumetric compressibility and/or dilatancy when loaded in uniaxial or triaxial tests. Both compressibility and dilatancy are also rate dependent: in slower tests, generally, more dilatancy and more compressibility is recorded. The strain rate effect on unconfined uniaxial compressive strength of concrete is presented by Watstein and Boresi [1952], Reinhardt [1987], Cowell [1996] and Malvern [1986], rate effects on tensile strength of concrete are given by Ross *et al.* [1989, 1995, 1996] and Weerheijm [1992], and the effects of confining pressure on concrete material are presented by Osborn [1982], and Osborn and Matuska [1978], Derucher *et al.* [1998], *etc.* The combined effects of intermediate strain rate and low confining pressure on the compressive strength of concrete are presented by Malvern and Jenkins [1990]. Considerable triaxial data on mortar, rock (*e.g.* rock salt, granite, sandstone, andesite, *etc.*), and sand are presented in Cristescu [1989] and in Cristescu and Hunsche [1998]. However, very little dynamic triaxial data have been reported.

Many constitutive relations for concrete such as that of Osborn [1982], Osborn and Matuska [1978] are available for use in hydrocode calculations, other material models are available in numerical codes such as EPIC (Johnson and Stryk [1992]), CTH (Bell [1994]) and HULL (Matuska *et al.* [1991]). In an effort to combine rate and hydrostatic effects and to describe both compressibility and dilatancy, a three dimensional nonassociated

elastic/viscoplastic (EVP) constitutive model has been developed by Cristescu [1989]. The general form of this equation is shown below:

$$\dot{\varepsilon}_{ij} = \underbrace{\frac{\dot{\sigma}_{ij}}{2G} + \left(\frac{1}{3K} - \frac{1}{2G} \right) \dot{\sigma} \delta_{ij}}_{\text{Instantaneous Response}} + \underbrace{k_T \left\langle 1 - \frac{W(t)}{H(\sigma_{mn})} \right\rangle \frac{\partial F}{\partial \sigma_{ij}}}_{\text{Transient Creep Response}} \quad (1)$$

where:

W = Irreversible Stress Workper unit volume
F = Viscoplastic Potential
H = Yield Function
 k_T = Viscosity Coefficient
K = Bulk Modulus
G = Shear Modulus

ε_{ij} = Strain Tensor
 σ_{ij} = Stress Tensor
 σ = Mean Stress
 δ_{ij} = Kronecker Delta
 $\langle A \rangle = 1/2 (A + |A|)$

No a priori assumptions regarding the specific mathematical expressions of the yield function $H(\sigma)$ and of the viscoplastic potential $F(\sigma)$ are made. These two functions are generally distinct (nonassociated). Also the two elastic parameters K and G , are generally not constant. Since geomaterials may exhibit both compressible and dilatant behavior, the concept of compressibility/dilatancy boundary (see Cristescu, [1989]) is integrated in the model. This permits to capture the non-linear compressibility observed for low shearing stresses and shear induced dilatancy observed for higher shearing stresses using a unique continuous yield function and a unique viscoplastic potential to be used for all confining pressures. This is a significant advantage of this model over rate sensitive cap models, since it captures in a continuous way the transition between the two regimes of volumetric behavior. The basic experiment required for the

EVP formulation is a triaxial compression test in which a specimen is first subjected to hydrostatic test followed by a deviatoric test. Using the triaxial test data, all the parameters involved in the EVP equation can be determined.

The Advanced Weapons Effects Facility (AWEF) of Eglin AFB recently acquired a 50.8mm (2.0 in) diameter split Hopkinson pressure bar (SHPB) and as part of this study, assistance was given in the assembly and check out of this device. As part of this check out procedure, several tests on concrete grout cubes were conducted to determine the effects of dynamic compression on the ultrasonic wave velocity of each of the cube's three orthogonal directions.

In rock, granite, concrete and other cementitious materials where random oriented microcracks are present, a phenomenon sometimes referred to as "axial columnar splitting under axial compression" occurs, where crack growth orients itself in a direction parallel to the maximum compressive stress. In uniaxial compression of concrete and rock, cracking occurs parallel to the compression load even though no lateral tensile stresses are applied. In comparison with the stress state under tension, compressive loading leads to much more crack arrest, reflected in a much longer interval of stable crack growth and a pronounced non-linear behavior (Weerheijm, [1992]). Similarly, diametrical cracking occurs in a splitting tensile or Brazilian test when a cylindrical specimen is loaded in compression along the cylinder length. Cracking in concrete and other quasi-brittle materials parallel to the maximum applied compression stress was first reported by Brace and Bombolakis [1963]. Fracture mechanics offers the basic tools, *i.e.* criterion for crack growth initiation and energy criterion, which deals with the energy supply and energy dissipation during crack growth. An overview on the application of fracture mechanics on concrete can be found in Mindess [1983]. A mathematical theory of the phenomenon, which doesn't make use of singular integral equations was developed

by Nemat-Nasser and Horii [1982]. Another approach is the Continuous Damage Mechanics approach (CDM). In CDM models, the internal damage is described by a scalar (e.g. Lemaitre and Chaboche [1984], Mazars[1980]), vector (e.g. Krajcinovic and Fonseka [1981]) or tensor (Chaboche [1995], Halm and Dragon [1996]). The main disadvantage of CDM models is that they do not describe the real mechanism of damage extension or arrest in concrete. Another approach is to combine the random material composition and crack development in the description of the concrete response fracture mechanics features and Monte Carlo techniques have been used (e.g. Zaitsev[1986]). Schreyer and Gao [1998] use a discontinuous bifurcation, theory to describe crack extension in compression.

Experimental verification and identification of axial cracking under dynamic axial compression using a split Hopkinson pressure bar (SHPB) are reported by Ross [1989], Malvern and Jenkins [1992],. In Malvern *et. al.*[1992] crack patterns observed in post test photographs taken after the specimen was soaked in concrete restorer, mixed with zyglo to enhance the patterns under ultraviolet light are reported. In Ross [1992] high speed photography was used to track crack formation during the dynamic testing. A computer imaging technique was used to determine crack density and crack growth. Correlation of experimental crack growth parameters experimentally determined by Malvern *et al.* [1992] and Ross [1992] and theory of Krajcinovic [1984], Budiansky and O'Connel [1976] and Taylor *et al.* [1986], were reasonable except for the prediction of Poisson's ratio. The specimens used by Ross [1992] were instrumented with electrical resistance strain gages in the axial and transverse directions. Both volumetric strain and Poisson's ratio were determined. The volumetric strain obtained by Ross [1992] indicated that after a rather linear compressive strain, swelling and axial cracking occurred, resulting in dilatancy and giving rise to an increasing Poisson's ratio rather than a decreasing value as

predicted by Budiansky and O'Connel [1976] and Taylor *et al.*[1986]. This axial cracking and dilatancy is also observed in rock and granite as mentioned previously in the citations from Cristescu [1989].

Further research using cylindrical mortar specimens was conducted by Ross [1998] using the SHPB on 50.4mm and 76.4mm diameter specimens. Mortar specimens were loaded in compression in several increments of the failure stress. Ultrasonic wave propagation speeds were measured axially both before and after testing. The axial ultrasonic wave speed changed very little with increasing compressive load. However, post test ultrasonic wave speeds measured in only one transverse direction to the loading showed a significant reduction in those specimens loaded at loads near the failure stress.

2. Objective

The major objective of this study will be to produce unconfined and confined, quasi-static and dynamic data on concrete, mortar and granite in order to fully develop a three dimensional elastic/viscoplastic constitutive model of type given by Eq. (1) for each of these materials. The secondary objective is to implement the newly developed constitutive models in a computational code in order to analyze the penetration of kinetic energy penetrators into concrete and granite or combinations thereof. The EVP constitutive equation models a solid body with viscous properties in which dynamic loadings propagate by two types of waves, i.e. both compression and shearing waves. Thus, the EVP model can describe dynamic compressibility, propagation of compression and shearing waves, and failure produced by overstress, which is a departure from the current practice. A minor objective is to initiate a preliminary study of damage in concrete due to dynamic loading.

3. Methodology/Approach

The basic experiments needed to obtain material properties for concrete, mortar and granite are quasistatic and dynamic tests for both confined and unconfined conditions. Quasistatic hydrostatic tests with several loading-unloading-reloading cycles are necessary to obtain basic information regarding the compressibility characteristics of the given materials. Also, from these tests the energy of deformation may be computed for determination of the hydrostatic part of the yield function $H(\sigma)$. Conventional triaxial compression (CTC) tests at several confining pressures are necessary to produce stress-strain behavior and volume change relations and thus determine basic effects of different variables such as (1) compaction pressure over a large range, (2) confining pressure on the pattern of volumetric behavior, (3) stress-path dependency, (4) strain rate and time to failure on strength, (5) strain rate on the compressibility/dilatancy boundary. The data obtained in such tests have direct bearing on the formulation and calibration of the proposed models since they permit to determine the deviatoric part of the yield function $H(\sigma)$, which is a relaxation boundary for dynamic loading, and the viscoplastic potential $F(\sigma)$.

The quasistatic tests for both confined and unconfined concrete tests were to be completed by Waterways Experiment Station (WES) under a separate agreement. Unconfined and confined quasistatic tests on concrete, mortar and granite were conducted at the AWEF using the newly acquired material test machine of 2700 kN compressive capacity. Confined and unconfined dynamic tests on concrete, mortar and granite were conducted by UFGERC using the 3.00 in (76.2 mm) diameter split Hopkinson pressure bar (SHPB). A confining pressure cell developed for the experiments of Malvern *et al.*, [1992] and the SHPB, will be used to accomplish the dynamic confined tests. Small cube specimens of grout concrete were tested quasistatically and dynamically to study columnar fracture and splitting, and the effects of these

fractures on the ultrasonic wave velocity in directions transverse to the compressive load direction.

4. Conclusions

Fairly low confining pressure in both quasistatic and dynamic tests will cause a considerable increase in the compressive strength of cementitious materials and geomaterials. In addition, the material response relative to dilatancy and fracture are changed due to confining pressure. Material fracture and total failure under unconfined compressive loadings may be prevented under low confining pressures. This reduction of fracture appears to have a more noticeable effect on mortar and granite than on concrete.

The EVP model captures the basic features of the material behavior such as strain-hardening, confining pressure, rate influence, creep and relaxation phenomena. Although the model developed is applicable to fully 3-D stress conditions, all the parameters involved can be determined from the results of a few quasistatic and dynamic tests. The agreement between model prediction and data is rather good.

Section II EXPERIMENTS

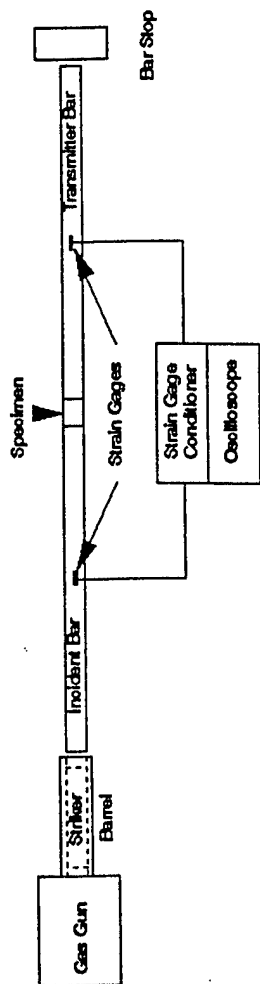
1. Introduction

Confined and unconfined, mortar, concrete, and granite tests were performed quasistatically using the MTS material test machine at the AF Advanced Weapons Effects Facility (AWEF) and dynamically using the University of Florida Split Hopkinson Pressure Bar (SHPB). For the confined pressure tests the pressure cell, designed especially for the SHPB, was used in both the MTS and SHPB. A schematic of the SHPB is shown in Figure 1 and a schematic of the pressure cell is shown in Figure 2.

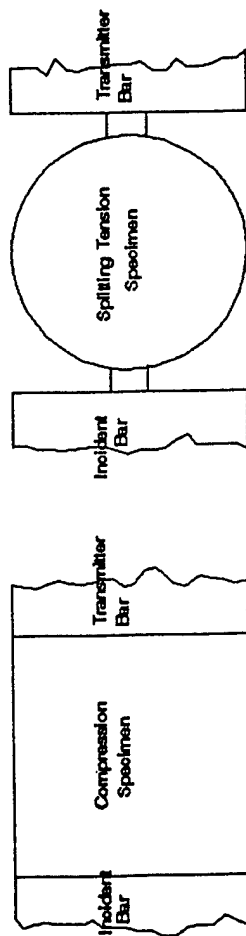
For all the tests, all specimens were nominally 76.2mm diameter, 76.2mm long (3"Dx3"L) and were tested in compressive. Each specimen was instrumented with two sets of diametrically opposed 25.4mm long (1.0"L) electrical resistance strain gages. One gage of each strain gage set was aligned in the longitudinal specimen direction and the other gage was aligned in the transverse or circumferential specimen direction. All strain gages were affixed near the mid-length of the specimen. This type instrumented specimen, shown in Figure 3, gives both specimen longitudinal and transverse strains, which may be used to determine the volumetric strain. The volumetric strain is defined as the sum of longitudinal, radial and transverse strains; however, due to the loading configuration on the cylindrical specimen it may be shown that the radial and transverse strains are equal. This gives a volumetric strain ϵ_v as the sum of the longitudinal strain ϵ_L plus twice the transverse strain ϵ_T , and written as

$$\epsilon_v = \epsilon_L + 2\epsilon_T \quad (2)$$

All loads and strains are recorded electronically so the formation of the volumetric strain can be performed rather easily in the computer. In the testing of confined geomaterials and concrete

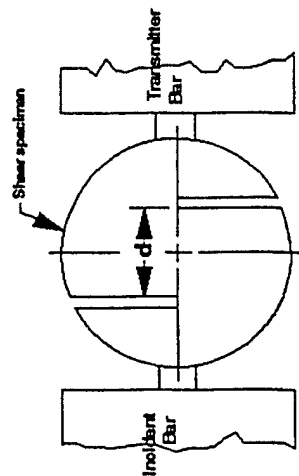


a) Split Hopkinson Pressure Bar (SHPB)



b) Specimen Arrangement for Compression Test

c) Specimen Arrangement for Splitting Tension Test



d) Specimen arrangement for shear test

Figure 1. Schematic of a split Hopkinson pressure bar (SHPB) showing an arrangement for the compressive, splitting tensile and shear specimens.

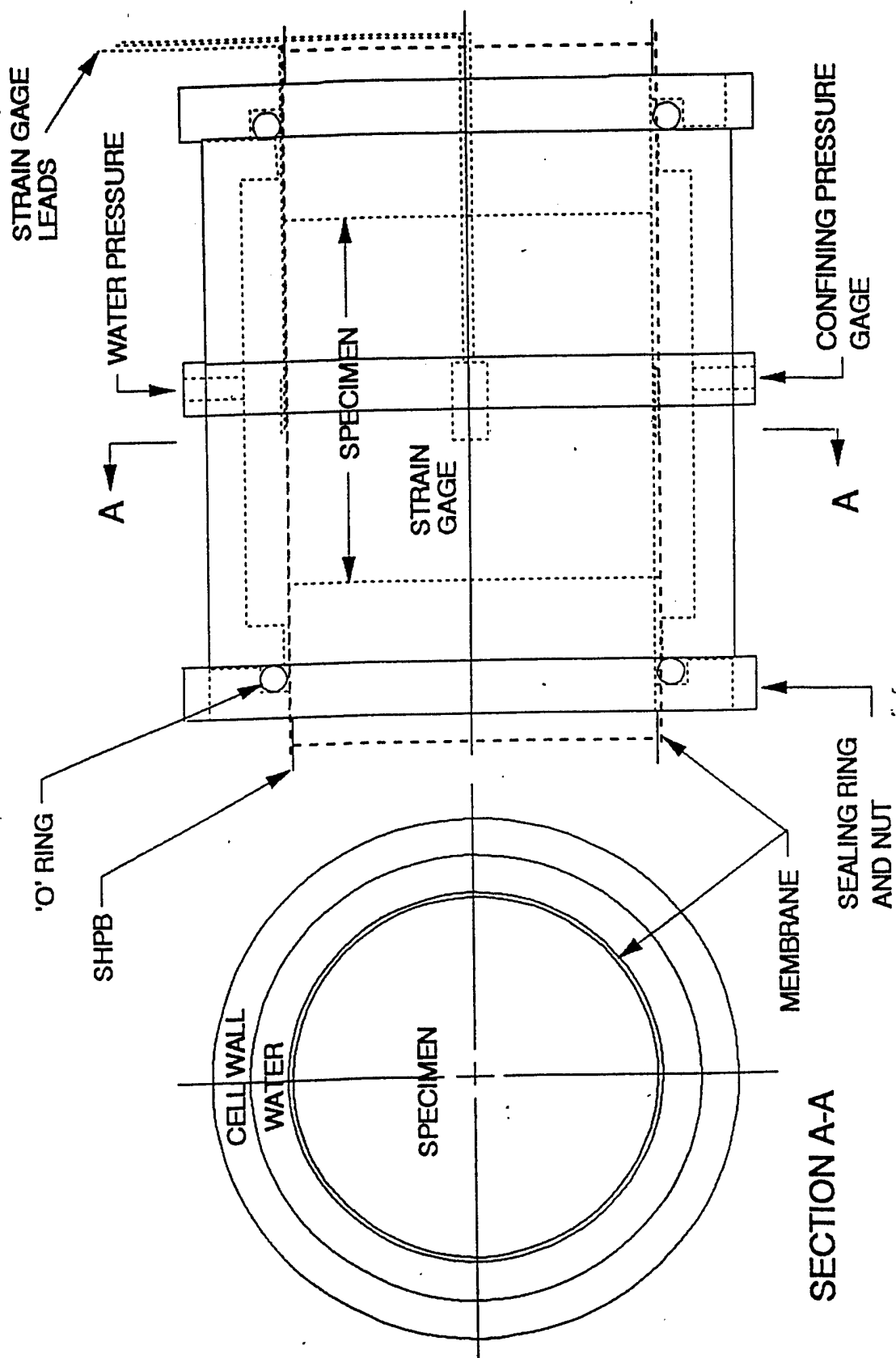


Figure 2. Schematic of confining pressure cell.

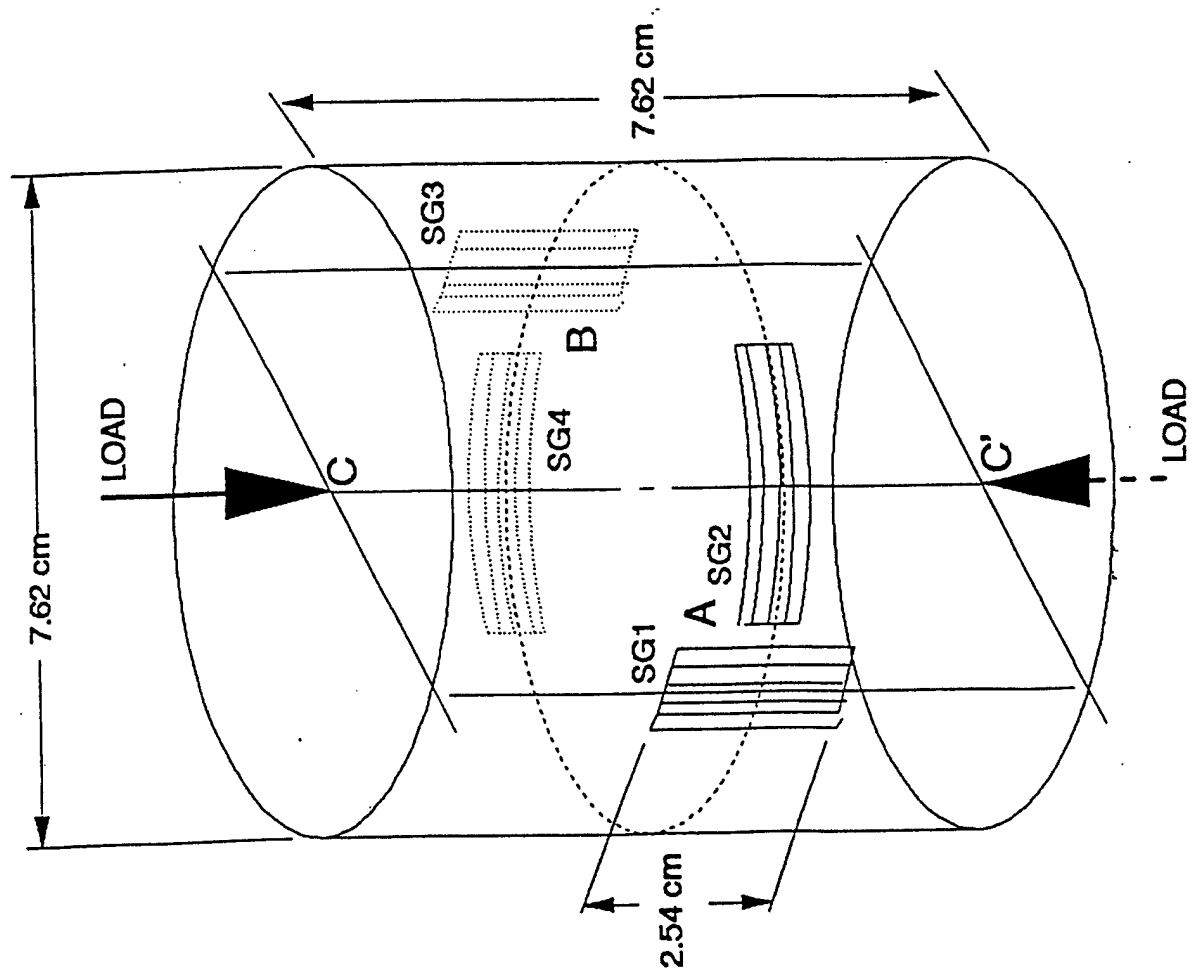


Figure 3. Schematic showing the strain gage locations on the test specimen.

(triaxial cell tests), compressive stresses and strains are considered positive and this sign convention is used in this study.

The significance of the volumetric strain is not readily apparent for a standard unconfined uniaxial concrete compression test. For this test radial expansion tends to occur immediately and as soon as the tensile strength is exceeded, considerable volumetric expansion, defined as dilatancy, occurs and the specimen fails at the peak compressive strength. For the unconfined concrete compression test the $2\varepsilon_T$ term of Eq. (2) will exceed the longitudinal strain term ε_L early in the test and the volumetric strain will change sign indicating severe expansion and dilatancy. However, if a transverse confining pressure is applied to the specimen during the axial compression then the radial expansion is restricted and the volumetric strain tends to remain positive and dilatancy is prevented. This results in an increased axial compressive strength. Some of these features will be evident and discussed later, using some of the data of the next sections.

2. Mortar Tests

Tests were continued in May – June 1999 on compressive tests of mortar. Some initial tests were conducted in late 1998, on mortar and one of those unconfined quasistatic tests, QSM3B, is included here. The results of this test are given for reference and marked as Figure 4, the stress-strain curve and Figure 5, the stress-volumetric-strain curve. The mix proportions for mortar are given in Table 1.

Two quasistatic unconfined modulus tests were conducted in May-June 1999 and one of those tests, QSM5, is included. Figure 6 shows the stress-time curve and the Figure 7 shows the stress-strain curve. The average modulus and average compressive strength are given on Figure 7 are 23.38 GPa (3.39×10^6 psi) and 55.48 MPa (8.04 ksi), respectfully.

TABLE 1

MIX PROPORTIONS FOR MORTAR

Portland Cement	450 g
Sand Sieve #4	1620 g
WRDA-19, 0.5%	3.7 g
"F" Fly Ash	297 g
Water, w/c = 0.55	411 g

TABLE 2

MIX PROPORTIONS FOR SAC-5 CONCRETE

Portland Cement, Type 1	445 lbs.
Fly Ash	94 lbs.
Sand, River Run	1417 lbs.
Gravel, River Run 3/8"	1749 lbs.
Water	246 lbs.
WRA, 300N	22 fl. oz.
WRA, Rhesbuild 716	54 fl. oz.

UNCONFINED MORTAR QUASISTATIC TEST

SPECIMEN QSM3B STRAIN RATE = $1.18\text{E-}6/\text{SEC}$

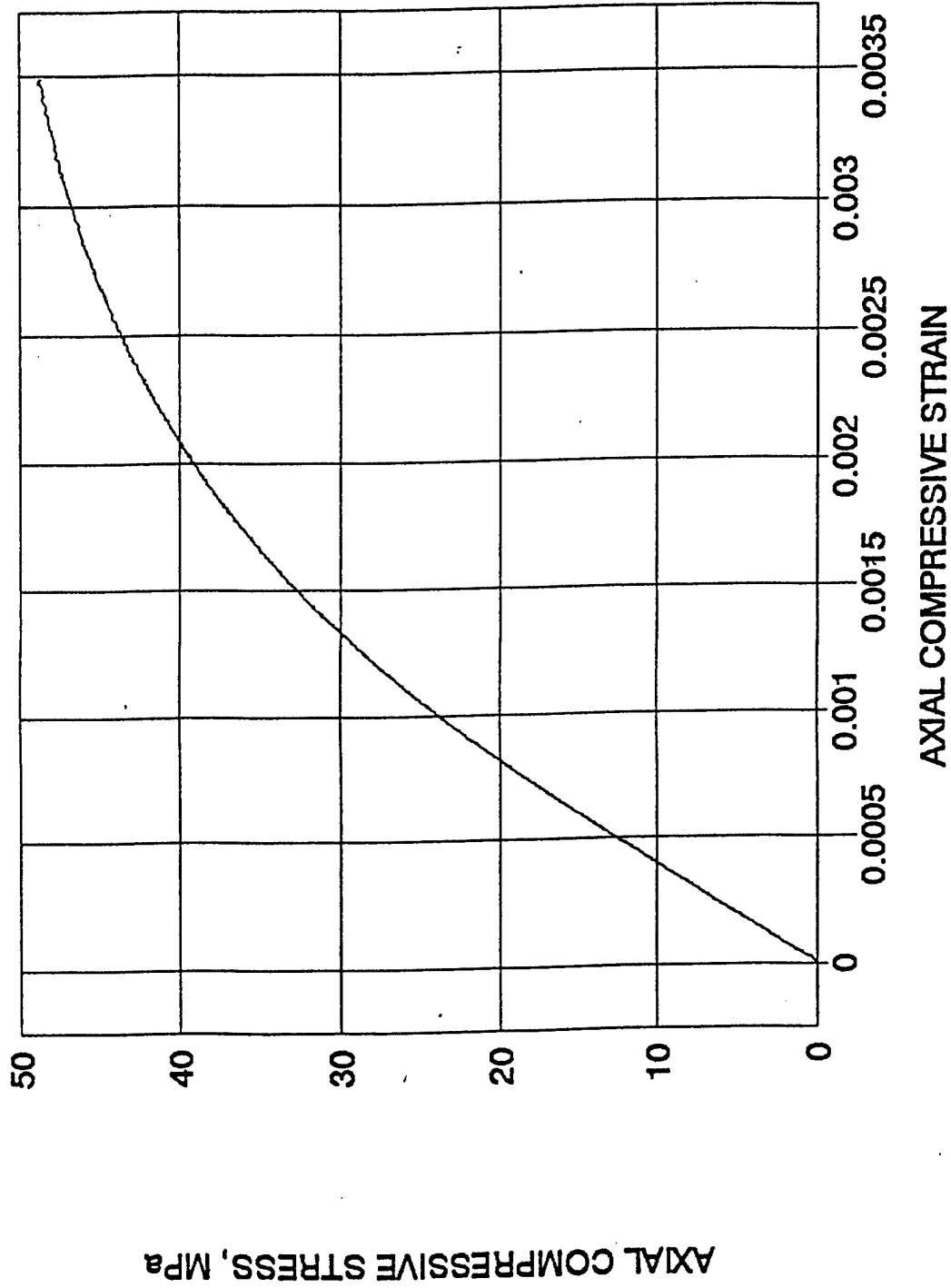


Figure 4. Stress-strain curve for mortar.

QUASISTATIC UNCONFINED MORTAR TEST

QSM3B, STRAIN RATE = 1.18×10^{-6} /SEC

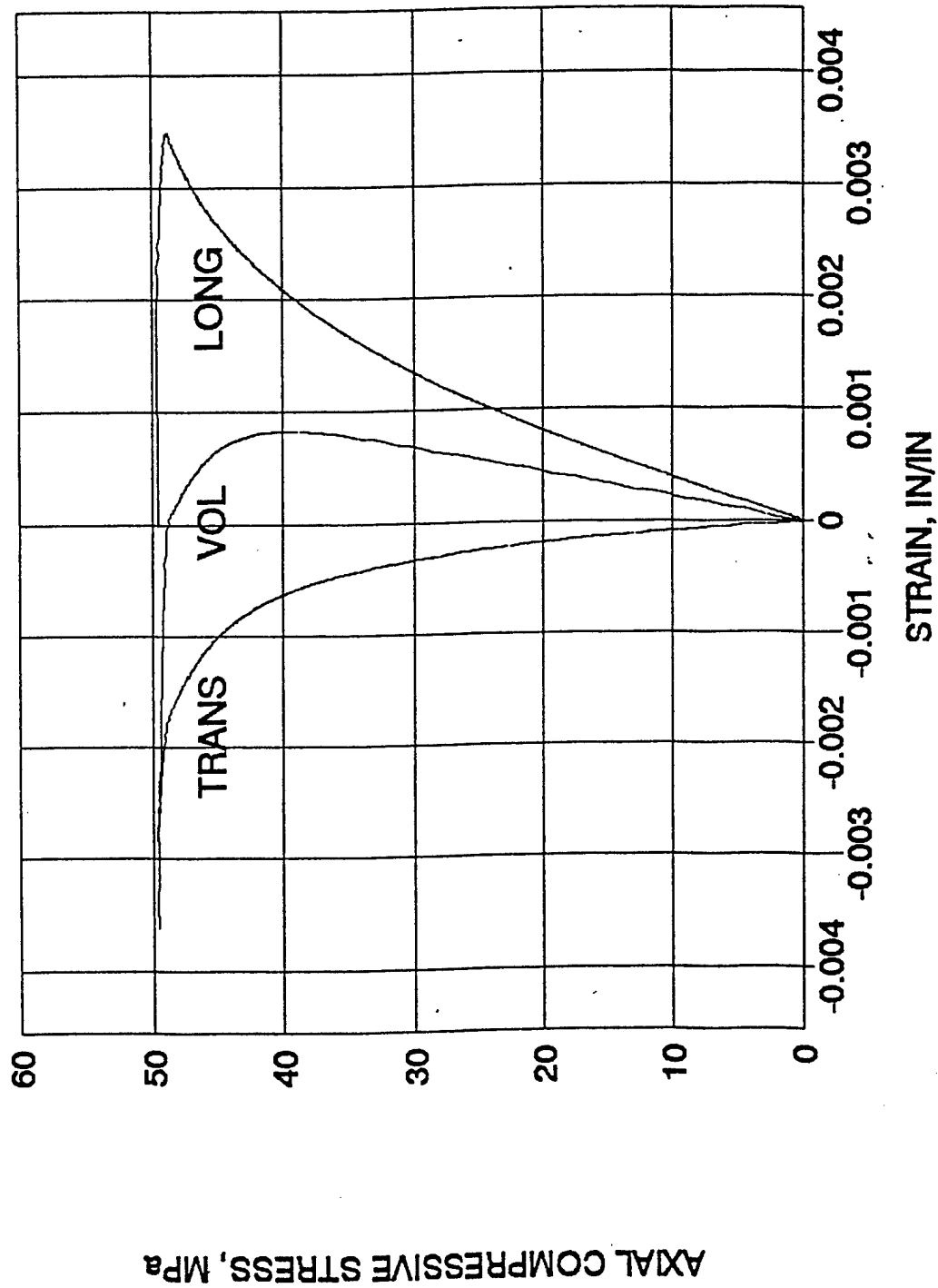


Figure 5. Longitudinal, transverse and volumetric strain for mortar.

QUASISTATIC MODULUS TEST FOR MORTAR

QSM-5, STRAIN RATE = $1.25E-6/SEC$

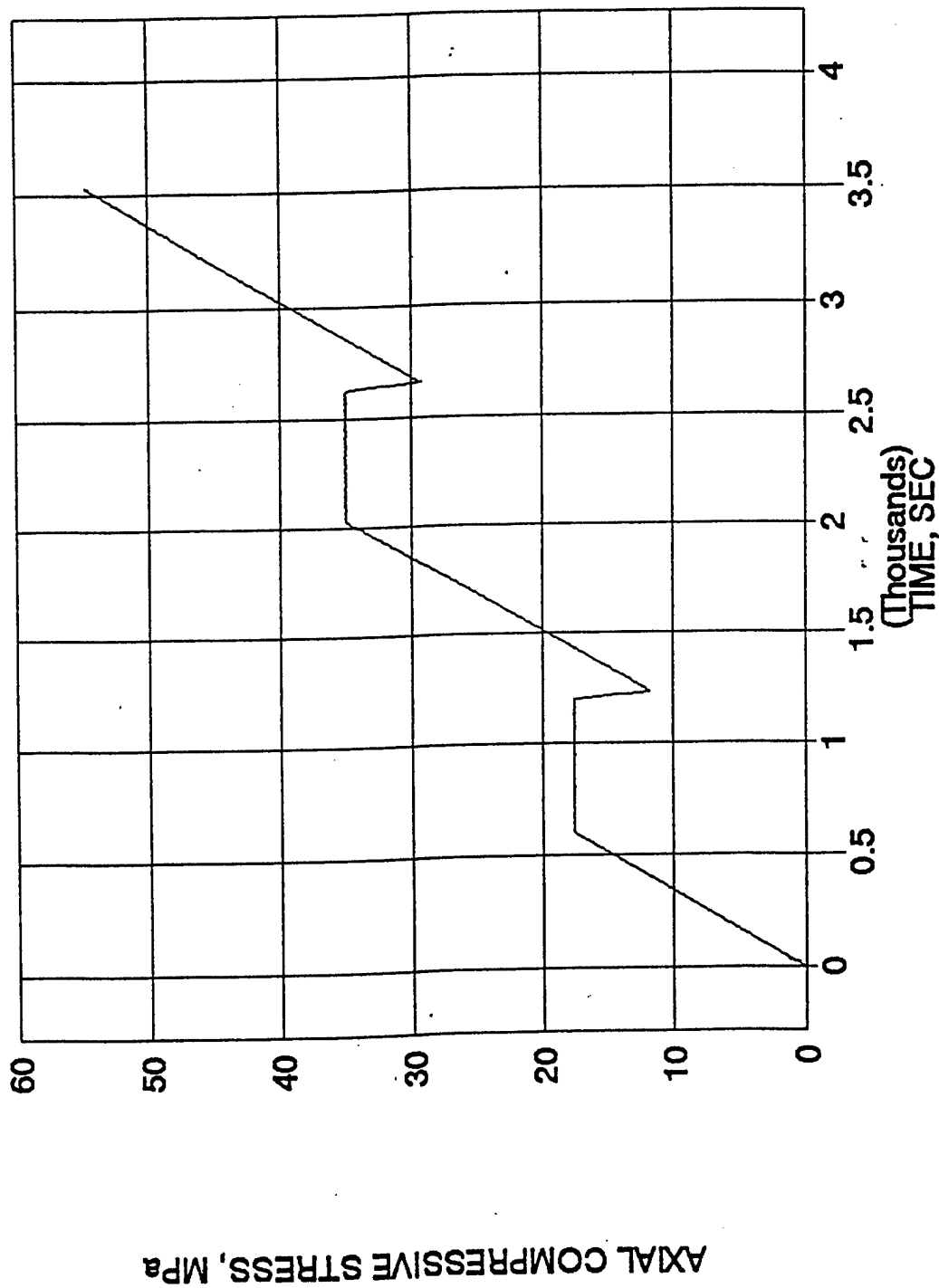


Figure 6. Modulus test for mortar.

QUASISTATIC MODULUS TEST FOR MORTAR

QSM-5, STRAIN RATE = $1.25E-6$ /SEC

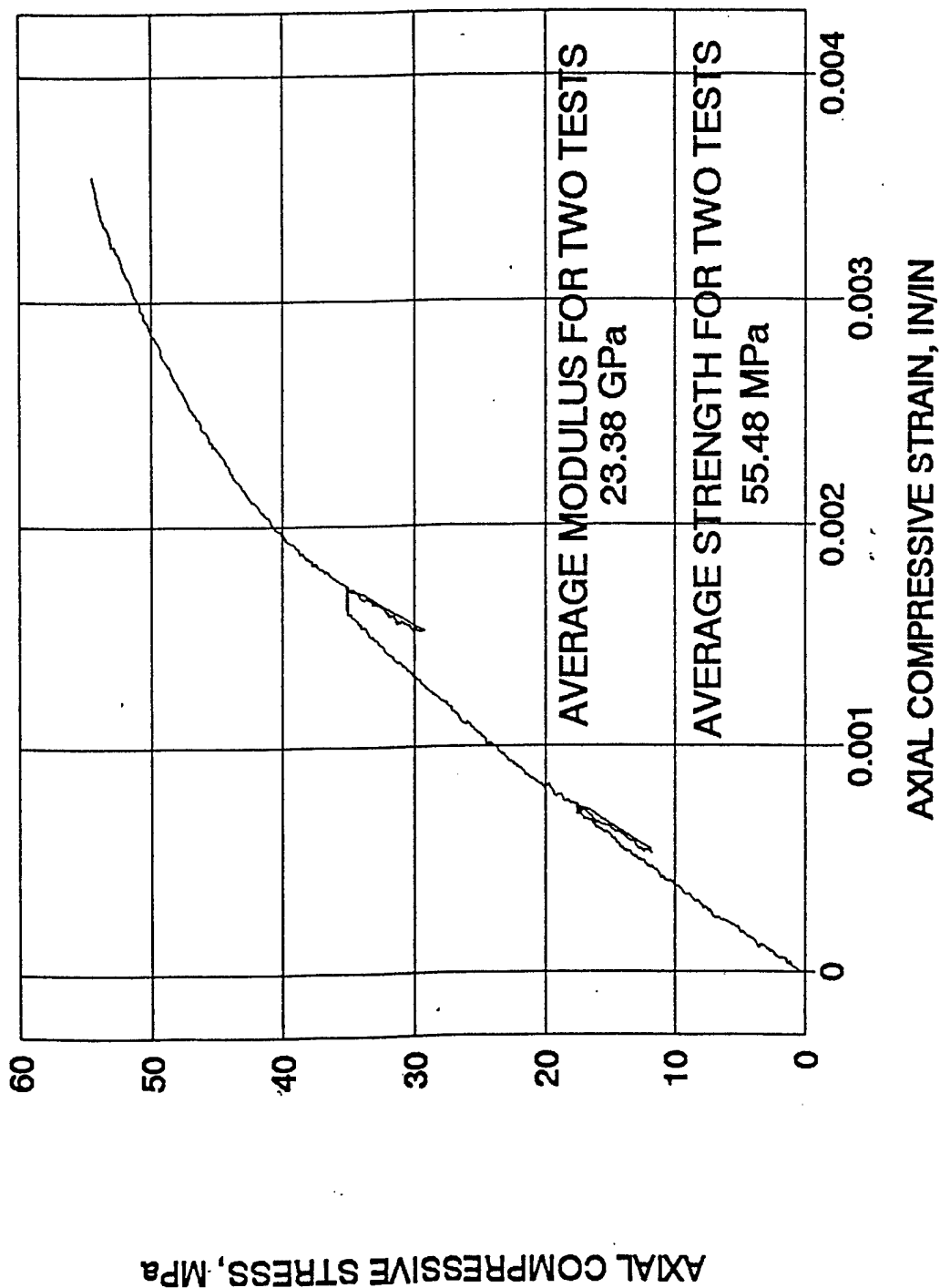


Figure 7. Stress-strain curve from modulus test of mortar.

Quasistatic confined mortar tests were conducted during May-June, 99 at confining pressures of 1.72 MPa (250 psi), 3.45 MPa (500 psi) and 6.90 MPa (1000 psi) at a strain rate of $1.25 \text{ E} - 6/\text{sec}$. A stress-strain curve and a stress-volumetric strain curve for each are given in Appendix A as Figures A-1 to A-8. An extra test for the 6.90 MPa confining pressure was analyzed and shown in Figures A-7 and A-8. This was done as the volumetric strain of QSMC9 of Figure A-6 never went negative and Figure A-8 confirms that the volumetric strain at the 6.90 MPa confining pressure shows very little negative strain or minimal swelling before failure.

Several dynamic confined mortar tests were performed in May-June 99 using the 76.2 mm diameter SHPB at the GERC. Selected confining pressure and strain rates were analyzed and shown in Appendix A as Figures A-9 to A-18. As indicated in the tests of late 1998 and noted here the confining pressure rises during the dynamic tests but appears to reach a maximum of approximately 12 – 15 MPa regardless of initial confining pressure or strain rate. The other observation worth noting is for the dynamic confined tests with initial confining pressure of 6.90 MPa (1000 psi), the volumetric strain is monotonically increasing for all strain rates tested. Based on this a quasistatic confined test at a confining pressure of approximately 10 MPa (the average confining pressure of the dynamic tests) would probably show the same general trend of a monotonically increasing volumetric strain. Details of all the tests discussed here are listed in Table 3.

3. Concrete Tests

Tests were continued in May – June, 1999 on compressive test of concrete. Two quasistatic unconfined modulus tests were conducted in May – June, 1999 and one of those tests, QSC-1, is included. Figure A-19 shows the stress-time curve and Figure A-20 shows the stress-

TABLE 3
COMPRESSIVE DATA FOR MORTAR

SPECIMEN	CONFINING PRESSURE – MPa	STRAIN RATE 1/SEC	FIGURE NUMBER
QSM3B	UNCONFINED	1.18E-6	4, 5
QSM5	UNCONFINED	1.25E-6	6, 7
QSMC5	1.72	1.25E-6	A-1, A-2
QSMC4	3.45	1.25E-6	A-3, A-4
QSMC9	6.90	1.25E-6	A-5, A-6
QSMC7	6.90	1.25E-6	A-7, A-8
DCMC27	1.72	140	A-9, A-10
DCMC20	3.45	80	A-11, A-12
DCMC30	6.90	52	A-13, A-14
DCMC24	6.90	67	A-15, A-16
DCMC25	6.90	123	A-17, A18

strain curve. The average modulus and average compressive strength given on Figure A-19 are 38.21 GPa (5.54×10^6 psi) and 69.52 MPa (10.08 ksi), respectively. The mix proportions for concrete are given in Table 2.

Several unconfined and confined quasistatic compressive tests on concrete were performed using the MTS material test machine at the AWEF. For the confined tests the same confining cell, used in the UFGERC SHPB, was used in the MTS test machine. Confining pressures of 1.81 MPa (263 psi), 3.45 MPa (500 psi) and 6.90 MPa (1000 psi) were used at a strain rate of 0.77×10^{-6} /sec. and those results are shown in Appendix A as Figures A-21 to A-26. Unconfined dynamic concrete tests were conducted using the UFGERC SHPB at strain rates of approximately 50/sec., 60/sec. and 100/sec. The results of these tests are shown in Appendix A as Figures A-27 to A-32. Several dynamic confined tests were performed on concrete at a confining pressure of 3.45 MPa (500 psi) and a strain rate of approximately 50/sec. Some of the results of these tests are shown in Appendix A as Figures A-33 to A-36. Some details of the tests discussed above are listed in Table 4.

4. Granite Tests

Several compressive strength tests were performed on rose granite whose quasistatic compressive strength and modulus are 20.16 Ksi (139.0 MPa) and 12.25 Msi (84.48 GPa), respectively, with a specific weight of 172 lbs/ft³ (2.21 kg/m³). One unconfined strength and modulus test is shown in Figure 8. The corresponding volumetric, transverse and longitudinal strains for the same specimen are shown in Figure 9. A quasistatic confined granite test, with 500 psi (3.45 MPa) confining pressure was performed and results are shown in Figures 10 and 11. Dynamic unconfined compression tests were performed in the SHPB and results of one of those tests are shown in Appendix A as Figures A-37 to A-38. Results of an additional dynamic

TABLE 4
COMPRESSIVE DATA FOR CONCRETE

SPECIMEN	CONFINING PRESSURE – MPa	STRAIN RATE 1/SEC	FIGURE NUMBER
QSC1	UNCONFINED	0.77E-6	A-19, A-20
QSCC1	3.45	0.77E-6	A-21, A-22
QSCC6	6.90	0.77E-6	A-23, A-24
QSCC12	1.81	0.77E-6	A-25, A-26
DCCU2	UNCONFINED	64	A-27, A-28
DCCU3	UNCONFINED	52	A-29, A-30
DCCU5	UNCONFINED	107	A-31, A-32
DCCC3	3.40	47	A-33, A-34
DCCC4	3.57	53	A-35, A-36

QUASISTATIC UNCONFINED GRANITE TEST

QSG-1, STRAIN RATE = $0.346E-6$ /SEC

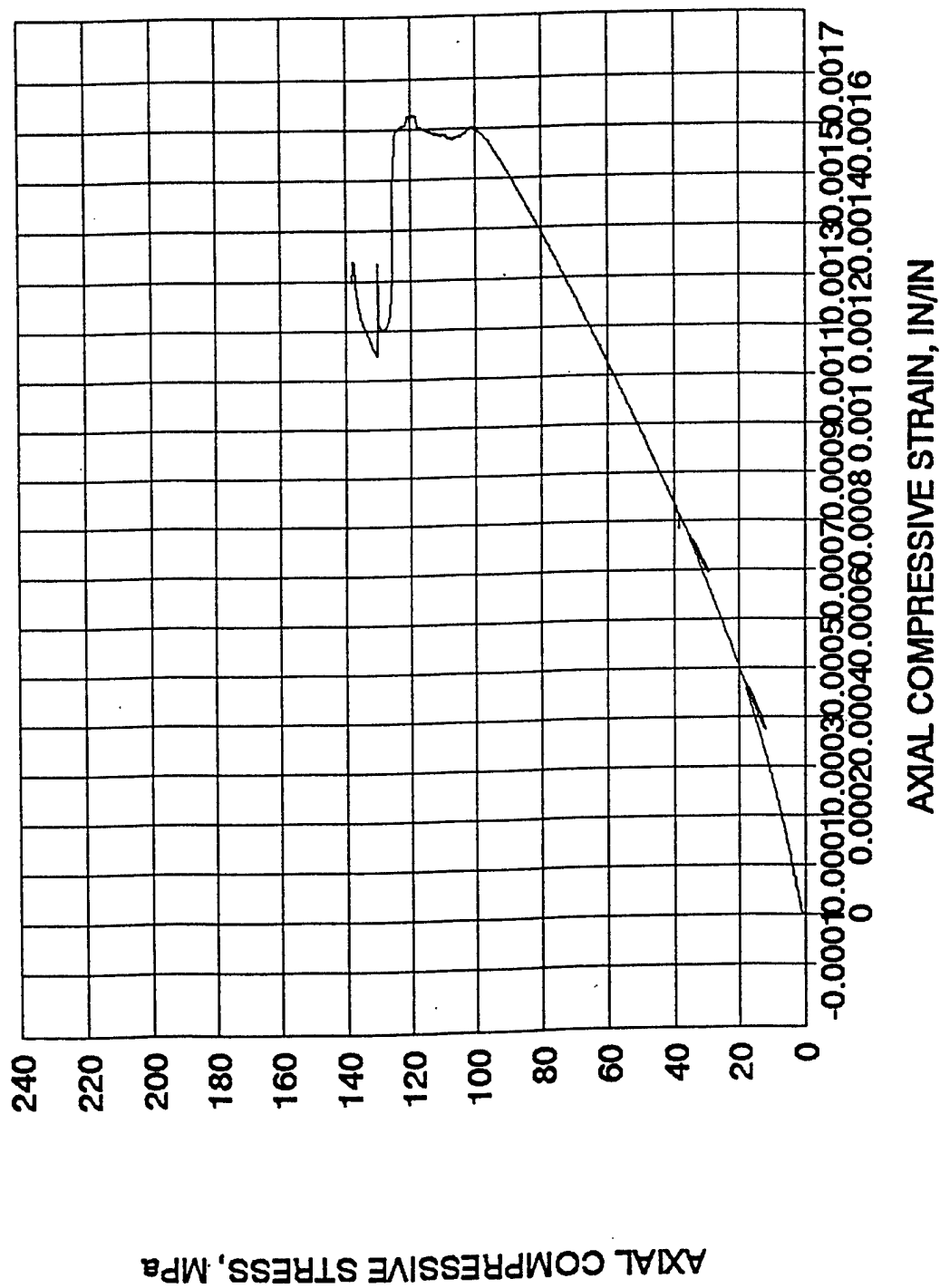


Figure 8. Stress-strain curve from modulus test of granite.

QUASISTATIC UNCONFINED GRANITE TEST

QSG-1, STRAIN RATE = 0.35E-6/SEC

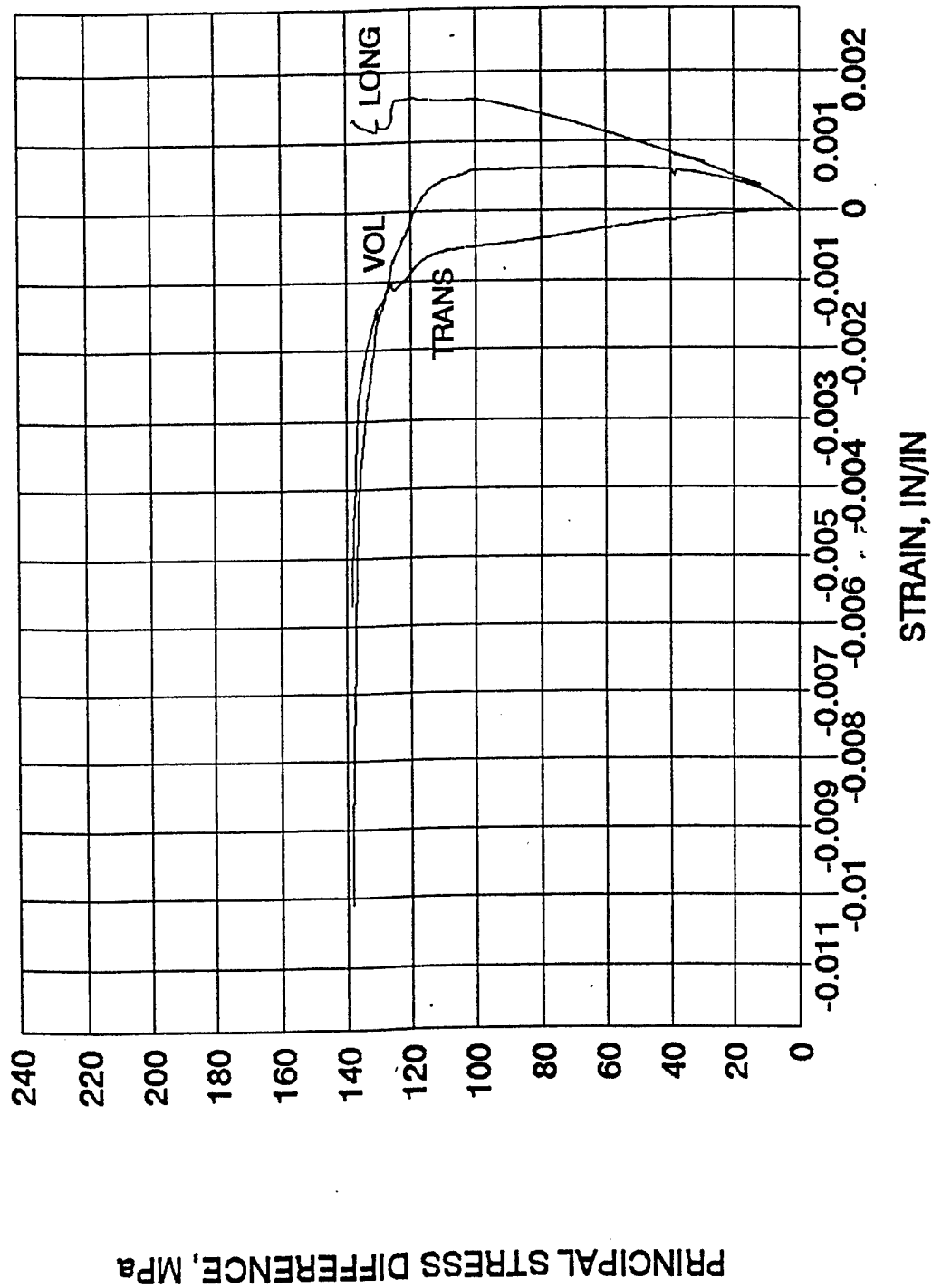


Figure 9. Longitudinal, transverse and volumetric strain for granite.

QUASISTATIC CONFINED TEST OF GRANITE

QSGC-3, CONFINING PRESSURE = 3.45 MPa, STRAIN RATE = 0.35E-6/SEC

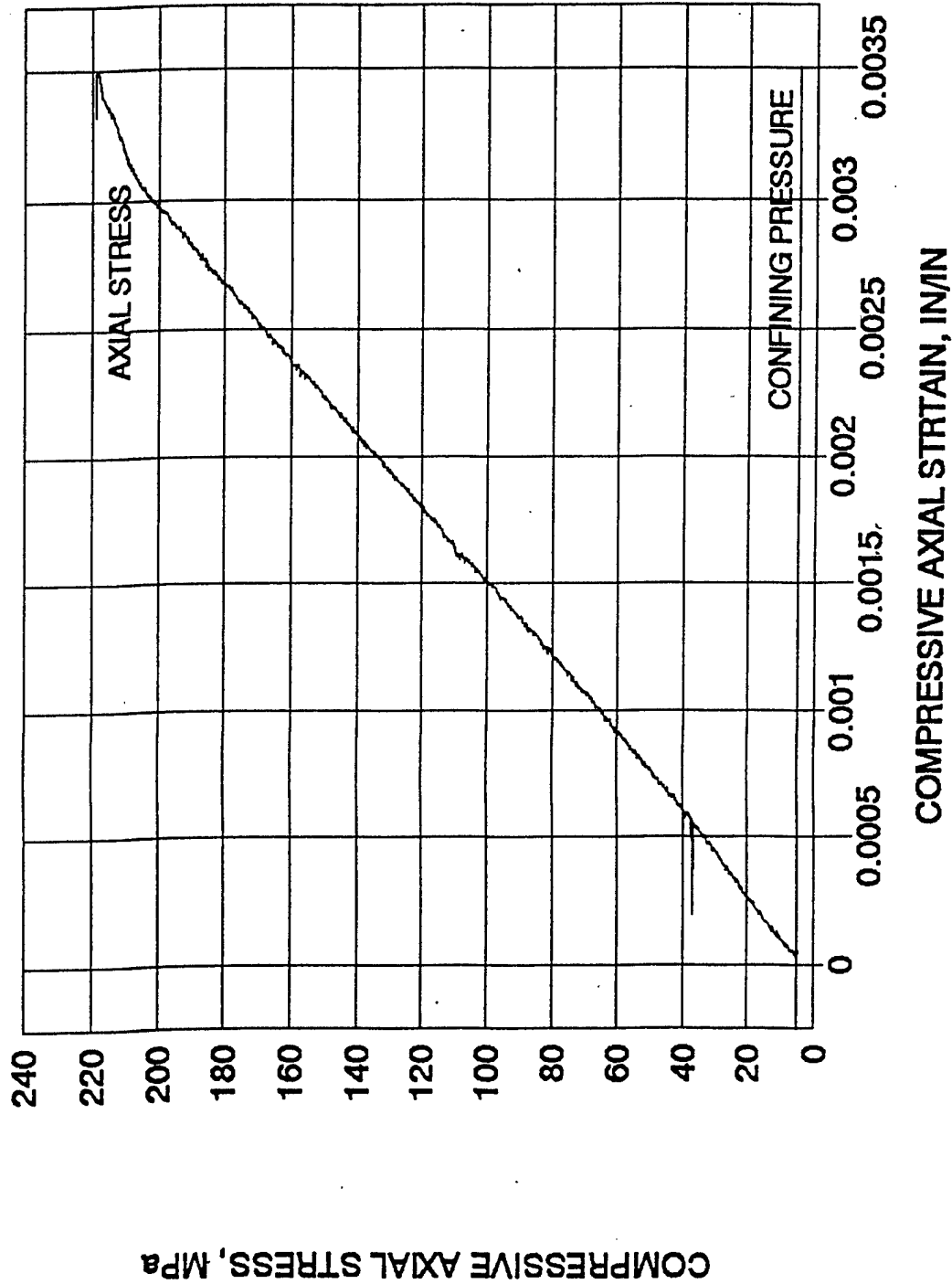


Figure 10. Stress-strain curve for quasistatic confined test of granite.

QUASISTATIC CONFINED TEST OF GRANITE

QSGC-3, CONFINING PRESSURE = 3.45 MPa, STRAIN RATE = 0.35E-6/SEC

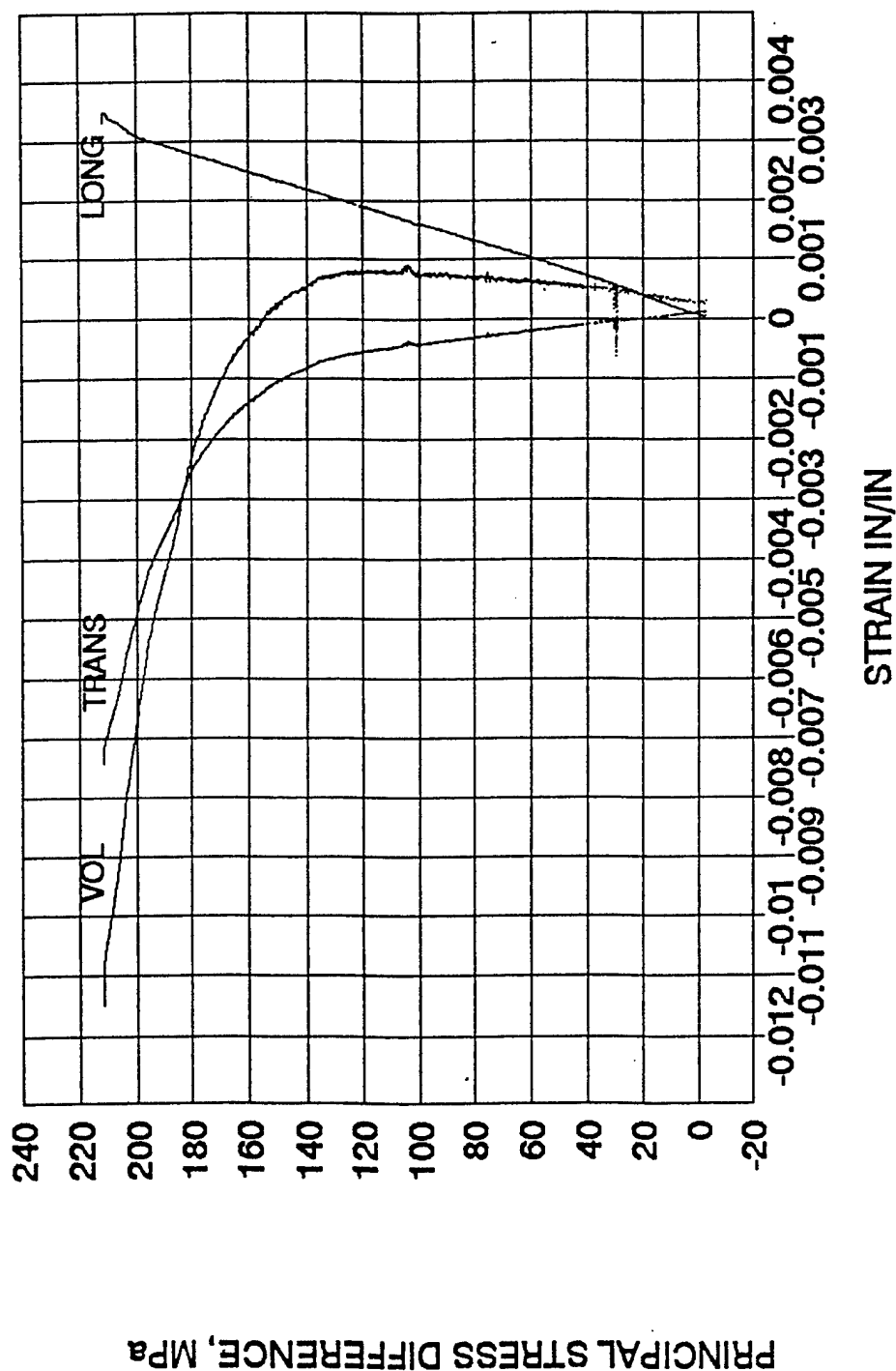


Figure 11. Longitudinal, transverse and volumetric strain for quasistatic confined test of granite.

unconfined granite are shown in Figures A-39 to A-40. The results of these dynamic unconfined granite tests appear to be somewhat different than similar tests on concrete and mortar. In observing the incident, reflected and transmitted strain traces we noticed rather different reflected pulse shapes than that of concrete tests. This will be discussed later in Section III. 1.

5. Ultrasonic Grout Tests

A. Background

Recently, the Advanced Weapons Effects Facility (AWEF) acquired a 50.8mm (2.0 in) diameter split Hopkinson pressure bar (SHPB) and as part of the Task 99-01, this device was aligned, leveled and exercised to determine its integrity. As part of the check out procedure a series of grout material cubes of nominally 35.92mm (1.414 in) on each edge, 50.8mm (2.0 in) diagonal on each face, were fabricated and tested in dynamic compression in the AWEF SHPB and quasistatic compression in the AWEF MTS material test machine. Mix proportions for the grout are given in Table 5. Prior to these tests each of the cube specimens were measured, as shown in Table 6 and tested ultrasonically using a Portable Ultrasonic Non-destructive Digital Indicating Tester (PUNDIT Mk-V) to measure the ultrasonic transit time in each of the orthogonal directions. The transducer frequency was 150 kHz. The cube faces were marked so that post-test transit times could be determined in the same directions. The objective of these tests was to determine the effect of a uniaxial compressive stress on the ultrasonic wave speed in the various directions of each specimen. The use of cubical specimens allows the ultrasonic measurement in three directions. Due to limited size of the 50.8mm diameter SHPB a small aggregate grout concrete material was used for the specimens. Also, due to the small specimen size, the results are presented in a normalized fashion by dividing the directional test data by each of the unstressed directional ultrasonic wave velocity or transit time.

TABLE 5

MIX PROPORTIONS FOR GROUT

295 kg (650 lbs.) Type I Portland Cement (3.15 s.g.)
 736 kg (1620 lbs.) #9 Crushed Limestone (2.74 s.g.)
 652 kg (1435 lbs.) Silica Sand (2.63 s.g.)
 0.77 l (26 oz.) Type A Water Reducer
 133 kg (292 lbs.) Water

TABLE 6

DIMENSIONS, TRANSIT TIMES AND WEIGHT FOR GROUT CUBES

Specimen#	Dim-X-Axis	Dim-Y-Axis	Dim-Z-Axis	Time---X-	Time---Y-	Time---Z--	Mass
	Inches	Inches	Inches	Millisec	Millisec	Millisec	Grams
#1	1.398	1.396	1.395	7.9	7.9	7.9	97.03
#2	1.382	1.402	1.392	7.9	7.9	8.2	95.73
#3	1.391	1.395	1.398	7.7	7.6	7.8	96.8
#4	1.387	1.396	1.401	7.5	7.6	7.5	97.76
#5	1.401	1.404	1.396	7.8	7.8	7.5	98.71
#6	1.397	1.398	1.4	7.7	7.7	7.8	96.78
#7	1.398	1.394	1.392	7.7	7.6	7.7	97.07
#8	1.394	1.405	1.39	7.6	7.7	7.4	98.06
#9	1.394	1.397	1.413	7.6	7.7	7.8	98.98
#10	1.387	1.402	1.401	7.6	7.7	7.7	98.79
#11	1.405	1.402	1.397	7.6	7.7	7.6	99.6
#12	1.398	1.397	1.396	7.6	7.7	7.8	96.72
#13	1.374	1.396	1.392	7.4	7.5	7.5	96.79
#14	1.396	1.402	1.4	7.5	7.5	7.7	98.27
#15	1.405	1.395	1.396	7.4	7.6	7.6	99.39
#16	1.401	1.402	1.405	7.6	7.6	7.6	97.95
#17	1.405	1.406	1.396	7.6	7.7	7.5	97.77
#18	1.401	1.389	1.4	7.6	7.6	7.7	96.84
#19	1.394	1.402	1.396	7.5	7.5	7.3	98.66
#20	1.399	1.404	1.396	7.7	7.6	7.6	97.33
#21	1.39	1.4	1.4	7.4	7.5	7.4	98.53
#22	1.394	1.399	1.403	7.7	7.7	7.8	98.04
#23	1.396	1.394	1.392	7.9	7.6	7.6	96.2
#24	1.399	1.394	1.397	7.8	7.8	7.8	96.21
#25	1.403	1.4	1.394	7.9	7.7	7.5	97.31
#26	1.392	1.4	1.404	7.7	7.7	7.8	96.95
#27	1.399	1.4	1.401	7.5	7.5	7.6	98.95
#28	1.404	1.391	1.394	7.7	7.7	7.7	97.25
#29	1.398	1.387	1.401	7.6	7.6	7.6	96.66
#30	1.397	1.398	1.396	7.6	7.6	7.6	95.95
#31	1.398	1.392	1.404	9.1	9.2	8.3	95.7

B. Quasistatic Tests

Several Compressive quasistatic tests were performed on the cube grout specimens using the 55 kips (12.35 nt) load cell of the AWEF MTS machine. Tests were run on some specimens with the ultrasonic transducers attached to opposite faces, which measured the ultrasonic wave transit time in a direction perpendicular to the loading direction. (See Figure 12.) The quasistatic tests were run at a compressive loading rate of 20 psi/sec (0.138 MPa/sec). An example of the data showing the axial loading and change in ultrasonic wave speed is shown later in the Results and Discussion Section.

C. Dynamic Tests

Dynamic tests on the grout cubes were performed using the 50.8mm diameter AWEF SHPB as shown schematically in Figure 13. The cubes were fabricated with the diagonal on each face of a nominal 2.0 in (50.8mm) length such that each loaded face fit inside the 50.8mm diameter of the loading faces of the incident and transmitter bars. (See Figure 13.)

The 50.8mm diameter SHPB was recently transferred from Tyndall AFB, FL to the AWEF, then aligned and leveled under Task 99-01. The principles and procedures of operation of this SHPB are discussed by Ross [1989]. In the compression mode as shown in Figure 13, a striker bar impacts the incident bar and generates a compressive stress pulse, which in time is twice the length of the transit time of the striker bar. This pulse travels down the incident bar and impinges on the specimen, which is sandwiched between the incident and transmitter bars. At the specimen, a portion of the pulse is reflected back into the incident bar and a portion of the pulse is transmitted into the transmitter bar. Specimen strain is proportional to the integral of the reflected pulse, specimen strain-rate is proportional to the reflected pulse and specimen stress is proportional to the transmitted pulse. A typical set of stress pulses, obtained for specimen No.

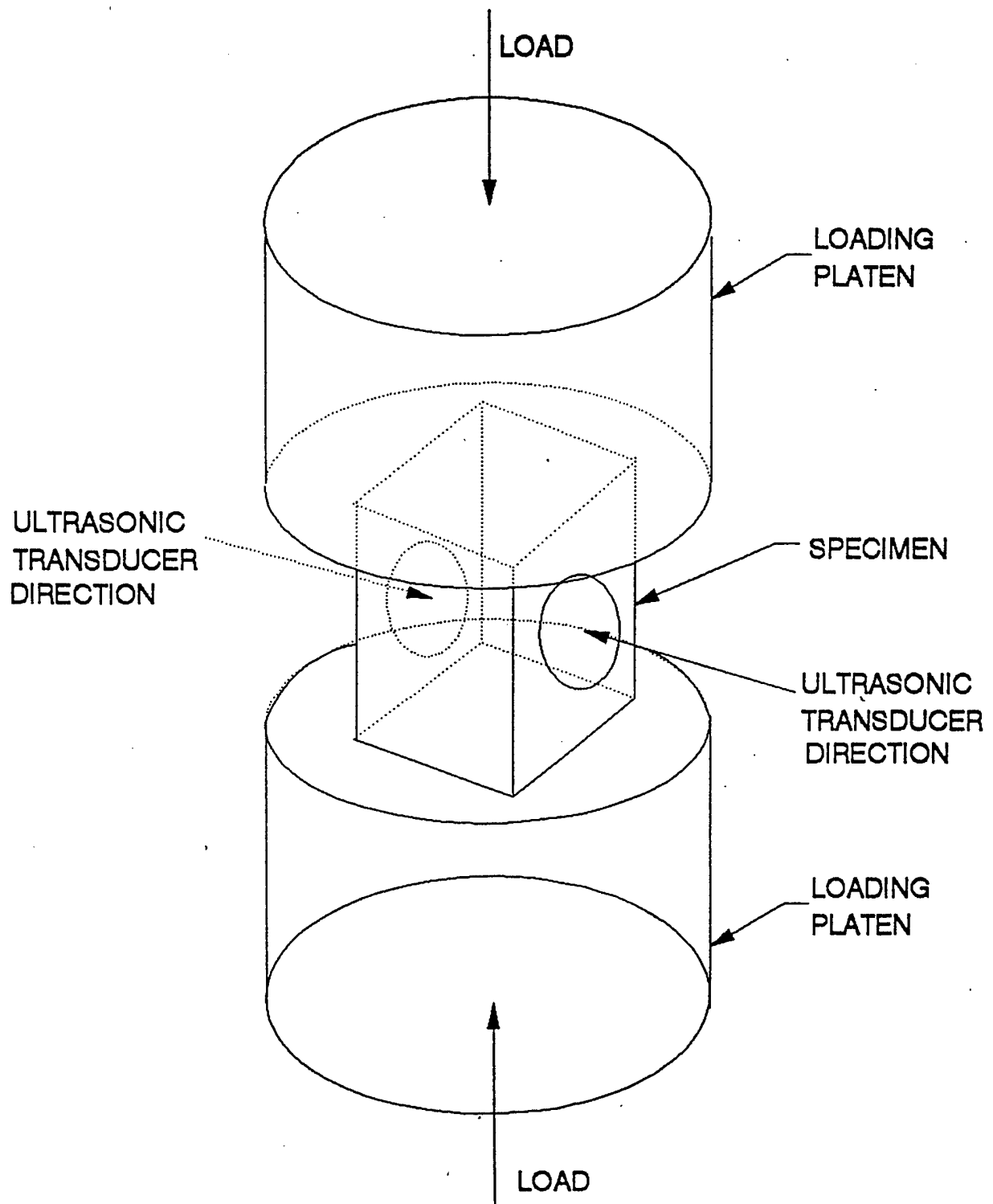
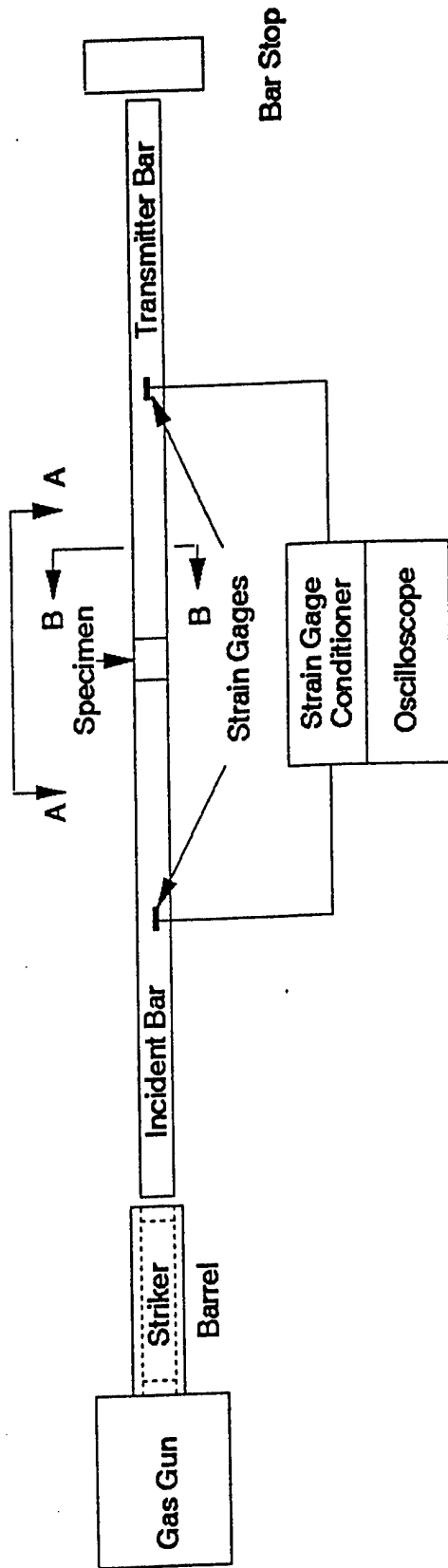
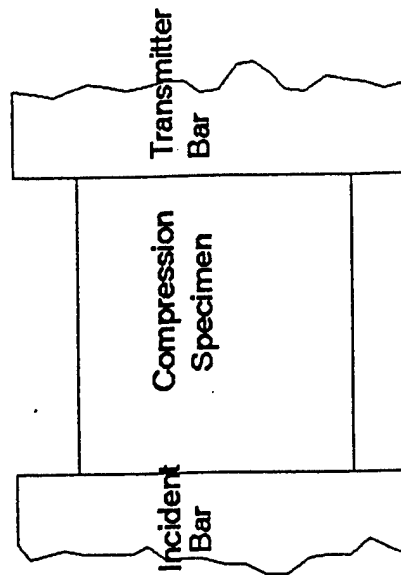


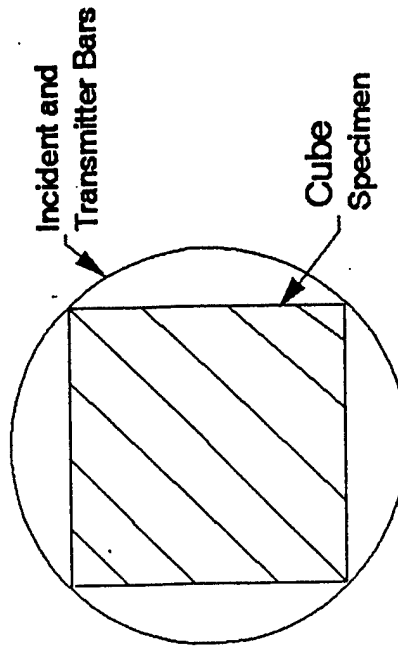
Figure 12. Schematic of quasistatic compressive cube test.



a) Split Hopkinson Pressure Bar (SHPB)



b) Top view A-A of specimen



c) Cross-section view B-B of specimen

Figure 13. Schematic of a split Hopkinson pressure bar (SHPB) showing the arrangement for the compressive cube specimen.

10, is shown in Figure 14. The striker bar is driven by compressed nitrogen gas, regulated in the gas gun. A plot of the average peak stress in the incident bar versus the gas gun pressure is shown in Figure 15.

For the grout specimens the SHPB was initially operated at the lowest gas gun pressure that would generate a stress pulse in the incident bar; approximately 5.0 psi (35kPa) which resulted in a specimen stress of approximately 1360 psi (9.38 MPa). Specimens were then tested in 0.5 psi increments up to 9.0 psi (62 kPa) at which the specimen fractured at a specimen stress of approximately 10,000 psi (69 MPa). The strain rate for these tests ranged from 1.0 to 20/sec. After each dynamic tests the ultrasonic wave speed was measured and the ratio of the transit times, pretest time divided by post test time, was determined and given in Table 7. This ratio which represents the ratio of pretest wave velocity to post test wave velocity, assuming the dimension changes during the test are negligible. This assumption appears reasonable as the strain in the loaded direction for most all concrete material is approximately 0.2 – 0.3 percent. In addition, a ratio of the dynamic compressive specimen stress to the average quasistatic compressive stress was determined and shown in Table 7. Generally, this stress ratio is referred to as the Dynamic Increase Factor (DIF) in the literature on the effects of strain rate on material properties.

INCIDENT STRESS VS GAS GUN PRESSURE 2.0 INCH DIAMETER SHPB

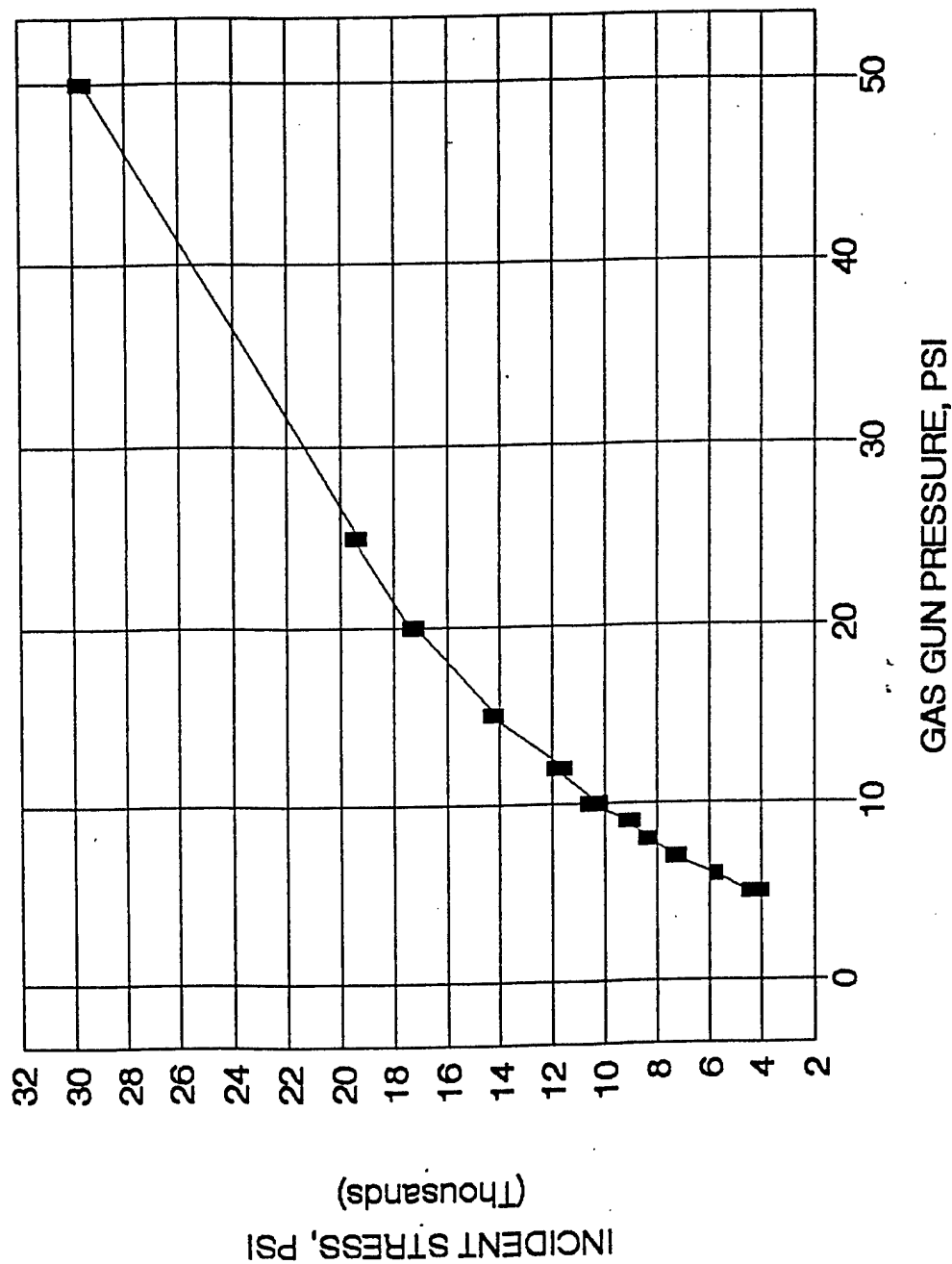


Figure 15. Average value of incident stress generated by impactor when driven by a given gas gun pressure.

TABLE 7
ULTRASONIC GROUT TESTS

SR = STEESS RATIO, TRANSMITTED STRESS (PSI)/7685 PSI
 UVR = ULTRASONIC VELOCITY RATIO
 = (PRETEST TRANSIT TIME)/(POST-TEST TRANSIT TIME)
 UVRL = VEL RATIO IN LOADED DIRECTION
 UVR1, UVR2 VEL RATIO IN OTHER DIRECTIONS

SPEC	SR	UVRL	UVR1	UVR2	(UVRL)^2	(UVR1)^2	(UVR2)^2
1	0.84244	1	0.95	0.99	1	0.9025	0.9801
2	0.92217	0.95	0.65	0.71	0.9025	0.4225	0.5041
3	0.48990	1	1	1	1	1	1
4	0.18347	1	0.98	0.97	1	0.9604	0.9409
5	0.16234	0.97	1	1	0.9409	1	1
6	0.34197	0.98	0.97	0.97	0.9604	0.9409	0.9409
8	0.49374	0.96	0.92	0.92	0.9216	0.8464	0.8464
9	0.56867	0.98	0.96	0.97	0.9604	0.9216	0.9409
10	0.94330	0.97	0.97	0.97	0.9409	0.9409	0.9409
11	0.71756	0.95	0.8	0.88	0.9025	0.64	0.7744
12	0.96348	0.96	0.85	0.85	0.9216	0.7225	0.7225
13	1.15560	0.97	0.83	0.89	0.9409	0.6889	0.7921
14	1.15272	0.91	0.57	0.56	0.8281	0.3249	0.3136
15	1.19210	0.89	0.61	0.67	0.7921	0.3721	0.4489
17	0.94523	0.9	0.59	0.59	0.81	0.3481	0.3481
18	0.89143	0.87	0.5	0.52	0.7569	0.25	0.2704
19	0.64072	0.95	0.39	0.91	0.9025	0.1521	0.8281
20	0.99902	0.92	0.62	0.73	0.8464	0.3844	0.5329
21	1.12582	0.93	0.78	0.86	0.8649	0.6084	0.7396
22	0.90872	0.95	0.95	0.95	0.9025	0.9025	0.9025
23	1.00190	0.92	0.88	0.89	0.8464	0.7744	0.7921
27	0.90008	0.97	0.9	0.96	0.9409	0.81	0.9216
28	0.64072	0.99	0.83	0.93	0.9801	0.6889	0.8649
29	0.37943	0.92	0.95	0.95	0.8464	0.9025	0.9025
30	0.79153	0.92	0.68	0.68	0.8464	0.4624	0.4624

Section III

RESULTS AND DISCUSSION

1. Experiments

a. Mortar, Concrete and Granite Tests

Generally, these tests were conducted to furnish data for calibration of the EVP Model as given in Section III.2. All of these tests are very time consuming and expensive. In particular the confined specimens for both quasistatic and dynamic tests require as much as three hours preparation time for each specimen. For the quasistatic confined high strength granite tests, at least two hours of MTS machine time was required for completion. In addition each test requires more than one hour for analysis. For the high confining pressure triaxial test run at WES, as much as eight hours are required to complete the test. Considering the amount of time required only a limited number of test could be completed.

In summary, as the strain rate or confining pressure increases the compressive strength increases. This trend also holds true for the principal stress difference at which dilatancy begins to occur. As the confining pressure increases the deviatoric stress (principal stress difference) at which the volumetric strain changes sign also increases. For a given axial stress and increasing confining pressure there is some confining pressure at which dilatancy is prevented from occurring.

The response of the material in terms of failure or fracture is highly dependent on the confining pressure. Only a small amount of confining pressure is required to prevent material fracture for mortar, concrete or granite. Complete specimen fracture occurs when the compressive strength (for a given strain rate) is exceeded. However, if approximately ten or

fifteen percent of the compressive strength of the material is applied as a hydrostatic stress then practically no visible fracture occurs.

During the dynamic tests of mortar, concrete and granite the general shape of the reflected portion of SHPB data was observed to change. In particular the shape of the reflected pulse of granite specimen is different than that of the concrete specimen.

Figure 16 shows the results of a dynamic unconfined mortar test with a fairly constant reflected shape with a transmitted pulse magnitude about half the incident pulse. This is typical of dynamic concrete and mortar tests. For the mortar specimen there was practically no visible damage to the specimen. The results of a dynamic unconfined granite test of similar impactor velocity are shown in Figure 17. Here again there was practically no visible damage to the specimen. However, the reflected pulse magnitude of the granite test (Figure 17) falls near zero about halfway through the pulse length and the peak transmitted pulse magnitude is approximately that of the incident pulse. When the impactor velocity is increased, such that the specimen is completely shattered into small pieces, the reflected pulse magnitude, as shown in Figure 18 falls almost to zero but increases again near the end of the transmitted pulse. These shapes are explained by observing the elastic properties of the materials. In comparison the characteristic impedances of the materials given in units of lbf-sec/in^3 , are 148.9 for steel, 55.0 for granite, 33.5 for concrete and 26.5 for mortar.

Assuming the initial reflection/transmission of the incident pulse of the SHPB at the incident/specimen interface is elastic, then the reflection coefficients of all the specimens will be negative indicating a tensile reflected pulse. The tensile reflection coefficient is a result of the impedance mismatch of the higher steel characteristic impedance and the lower values of the other materials. As a portion of the compressive incident pulse is transmitted into the specimen a

SHPB UNCONFINED MORTAR TEST

IMPACT VELOCITY = 7.94 M/SEC

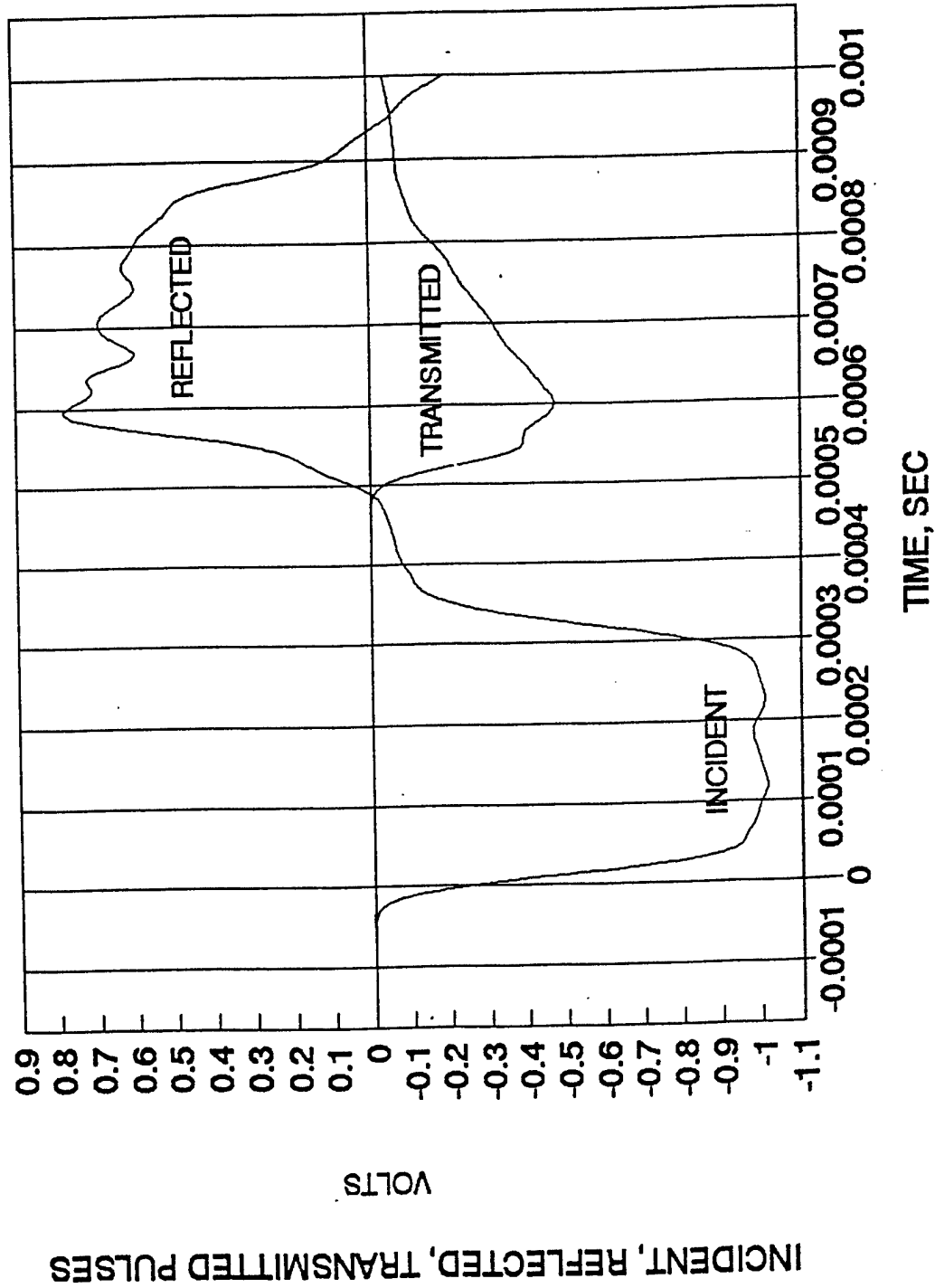


Figure 16: Incident, reflected and transmitted pulse for dynamic mortar test.

SHPB UNCONFINED GRANITE TEST

IMPACT VELOCITY = 6.62 M/SEC

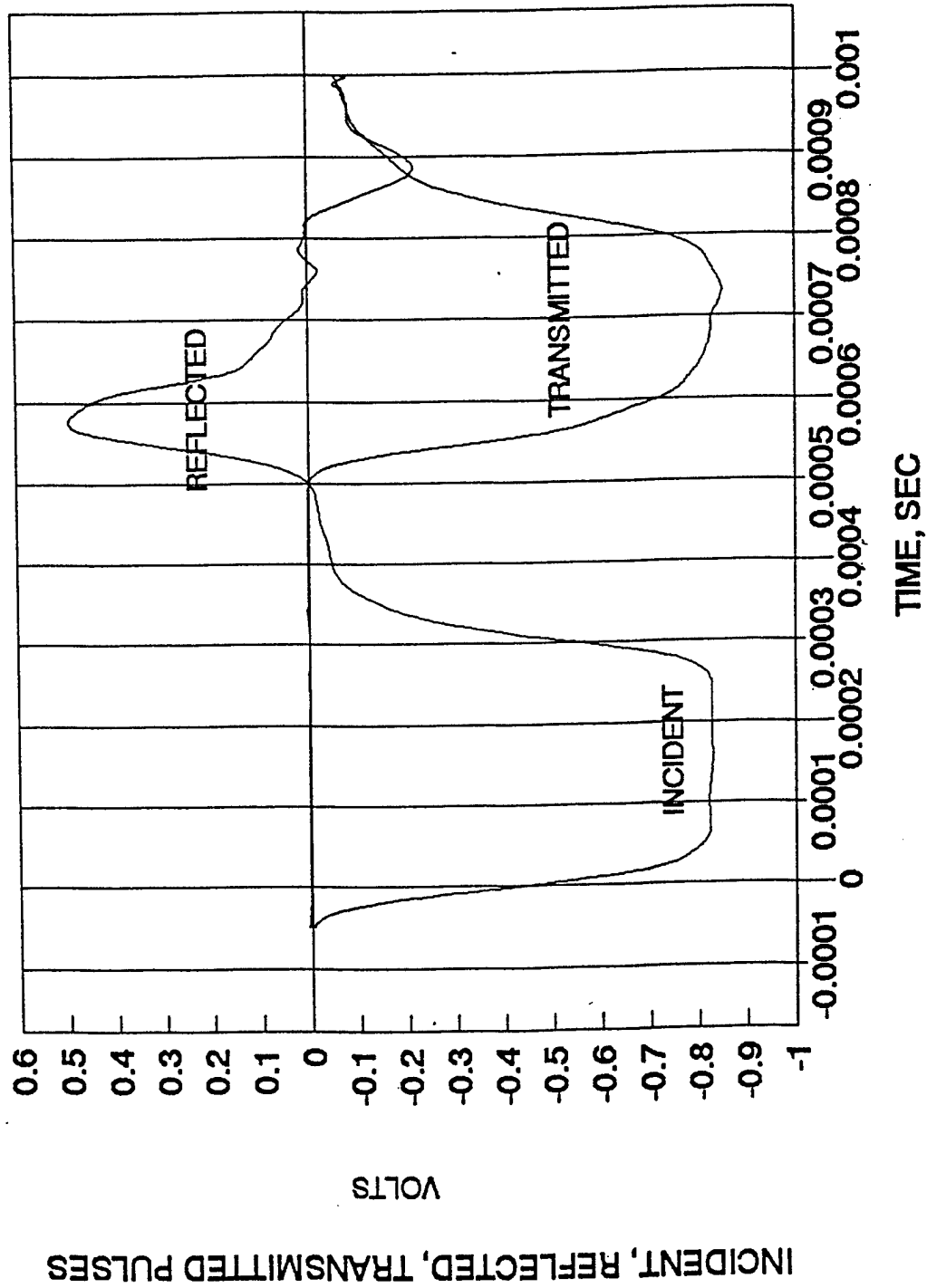


Figure 17. Incident, reflected and transmitted pulses for dynamic granite test.

SHPB UNCONFINED GRANITE TEST

IMPACT VELOCITY = 10.26 M/SEC

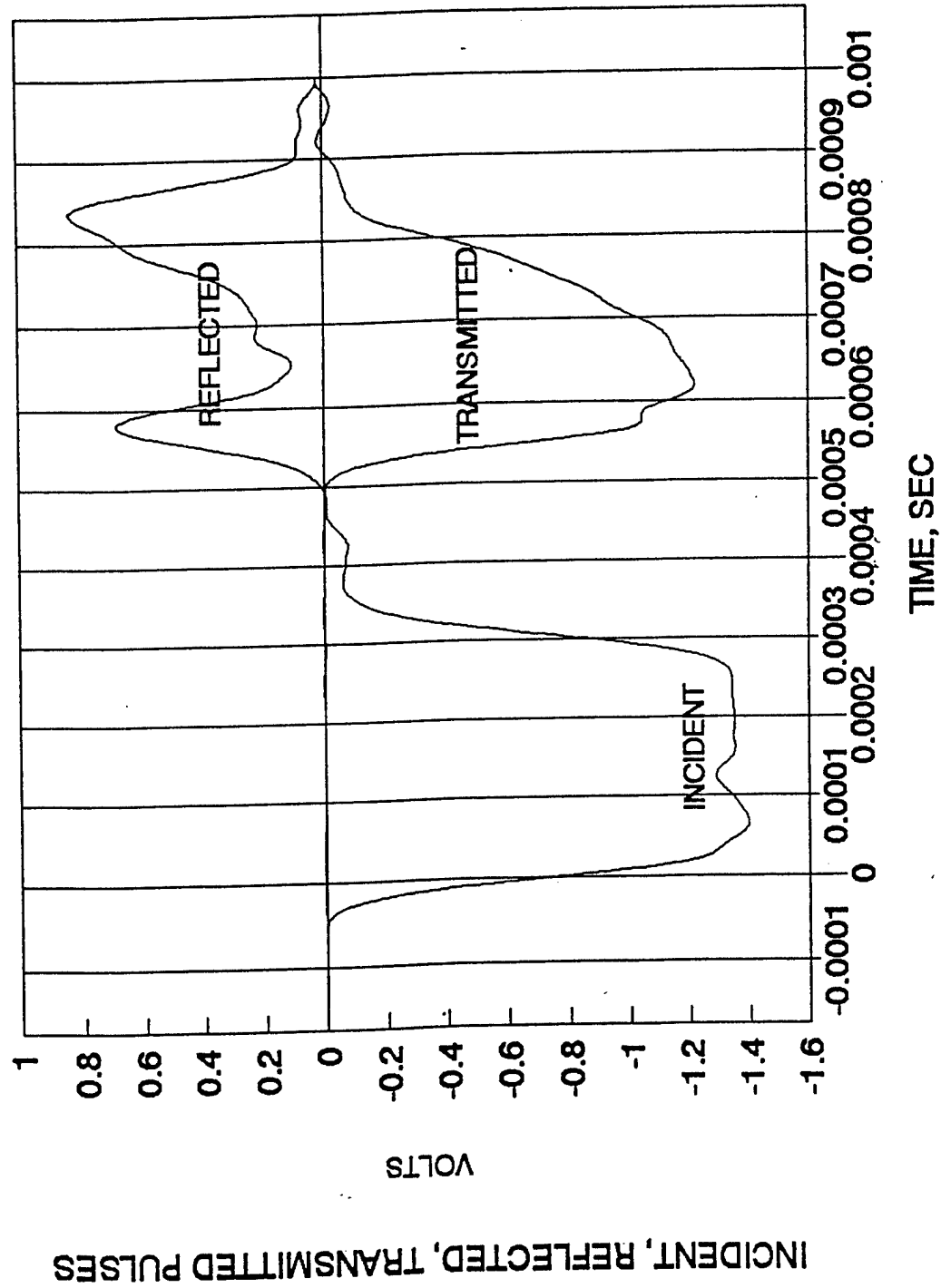


Figure 18. Incident, reflected and transmitted pulses for dynamic granite test.

reflection/transmission occurs at the specimen/transmission bar interface. Both reflection and transmission coefficients are positive here, therefore both reflected and transmitted pulses are compressive. The compressive pulse reflected back into the specimen is now trapped in the specimen due to the mismatch of the characteristic impedances. This pulse is now reflected and transmitted as a compressive pulse at each interface. The initial tensile reflected pulse is now reduced in magnitude, after the double transit time in the specimen, by the compression pulse transmitted into the incident bar. The amount of reduction of the initial tensile reflection is dependent on the magnitude of specimen characteristic impedance relative to the steel value. The higher the specimen characteristic impedance the larger the percentage reduction of the initial reflected tensile pulse. Thus, the relative reduction in the granite specimen is greater as shown in Figure 18 for granite when compared to Figure 16 for mortar.

If the specimen remains intact and relatively elastic the reduction in tensile reflected pulse remains at approximately this value for the remainder of the reflected pulse as evident in Figure 17 for a low impact test of granite. For higher impact tests, causing high strain rate effects, the specimen begins to fracture then, the magnitude of the reflected tensile pulse rises again as shown in Figure 16 for mortar and Figure 18 for granite.

b. Grout Tests

As discussed by Schreyer and Gao [1998] and Nemat Nasser and Horii [1982] columnar fracture of cementitious material under uniaxial compression occurs in planes that are parallel to the loading axis. This phenomenon was observed in both the quasistatic and dynamic grout tests listed in Section II. 5. Fracture planes as shown schematically in Figure 19 were observed in several specimens. Post test ultrasonic transit times measurements of all the dynamic grout tests showed that transit times, of one or both transverse measurements, was always greater than the

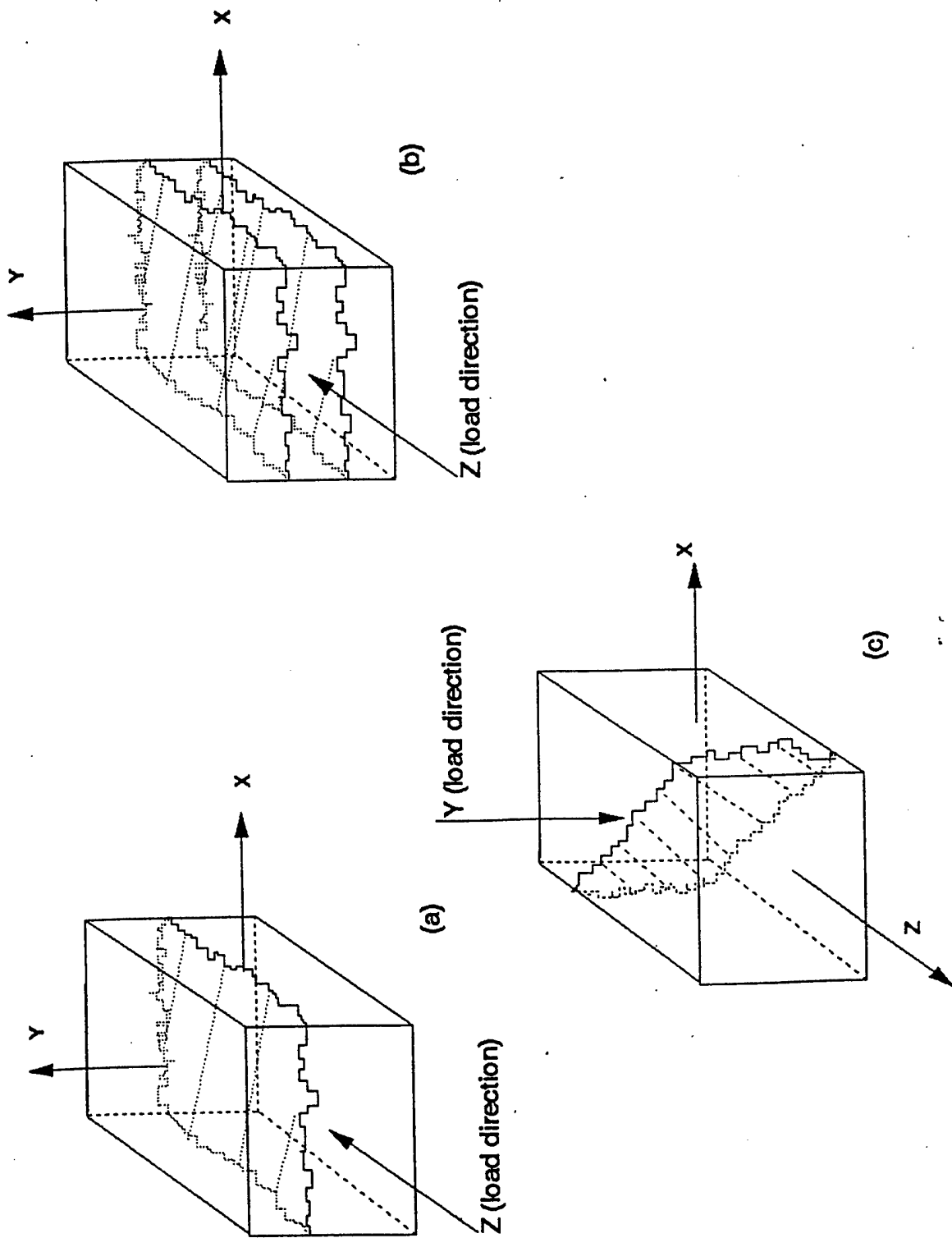


Figure 19. Schematic of fracture planes. (a) Plane approximately parallel to the XZ plane. (b) Two planes approximately parallel to the XZ plane. (c) Plane diagonal across the XZ plane, but approximately parallel to Y axis.

measurement made in the loaded direction. For example, when a cube is loaded in the z direction a fracture plane may occur in the xz plane, such as in Figure 19a, and the transit time in y direction will be greater than the other two directions. For multiple planes, such as in Figure 19b, a schematic of specimen No. 19, the transit time in the y direction will be much larger than the other two directions. However, for a y load direction as in specimen no. 30, where a fracture plane occurred diagonally, as shown in Figure 19c, the transverse transit times of directions x and z were approximately equal and greater than the y or loaded direction transit time.

To show the effect of increasing peak dynamic transmitted stress the transit time rates of Table 7 are plotted in Figure 20 versus the stress ratio. The stress ratio here is the peak transmitted stress divided by the average quasistatic strength of the cube tests. The ultrasonic wave velocity ratio, UVR, defined as the ratio of wave velocities in a certain direction before and after the compressive test may be formed in the following way. Assuming the transit distance does not change during the test,

$$\text{UVR} = T_b/T_a = V_a/V_b \quad (3)$$

where T_b is transit time before test, T_a is transit time after test, V_b is wave velocity before the test and V_a is velocity after the test. In some cases a damage parameter may be related to a material modulus ratio and wave velocity V may be related to the material modulus E by the equation

$$V = (E/\rho)^{1/2} \quad (4)$$

where ρ is the material density. Assuming the density change is negligible in the tests a ratio of moduli before and after the test may be formed by squaring Eq. (4) and dividing V_b^2 by V_a^2 to give

$$(V_a/V_b)^2 = (\text{UVR})^2 = E_a/E_b \quad (5)$$

VELOCITY RATIO VS STRESS RATIO ULTRASONIC GROUT TESTS

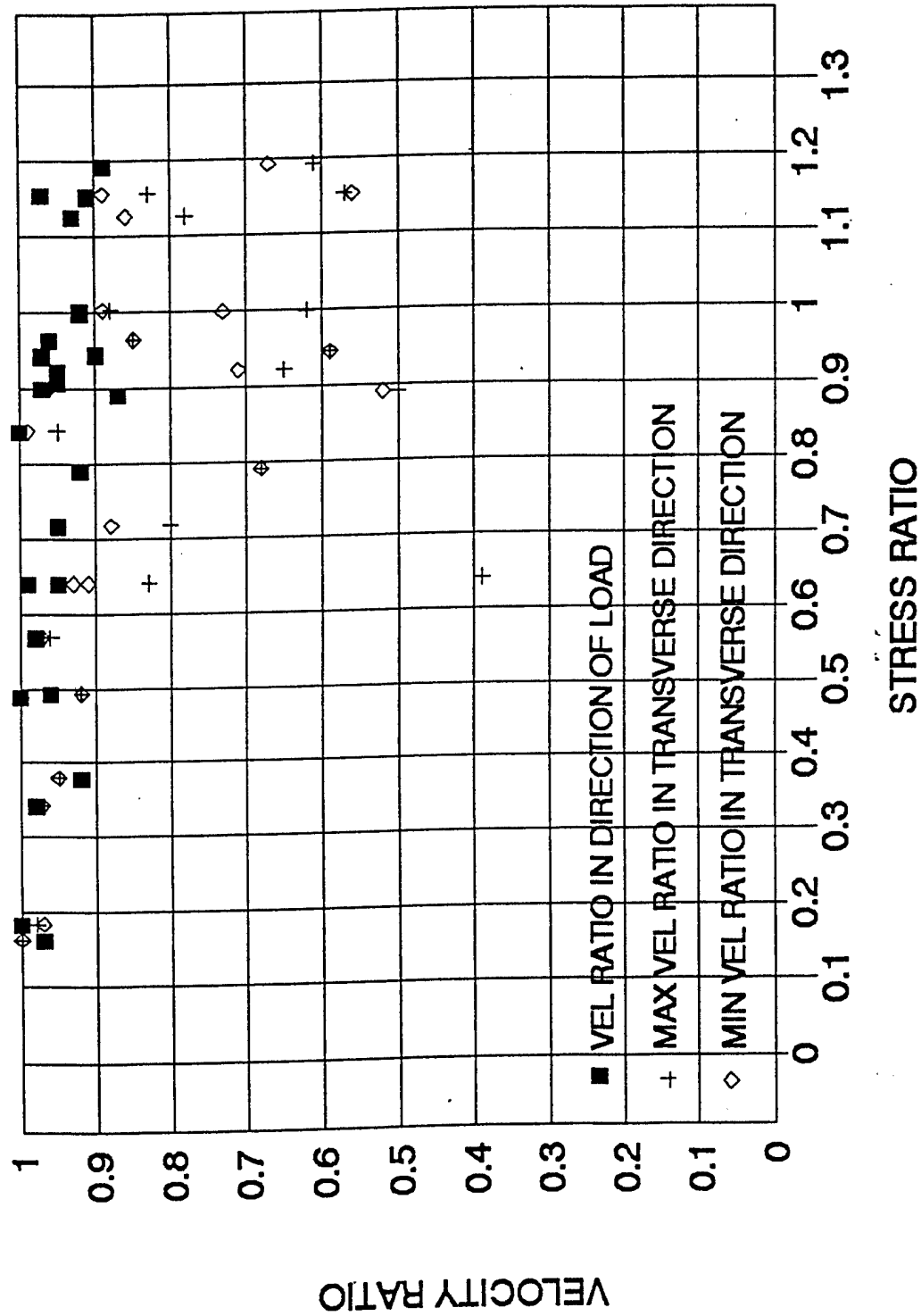


Figure 20. Ultrasonic grout tests using the SHPB as a loading device.

where E_b is modulus before the dynamic test and E_a is modulus after the dynamic tests. The modulus ratio may be determined by the velocity ratio squared and is plotted in Figure 21 versus the stress ratio. The major conclusion here is that due to the fracture planes forming parallel to load direction, ligaments of continuous material parallel to the load direction channel the ultrasonic waves across the loaded length of the specimen. However, ultrasonic waves trying to move perpendicular to the fracture planes are impeded and multiple reflections and transmissions increase the transit time or reduce the wave velocity. This phenomenon is then accompanied by a reduction in transverse modulus and tensile strength. Reduction of dynamic tensile stresses were observed in a study by Ross [1998], where cylinders were subjected to a splitting tensile test after an application of a longitudinal dynamic compressive stress.

Based on the data shown in Figure 21 the modulus ratio in the loaded direction decreases only approximately 20% at or near the peak load, whereas the modulus in the transverse direction begins to show a rather large decrease up to more than 50% at the quasistatic strength. A comparison of data obtained in the dynamic and quasistatic tests are shown in Figures 22a and 22b. In work reported by Ahrens [1998], Ross [1998] and here, it appears that ultrasonic wave velocity reduction of approximately 30 to 40% indicates a modulus reduction greater than 50% which might be considered zero strength for cementitious material. However, this does not mean a modulus reduction in one direction will predict a damage parameter that is effective for all directions. This is borne out in the experiments where transit times or ultrasonic wave velocities were different in all three directions.

The scatter in the data when comparing quasistatic and dynamic data of Figures 20 and 21 is most likely based on the fact that a set of the quasistatic data are taken from one specimen,

(VELOCITY RATIO) ~ 2 VS STRESS RATIO

ULTRASONIC GROUT TESTS

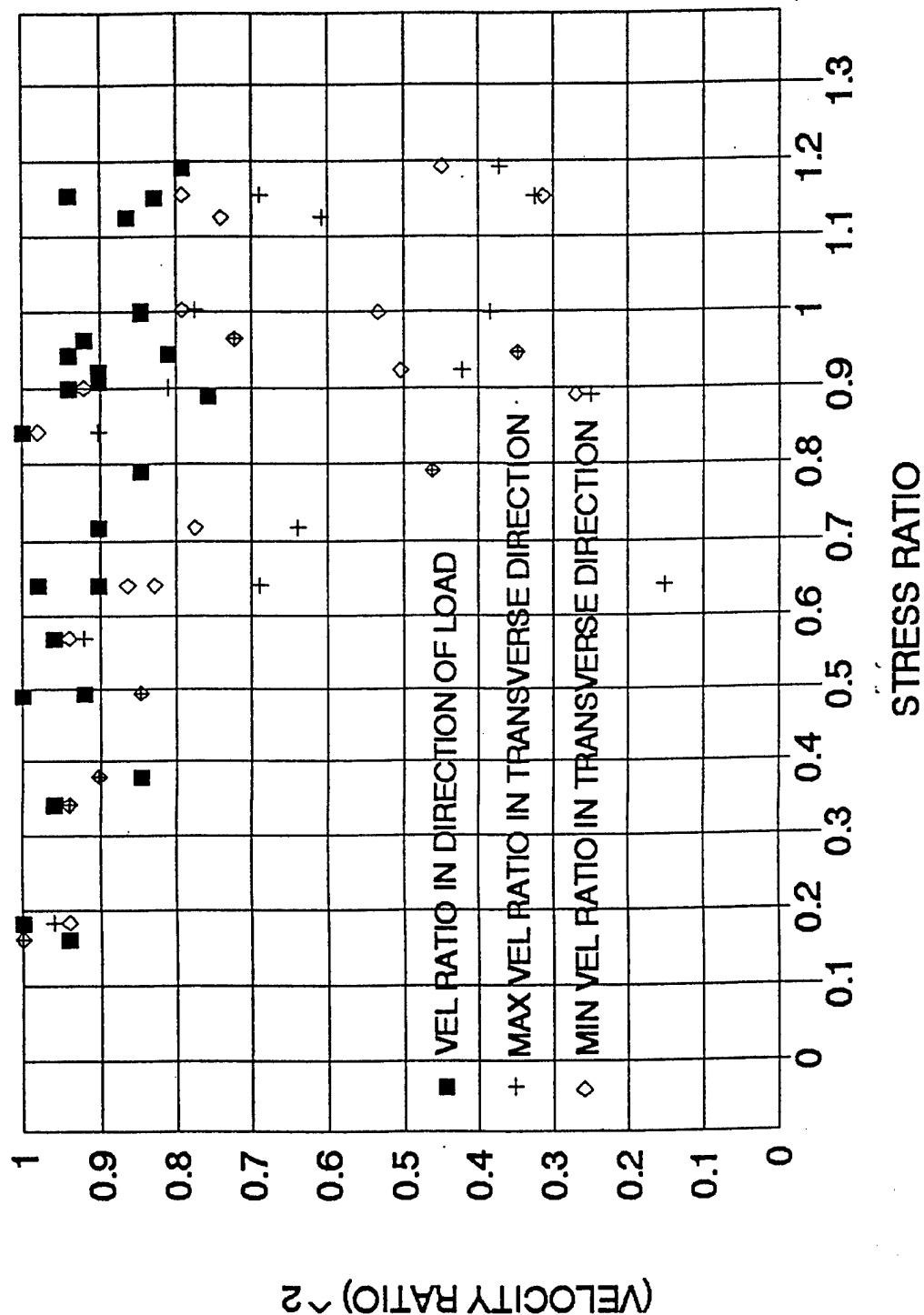


Figure 21. Ultrasonic grout tests using SHPB as a loading device.

VELOCITY RATIO VS STRESS RATIO

ULTRASONIC GROUT TESTS

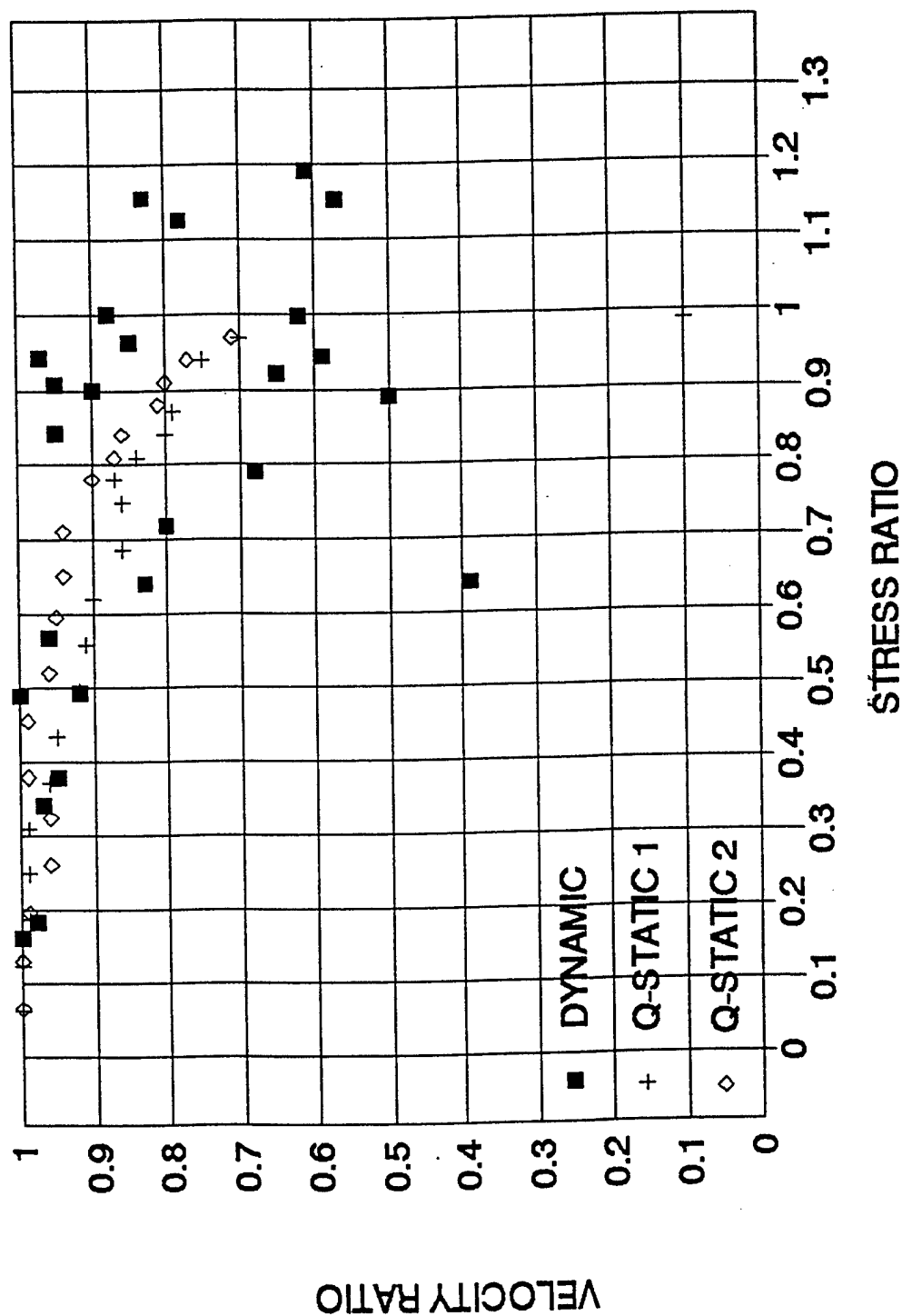


Figure 22a. Ultrasonic grout tests comparison of data obtained in dynamic tests with data obtained in quasistatic tests.

(VELOCITY RATIO) ² VS STRESS RATIO

ULTRASONIC GROUT TESTS

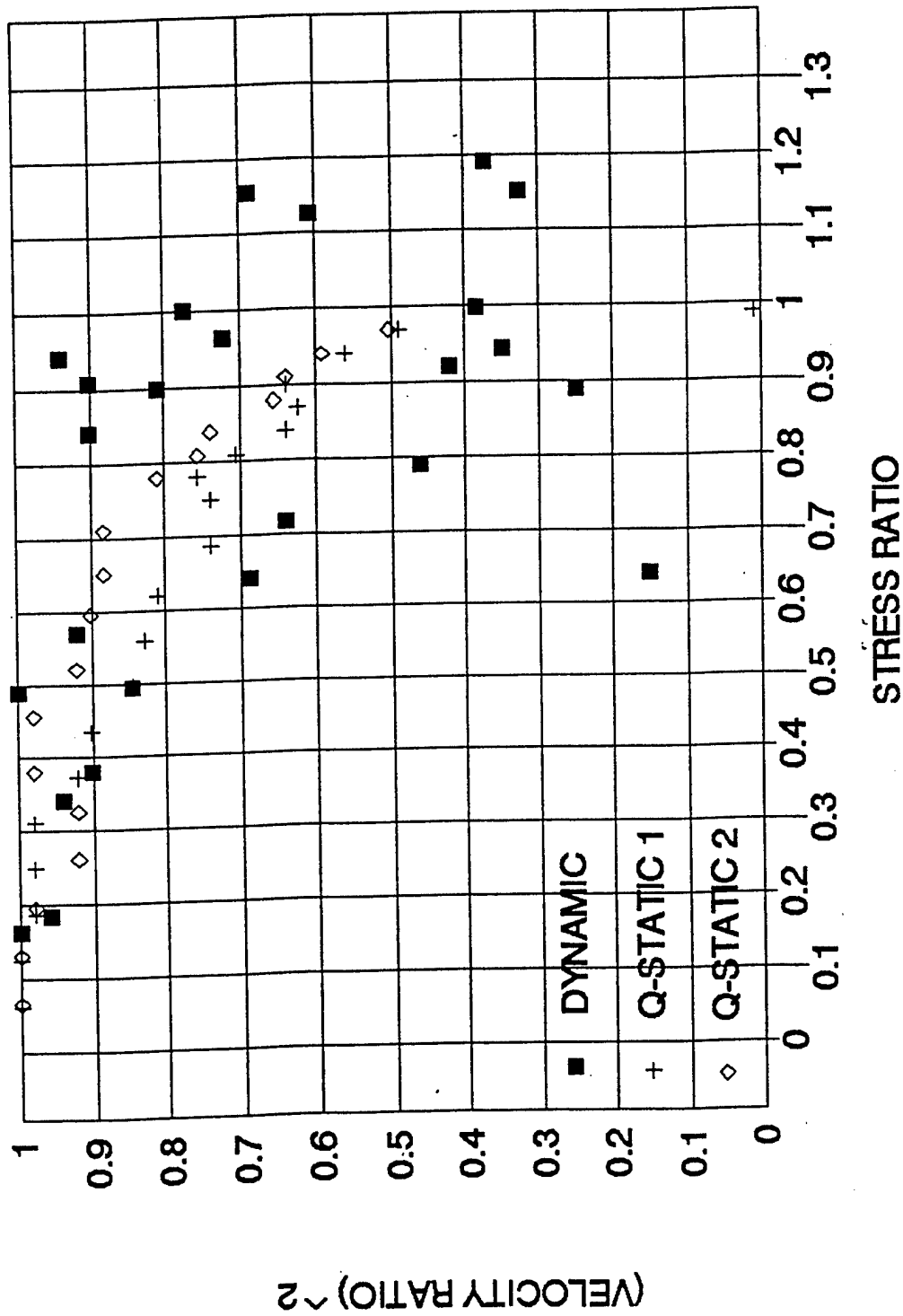


Figure 22b. Ultrasonic grout tests comparison of data obtained in dynamic tests with data obtained from quasistatic tests.

whereas the dynamic data was taken from some 25 specimens. Scatter of properties data from one concrete specimen to another is in many cases quite large.

2. ELASTIC/ VISCOPLASTIC MODEL

a. Introduction

The slow deformation in time of metals and geomaterials, mainly at high temperatures has been studied both from theoretical and experimental standpoint since the beginning of this century. The theory of viscoplasticity of metals, rooted in the works of Ludwik, and Prandtl (for a history of the main concepts see Nadai [1950], [1963], and Bell [1973]) has been extensively developed, mainly in the second half of the century. What concerns geomaterials, such as rocks and soils, their slow deformation and motion were observed since the beginning of mankind. However, a scientific approach and description of these phenomena are of relatively recent date. While, for metals, inelasticity can be explained in principle by means of the mechanics and physics of dislocation nucleation and propagation, for most rocks it is mainly the mechanisms of closure and/or opening of microcracks (and sometimes of pores) and their multiplication which explain the inelastic properties: compressibility and/or dilatancy, damage, creep, failure, etc. Dislocation mechanisms also have a role in individual crystal deformation. Irreversible volumetric deformation during creep is responsible for an increased complexity of the constitutive laws for geomaterials.

The first to report that sandstone is dilatant in uniaxial compression tests seems to be Bauschinger in 1879 (see Bell, [1973]). Afterwards, Bridgman [1949] has found that in uniaxial compression tests, soapstone, marble and diabase are dilatant at high applied stresses. He was the first to mention that dilatancy is produced by "rapid creep". Also, he suggested that irreversible compressibility is due to closing of pores, while dilatancy – to the opening of pores. Further

pioneering experimental work concerning compressibility and/or dilatancy of rocks is due to Brace *et al.* [1966] and Bieniawski [1967], among others. For early papers concerning compressibility and/or dilatancy of rocks, see for example Cristescu [1989], Cristescu and Hunsche [1998], while for soils see Schofield and Wroth [1968] and Wood [1990].

To formulate a general elasto/viscoplastic constitutive equation for a geomaterial the following ingredients are required:

- Elastic parameters at various stress states;
- Yield function and the compressibility/dilatancy boundary which can be determined from quasistatic and dynamic confined tests;
- Viscoplastic potential, since for most geomaterials it is expected that the yield function is not a potential for the irreversible deformation;
- Short-term failure surface.

However, a 3-D model that could capture the main features of the behavior for high pressures and high loading rates can be developed based on a series of quasistatic tests at several confining pressures (at least 4 different confining pressures) and dynamic unconfined and confined data at different strain rates and at least 2 different confining pressures. The basic steps in the development of this model are:

- determination of the elastic parameters;
- determination of the relaxation boundaries for axial and radial strain, based on which relaxation boundary for volumetric and deviatoric deformation, respectively can be constructed;
- determination of viscosity coefficients for volumetric and deviator deformation should be determined from data obtained in tests at several different loading rates.

This second approach was followed in developing a new a 3-D elastic/viscoplastic model for concrete. First, we present and analyze the available experimental data and give a rationale for selecting only the quasi-static results obtained at GERC as a basis for constructing the model. The structure of the proposed constitutive equation and a procedure for determining the material parameters based on a minimal set of data is given. Finally, the model predictions for quasi-static conditions and dynamic unconfined and confined conditions are tested against the data. The comparison is good, with a degree of accuracy within the natural scatter of the data.

b. Experimental basis

On concrete, unconfined compression tests (see Figure A-19) and confined compression tests at confining pressures of 1.8 MPa, 3.45 MPa, and 6.9 MPa (Figures A-26, A-22, and A-24, respectively) have been performed at UF/GERC. The loading path in the unconfined test (QSC-1, strain rate of $0.77 \cdot 10^{-6} / s$) consisted of monotonic loading up to 17.5 MPa, at which level the axial stress was held constant for a time interval of 9.5 minutes. Instantaneous creep was recorded even at this low stress level. At the end of the creep stage, partial unloading followed by fast reloading showed irreversible strain. Although, slight hysteresis was observed, the unloading could be considered as elastic, the value of the Young modulus E determined from the unloading slope being of 38 GPa. At 35 MPa another 9.5 minutes creep-reloading-unloading cycle have been performed, the value of E was found to be of 42.5 GPa. This test was repeated, this time the specimen was instrumented with axial strain gages and lateral strain gages. The axial stress vs. volumetric strain curve obtained in this latest test (see Figure 23) shows compressibility up to 50 MPa and strong volume expansion (dilatancy) up to failure. The value of the bulk modulus estimated from the tangent to the quasilinear middle portion of the curve is of 16.85 GPa. The average E obtained from both unconfined tests is of 40 GPa.

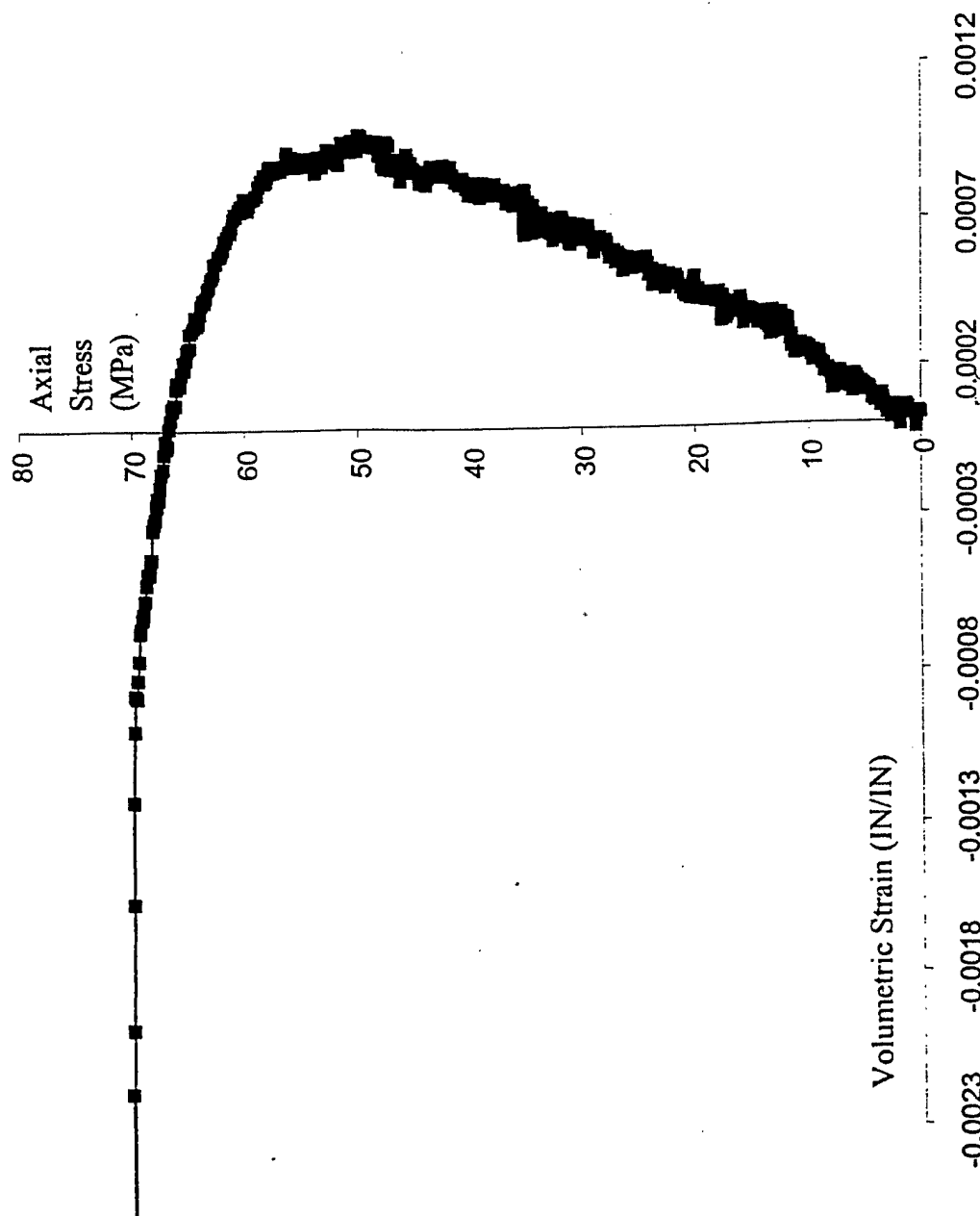


Figure 23: Axial Stress vs. Volumetric Strain curve obtained in the unconfined compression test QSC-2.

In the confined tests the loading was increased monotonically. In all the tests, the deviatoric stress vs. axial stress curve show an initial nonlinear portion (generally, attributed to closing of existing microcracks) followed by a quasilinear portion, and a final nonlinear portion with opposed concavity (see Figure 24); the deviatoric stress vs. volumetric stress curve show that with increasing deviatoric stress the material becomes strongly dilatant (see Figure 25). Dilatancy is defined globally as irreversible increase in volume. It is clearly seen that an increase of the confining pressure results in an increase of the dilatancy threshold. Although it is difficult to separate the elastic contribution to the strain from the irreversible one, an approximate estimate of E , and K can be obtained from the slope of the quasilinear part of the $(\sigma_1 - \sigma_3)$ vs. ϵ_v curve, and $(\sigma_1 - \sigma_3)$ vs. ϵ_1 , respectively. In Table 8 we present the estimates of the elastic moduli as obtained from all the tests. An average value of K of 17.29 GPa has been obtained from those confined tests, while the corresponding mean value for the Poisson ratio ν was found to be of 0.22.

TABLE 8
ELASTIC MODULI AS DETERMINED FROM THE QUASI-STATIC GERC TESTS.

Confining pressure (MPa)	E (GPa)	K (GPa)
0	40	16.85
1.8	31.66	13.83
3.45	26.56	11.5
6.9	36.04	25.62

As discussed in the previous section (III.2.a), in order to better characterize the influence of the confining pressure on the deformation and fracture of the material, confined triaxial quasi-static data at very high confining pressures are necessary. High-confining triaxial test have been

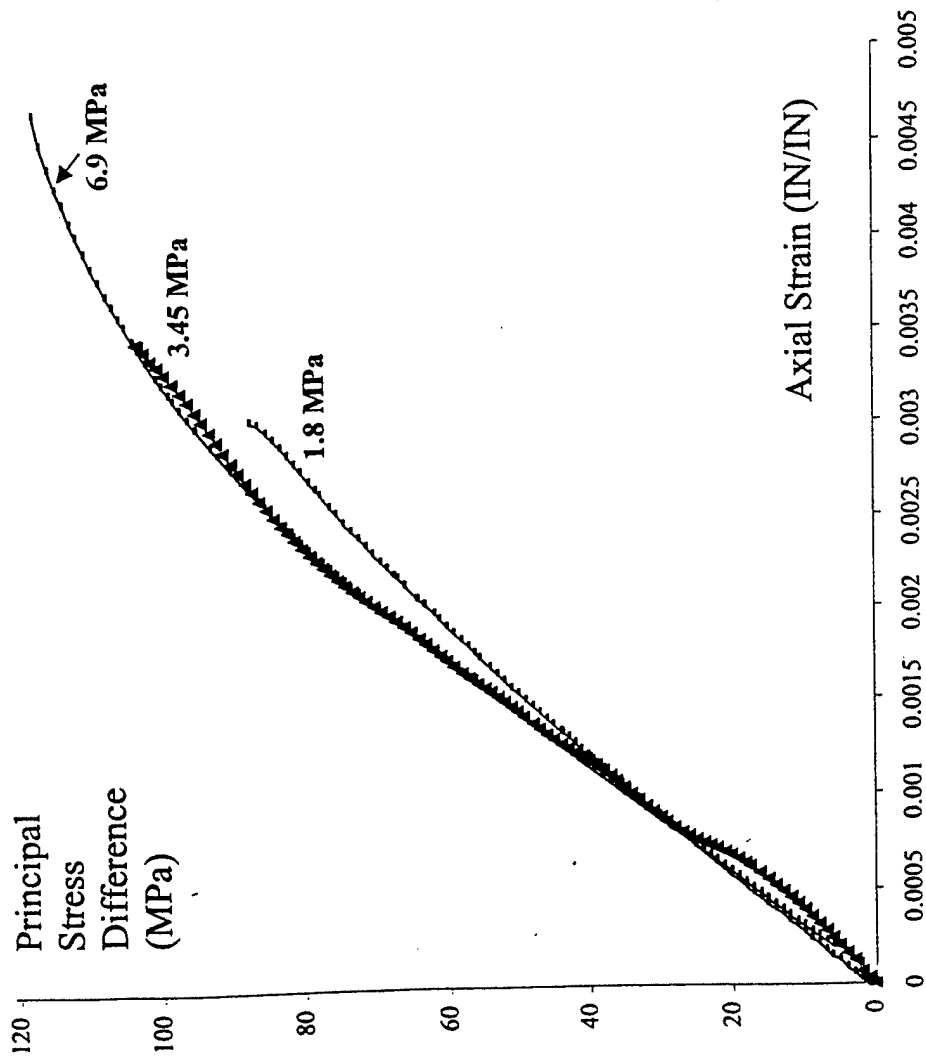


Figure 24: Comparison of the deviatoric stress vs. axial strain curves obtained in quasi-static confining compression tests QSSC12 (1.8 MPa confining), QSCC1 (3.45 MPa confining), and QSCC6 (6.9 MPa confining).

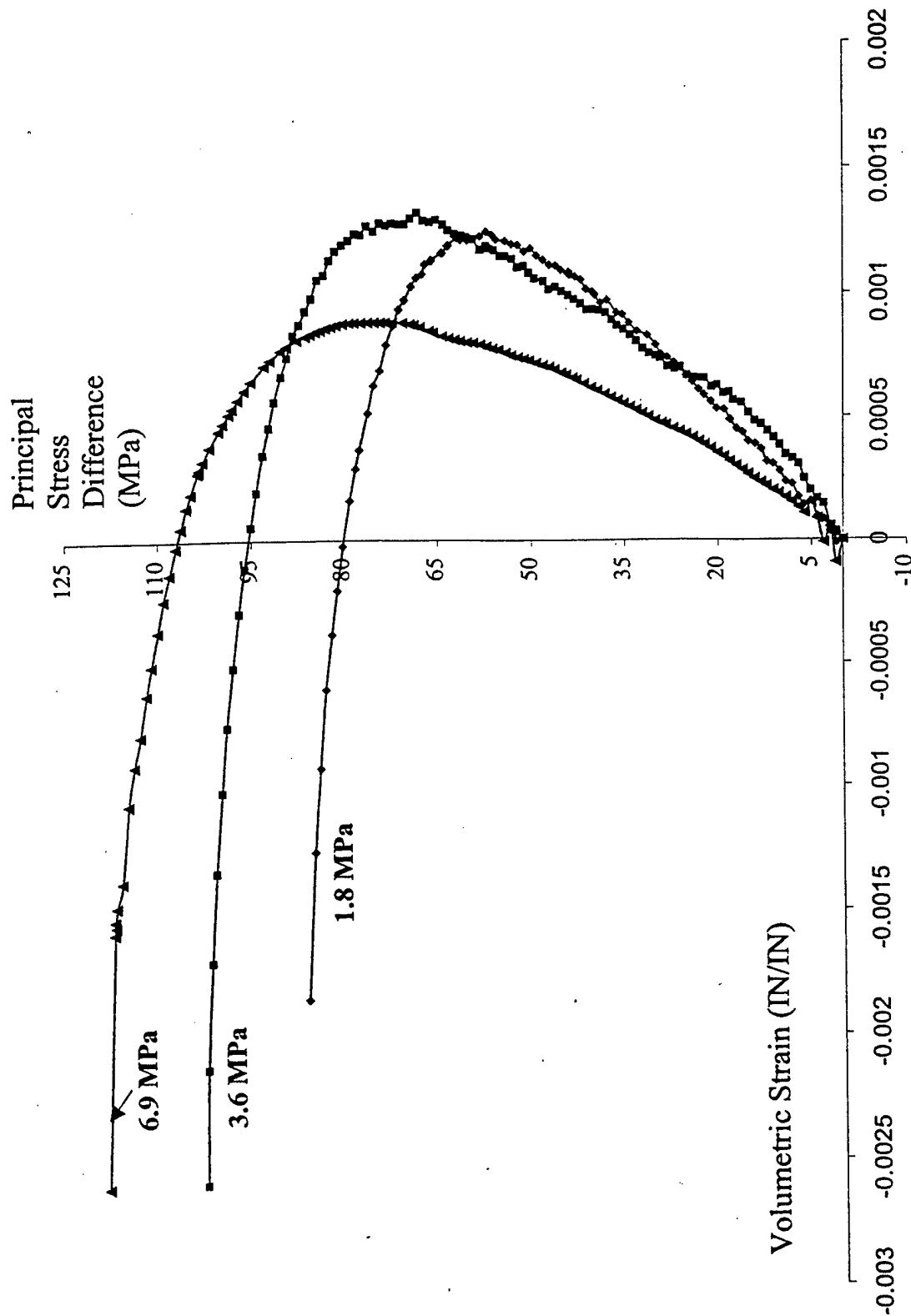


Figure 25: Deviatoric stress vs. volumetric strain curves obtained in the quasi-static confined tests QSSC12 (1.8 MPa), QSSC1(3.46 MPa), and QSSC6 (6.9 MPa) showing compressibility for low stress levels and pronounced dilatancy for high stress levels.

carried out at WES under 150 MPa, 300 MPa, and 450 MPa confining pressure, respectively. The results of the 150 MPa confined test are presented in Figure 26 to 29. In the hydrostatic phase of this test, 5 loading-creep-unloading -reloading cycles have been performed (Figure 26). The material exhibited volume decrease by creep when the load is held constant. From the unloading slopes the bulk modulus K has been evaluated. As expected, the bulk modulus is an increasing function of the applied pressure (see Table 9).

TABLE 9

**BULK MODULUS K AS DETERMINED FROM THE
HYDROSTATIC PART OF QUASI-STATIC WES TEST 150 MPa -4TH TRY**

Cycle # and Pressure level (MPa)	K (GPa)
Cycle # 1: 9.3	15.1
Cycle # 2: 36.75	16.08
Cycle # 3: 72.17	20.98
Cycle #4: 110	22.81
Cycle #5: 148	24.58

In the deviatoric part of the test, 4 loading-creep-unloading-reloading cycles have been performed. Figures 27-28 show the axial and radial strains as functions of the applied deviatoric stress ($\sigma_1 - \sigma_3$). The material exhibits irreversible time-dependent behavior. Under constant load, the axial deformation is increasing. For the first 2 cycles, the absolute value of the radial strain decreases under constant load, whereas in the last 3 cycles, the creep changes direction *i.e.* the radial deformation increases under constant load (see inset Figure 28). This change in creep direction can be attributed to the mechanisms of closure/opening of microcracks. More precisely, it seems that the first 2 cycles were performed at stress levels at which the material is compacting (*i.e.* the stress states are below the compressibility/dilatancy boundary) while the other cycles

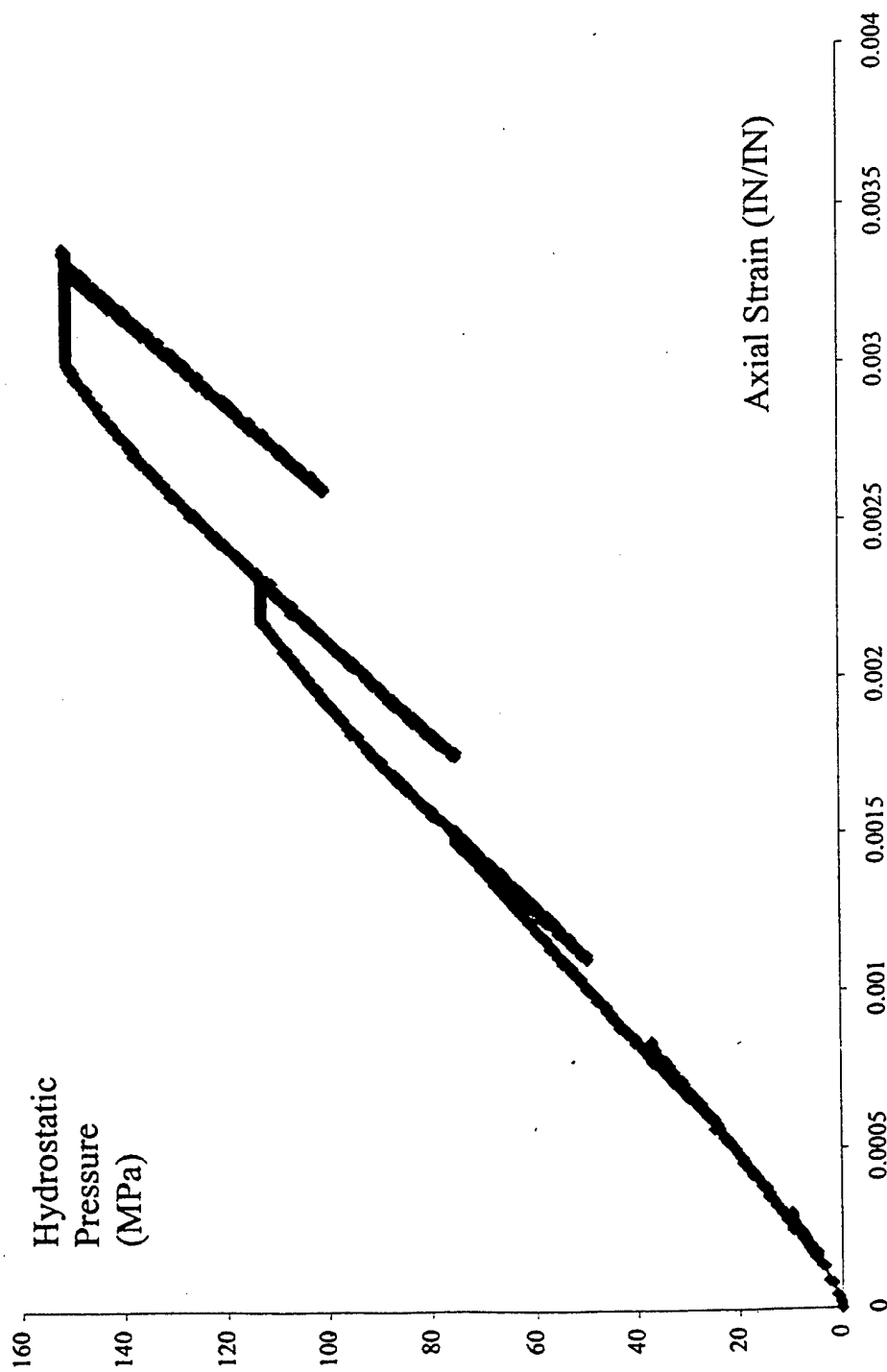


Figure 26: Hydrostatic Pressure vs. Axial Strain curve obtained in WES test 150 MPa -4th try.

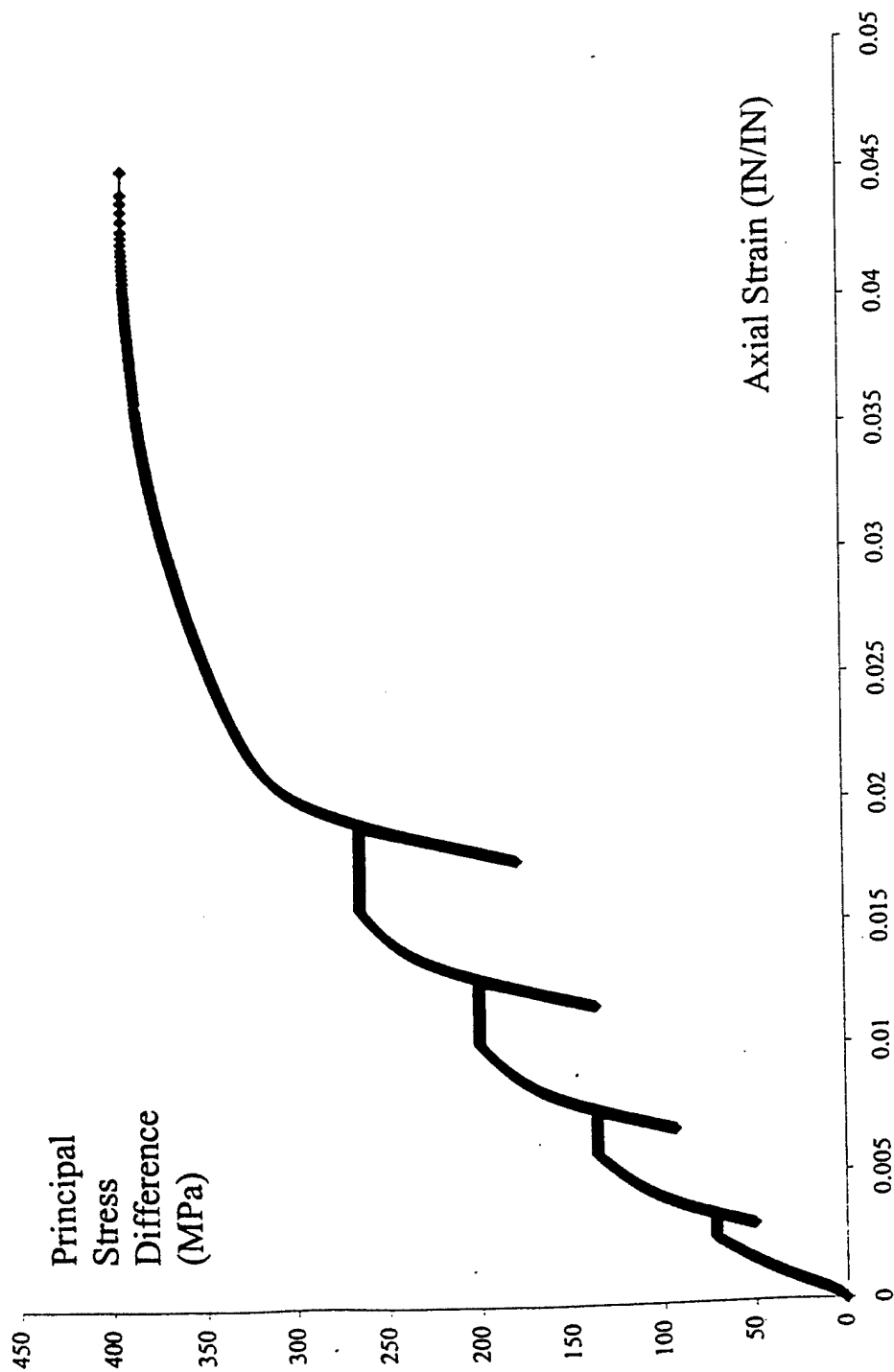


Figure 27: Deviatoric stress vs. axial strain curve obtained in the WES quasi-static test (150 MPa, 4th try), confining pressure of 150 MPa

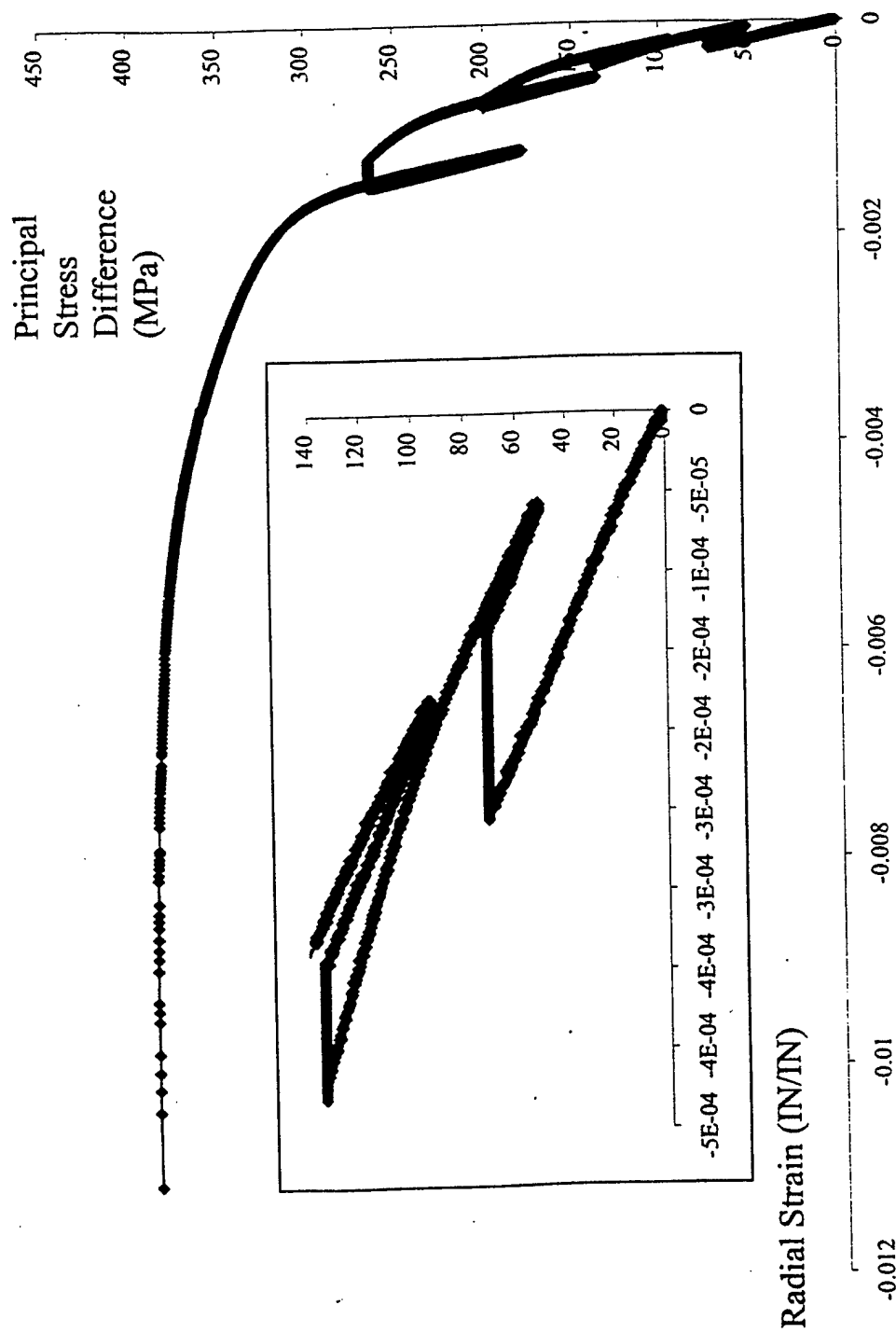


Figure 28: Deviatoric stress vs. Radial Strain curve obtained in WES test at 150 MPa confining pressure (150 MPa-4th try);
 Inset: first 2 cycles show creep compressibility whereas in the next cycles creep dilatancy is observed.

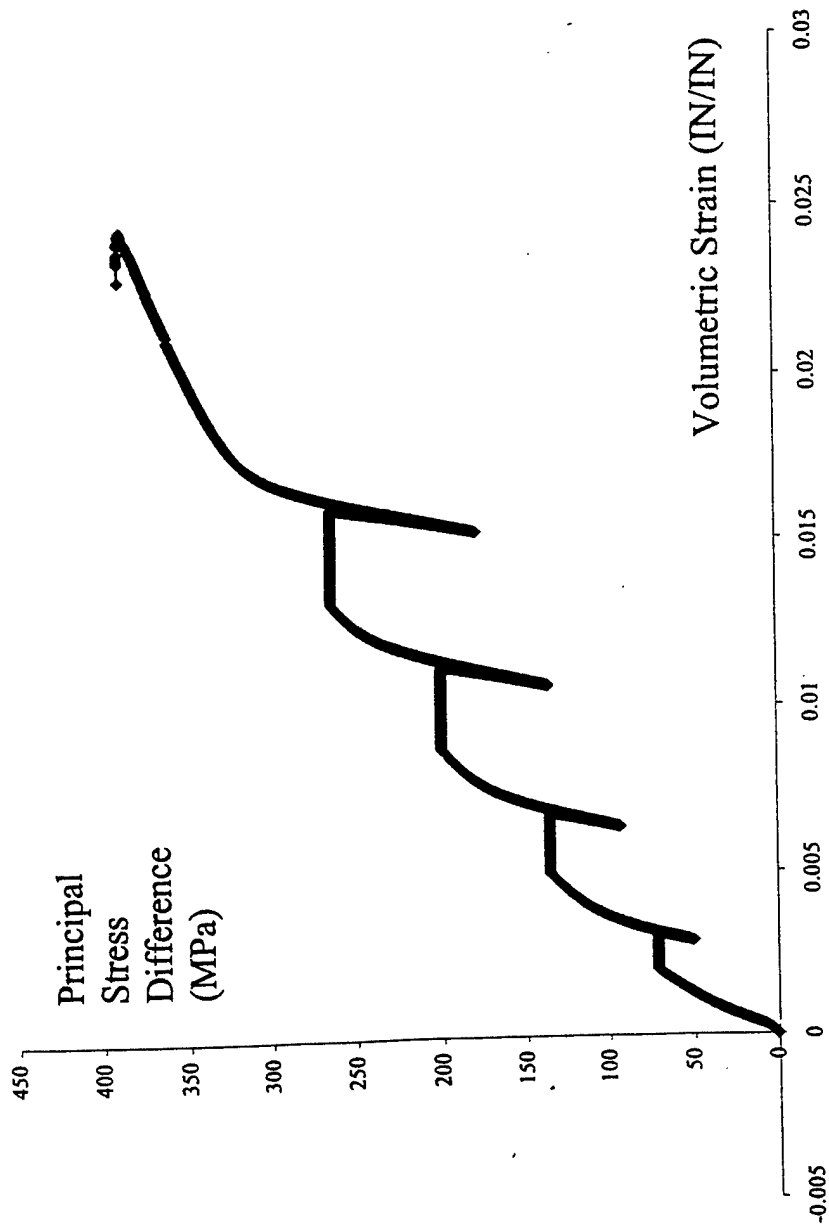


Figure 29: Deviatoric stress vs. Volumetric Strain curve obtained in WES test at 150 MPa confining pressure (150 MPa-4th try) showing no dilatancy.

were at stress levels belonging to the dilatant domain (beyond the compressibility/dilatancy boundary, where the material dilates). However, the deviatoric stress vs. volumetric strain curve (Figure 29) shows that the onset of dilatancy is very close to the fracture point. The volumetric strain ε_v was computed based on the measured values of the axial strain ε_1 and of the radial strain ε_3 using the formula: $\varepsilon_v = \varepsilon_1 + 2\varepsilon_2$.

The values of the elastic moduli determined from the deviatoric part of the test are given in Table 10. The average values of the elastic moduli obtained from the last 3 cycles are: $E = 61.52$ GPa, $\nu = 0.22$ and $K = 37.04$ GPa.

The same trends have been observed in the tests at 300 MPa and 450 MPa confining pressure, respectively. The results of the 300 MPa confined test are presented in Figure 30 to 33. In the hydrostatic phase of this test, 5 loading-creep-unloading-reloading cycles have been performed (Figure 30). The bulk modulus values determined in the hydrostatic part of the test are given in Table 11, while the estimates of the elastic moduli determined from the deviatoric part of the test are given in Table 12. The average values of the elastic moduli obtained from the last 3 cycles are: $E = 61.30$ GPa, $\nu = 0.27$ and $K = 49$ GPa.

TABLE 10
ELASTIC MODULI DETERMINED FROM THE DEVIATORIC
PHASE OF THE QUASI-STATIC WES TEST 150 MPa -4TH TRY

Deviatoric stress level (MPa)	E (GPa)	ν	$K=E/3(1-2\nu)$ (GPa)
Cycle1: 70	33.72	0.02	11.74
Cycle 2: 135	71.07	0.22	42.9
Cycle 3: 200	56.9	0.225	34.5
Cycle 4: 240	56.6	0.2	33.74

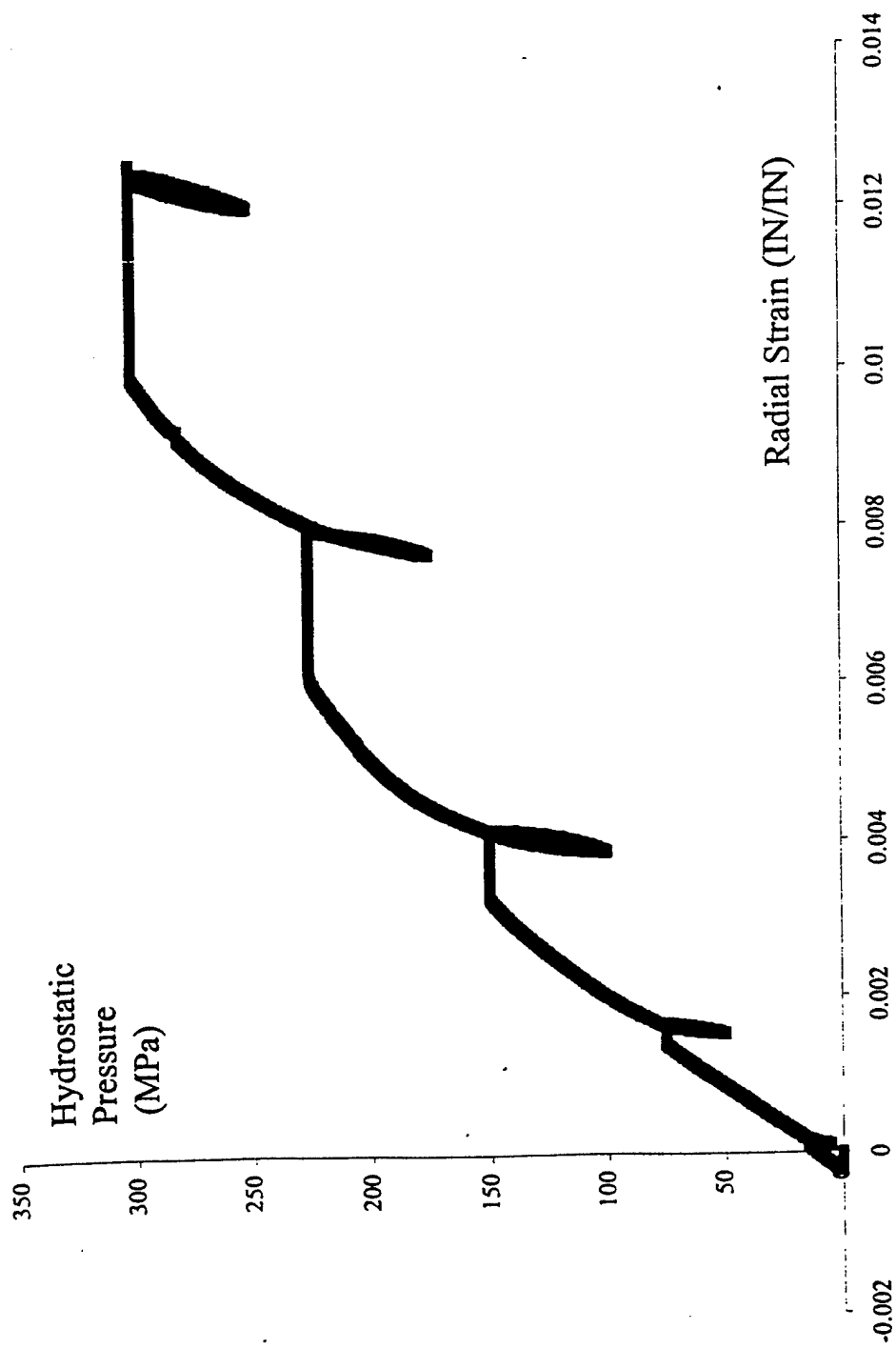


Figure 30: Hydrostatic Pressure vs. Radial Strain curve obtained in WES test 300 MPa-2nd try.

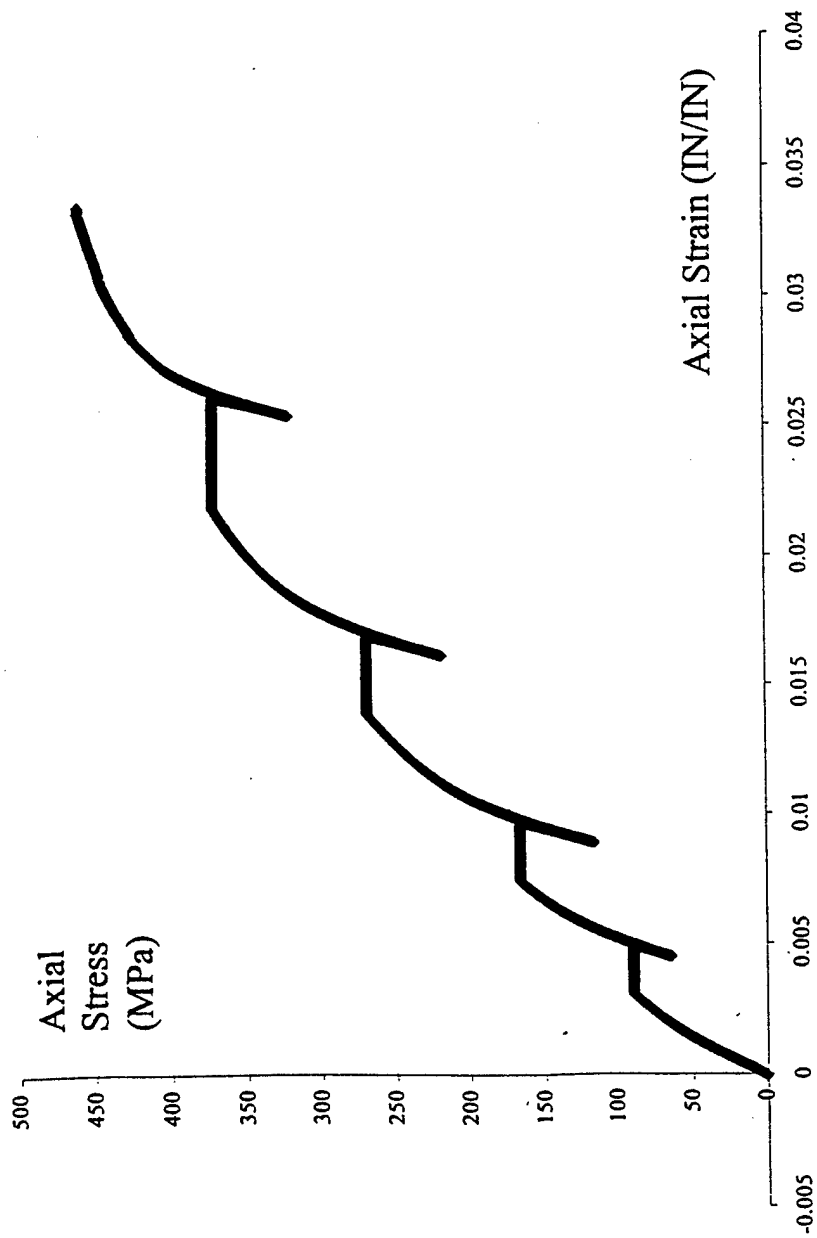


Figure 31: Deviatoric stress vs. Axial Strain curve obtained in the deviatoric part of WES test at 300 MPa confining pressure (300 MPa-2nd try).

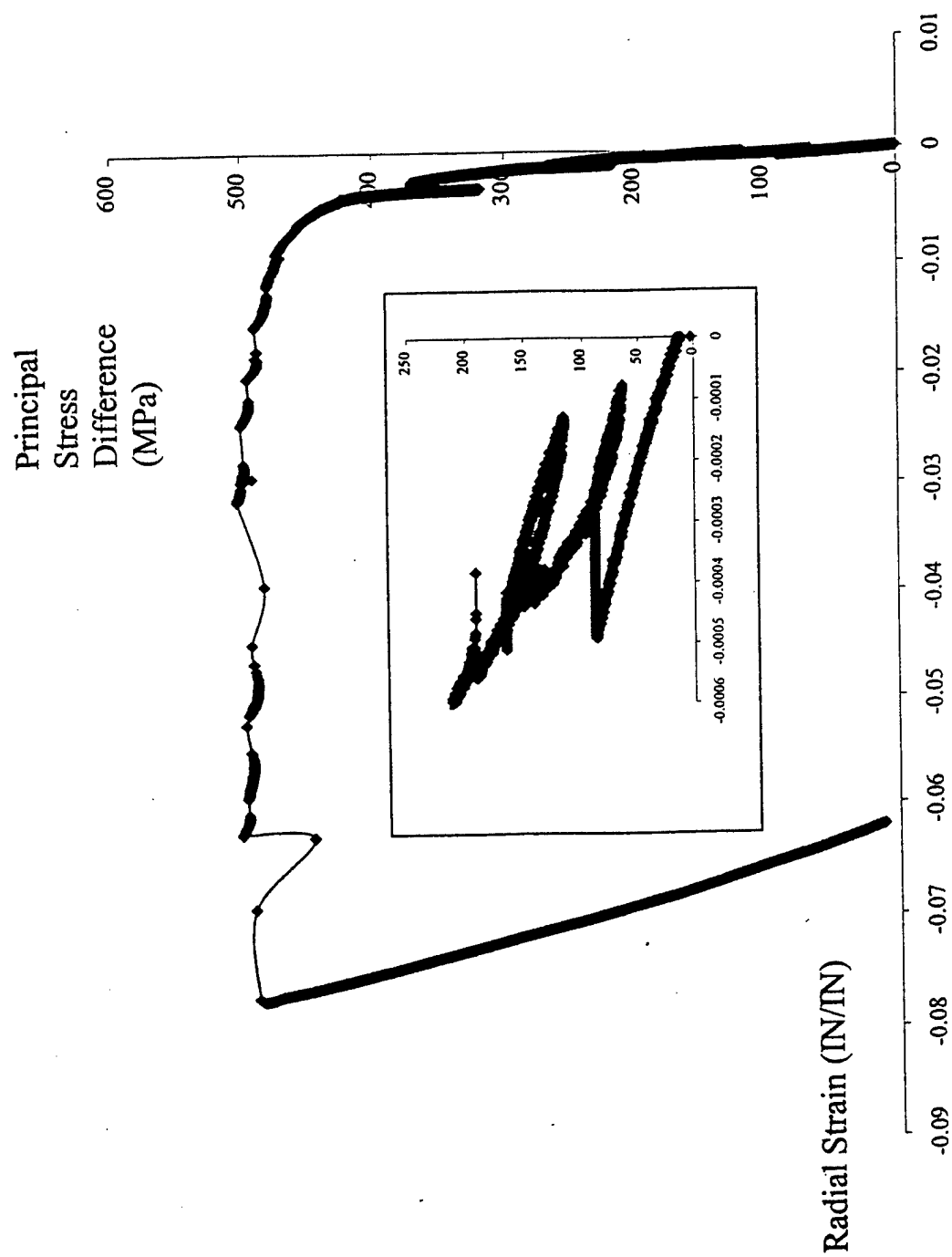


Figure 32: Deviatoric stress vs. Radial Strain curve obtained in the deviatoric part of WES test at 300 MPa confining pressure (300 MPa-2nd try); Inset: first 3 cycles, showing creep compressibility.

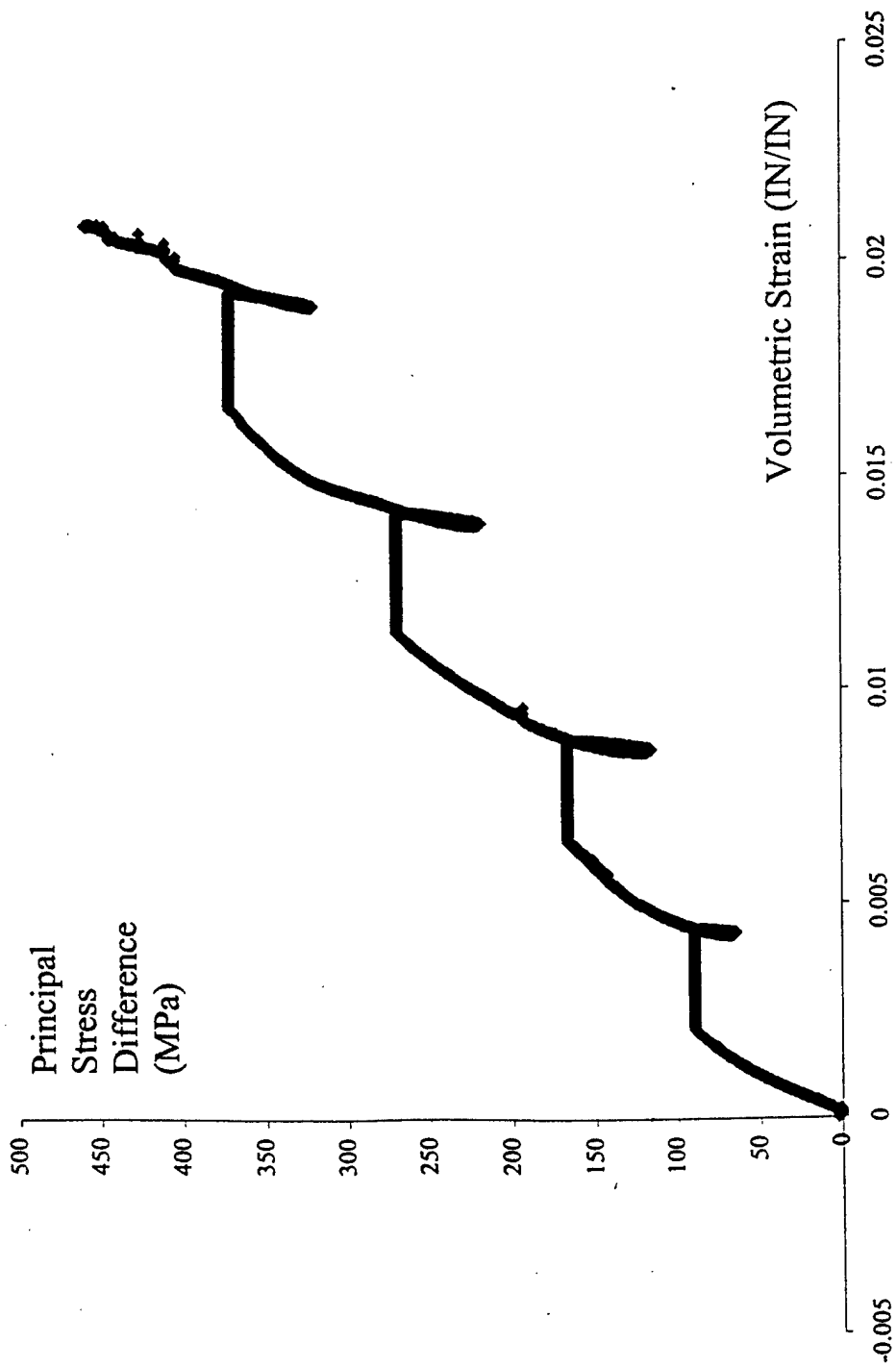


Figure 33: Deviatoric stress vs. Volumetric Strain curve obtained in WES test at 300 MPa confining pressure (300 MPa-2nd try) showing no dilatancy.

TABLE 11
BULK MODULUS K AS DETERMINED FROM THE HYDROSTATIC
PART OF QUASI-STATIC WES TEST 300 MPA -2ND TRY.

Cycle # and Pressure level (MPa)	K (GPa)
Cycle # 1: 75	21.6
Cycle # 2: 150	59.77
Cycle # 3: 226	49.4
Cycle #4: 300	39.78

The results of the 450 MPa confined test are presented in Figures 34 to 37. In the hydrostatic phase of this test, 5 loading-creep-unloading-reloading cycles have been performed (Figure 34). The bulk modulus values determined in the hydrostatic part of the test are given in Table 13, while the estimates of the elastic moduli determined from the deviatoric part of the test are given in Table 14. The average values of the elastic moduli obtained from the last 3 cycles are: $E = 64.81$ GPa, $\nu = 0.23$ and $K = 40.87$ GPa. The average values of the elastic moduli as determined from the deviatoric phase of each WES test are given in Table 15.

TABLE 12
ELASTIC MODULI DETERMINED FROM THE DEVIATORIC
PHASE OF THE QUASI-STATIC WES TEST 300 MPA -2ND TRY

Deviatoric stress level (MPa)	E (GPa)	ν	$K=E/3(1-2\nu)$ (GPa)
Cycle 2: 135	57.66	0.35	63.65
Cycle 3: 200	62.37	0.275	46.47
Cycle 4: 240	63.52	0.2	36.25

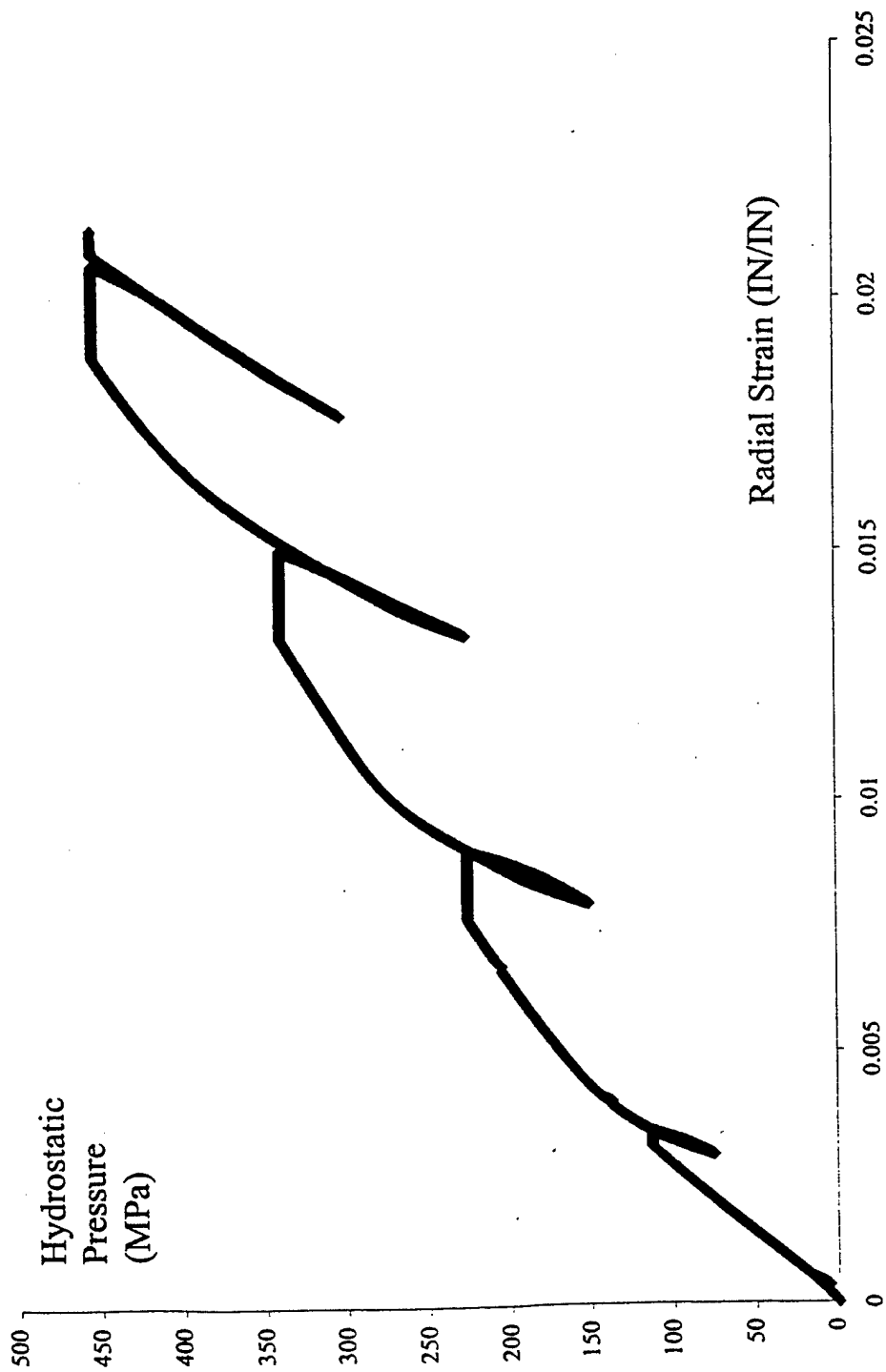


Figure 34: Hydrostatic Pressure vs. Radial Strain curve obtained in WES test 450 MPa-2nd try.

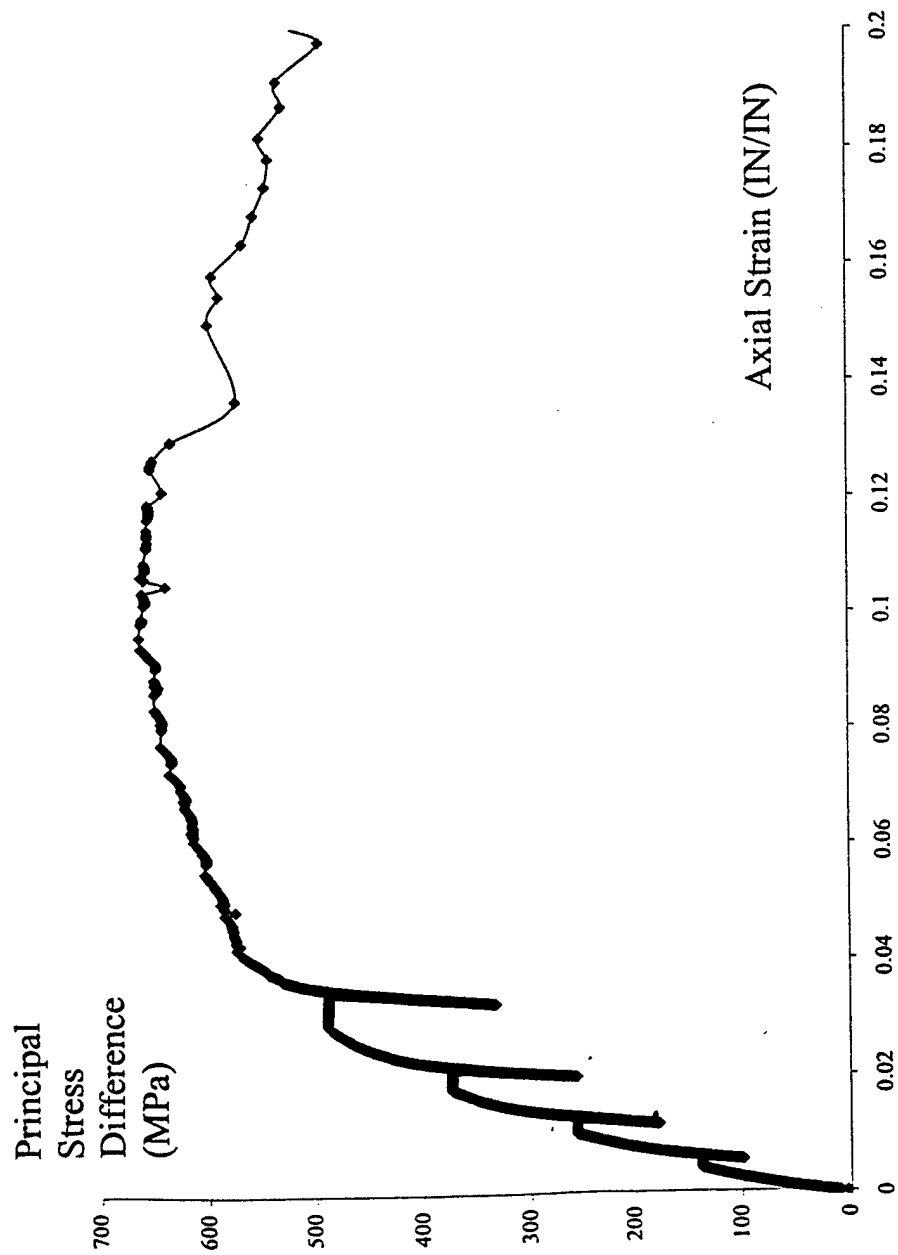


Figure 35: Deviatoric stress vs. Axial Strain curve obtained in the deviatoric part of WES test at 450 MPa confining pressure (450 MPa-2nd try).

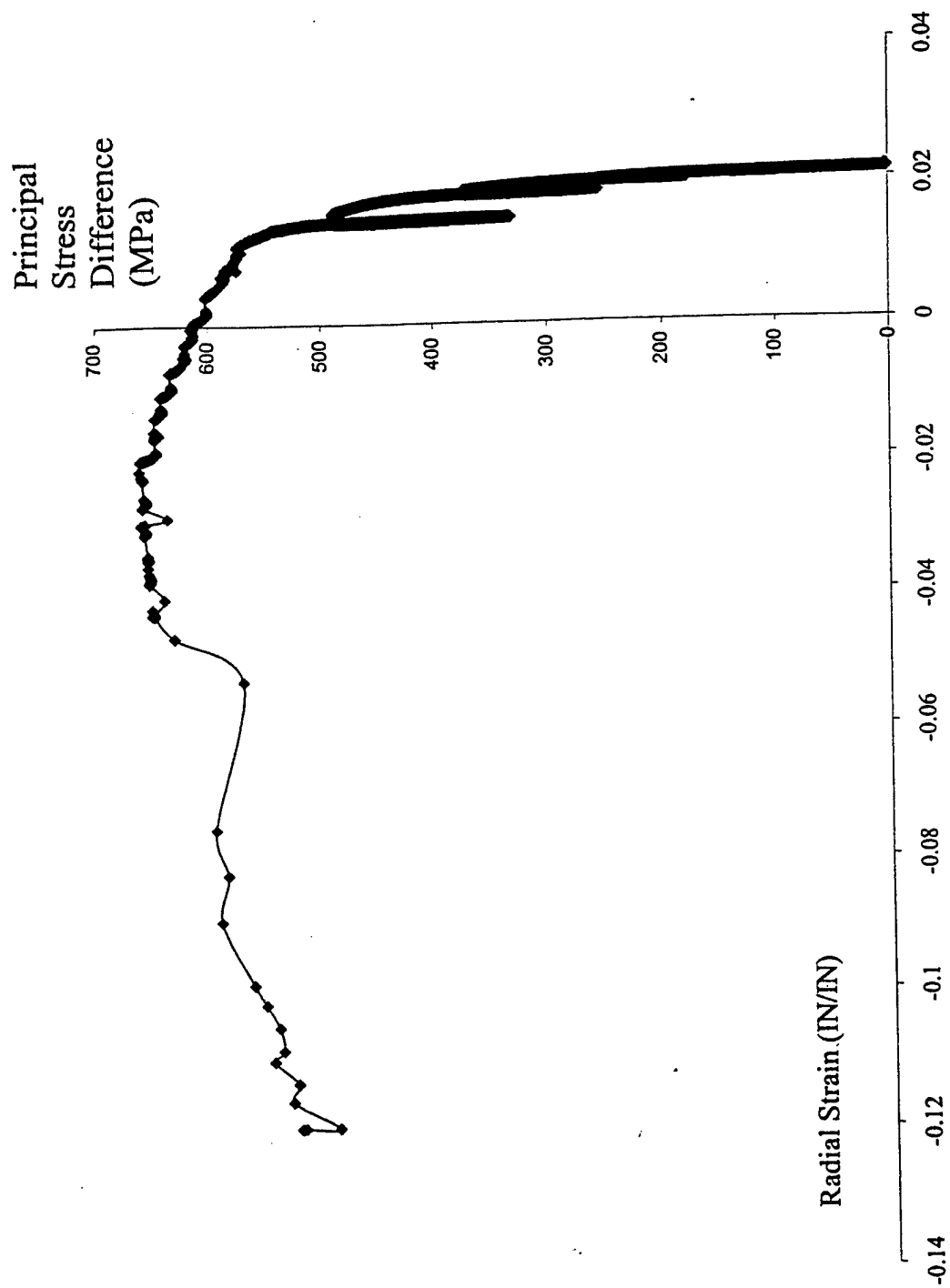


Figure 36: Deviatoric stress vs. Radial Strain curve obtained in the deviatoric part of WES test at 450 MPa confining pressure (450 MPa-2nd try).

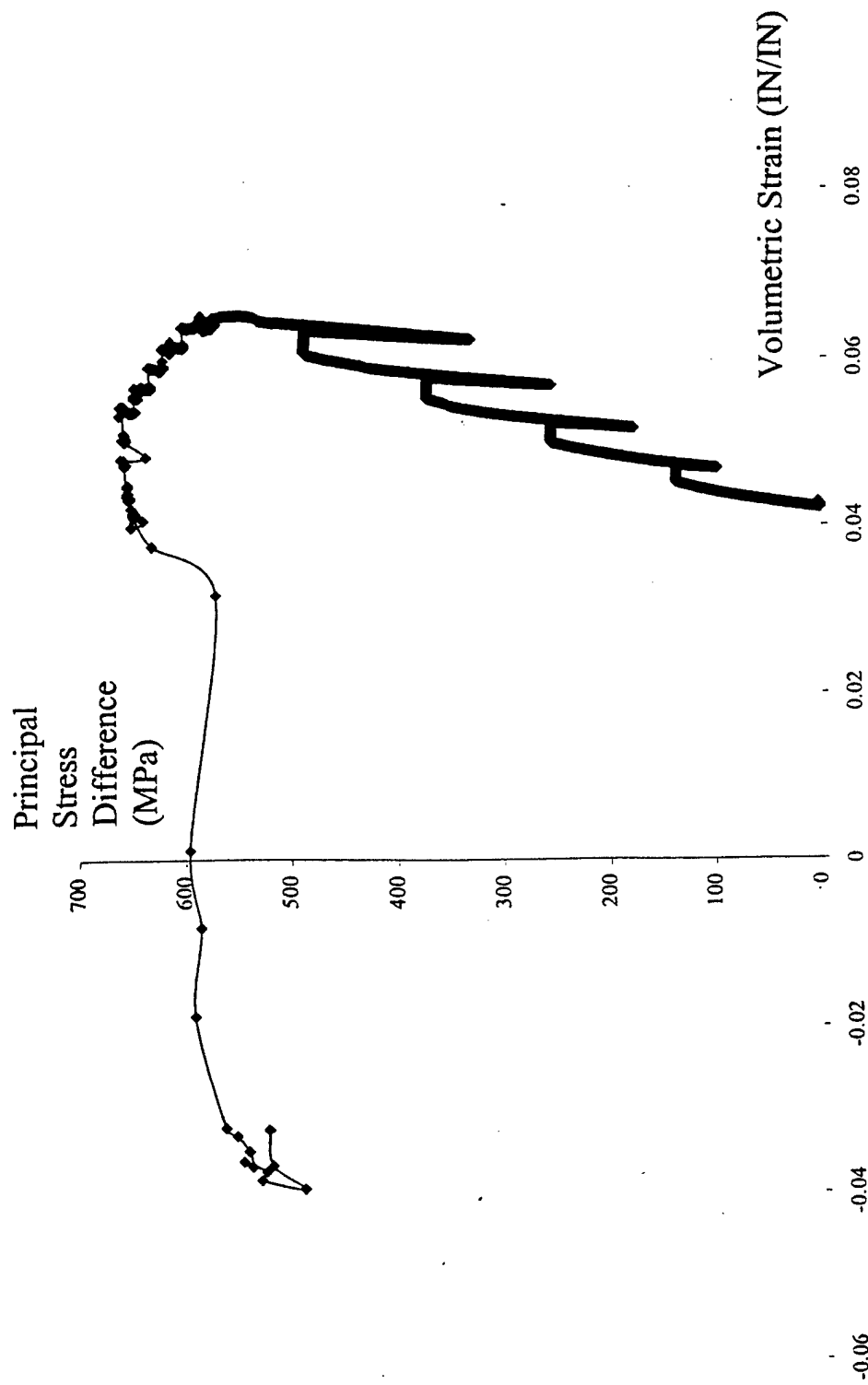


Figure 37: Deviatoric stress vs. Volumetric Strain curve obtained in the deviatoric part of WES test at 450 MPa confining pressure (450 MPa-2nd try).

TABLE 13

**BULK MODULUS K AS DETERMINED FROM THE HYDROSTATIC
PART OF QUASI-STATIC WES TEST 450 MPA -2ND TRY.**

Cycle # and Pressure level (MPa)	K (GPa)
Cycle # 2: 112	30.17
Cycle # 3: 225	23.8
Cycle # 4: 337	21.87
Cycle #5: 450	19.36

TABLE 14

**ELASTIC MODULI DETERMINED FROM THE DEVIATORIC
PHASE OF THE QUASI-STATIC WES TEST 300 MPA -2ND TRY.**

Deviatoric stress level (MPa)	E (GPa)	ν	$K=E/3(1-2\nu)$ (GPa)
137	60.33	0.026	21.24
256	62.91	0.213	36.63
373	65	0.217	38.28
240	47.71	0.26	47.71

TABLE 15

**AVERAGE VALUES OF THE ELASTIC MODULI AS DETERMINED
FROM THE DEVIATORIC PHASE OF EACH WES TEST .**

Confining pressure (MPa)	ν (average)	K (average) (GPa)
150	0.22	37.04
300	0.27	49
450	0.23	40.87

Due to the observed scatter of the elastic parameters, in the constitutive equation we have assumed linear elastic response. For the Young modulus we have taken the average dynamic value $E = 60$ GPa and a Poisson's coefficient $\nu = 0.22$.

The high confining pressure data do not correlate with the low confining data obtained at GERC. The volumetric profiles for high confining pressures show that the material is compressible, while for low confining pressures the material exhibits both compressible and dilatant behavior. Therefore, it was decided to use only the low confining data for the calibration of the elastic/viscoplastic model.

c. Structure of the constitutive equation

The experimental data show that the material exhibits strong strain-rate sensitivity. A natural framework in which the main features of the observed behavior can be modeled is offered by the viscoplasticity theory. In this approach it is considered that the instantaneous response is elastic, the total strain increment observed in the material being the sum of the elastic and irreversible (rate-dependent) components.

The general form of the constitutive equation is

$$\dot{\epsilon} = \dot{\epsilon}^E + \dot{\epsilon}^I \quad (6)$$

$$\dot{\epsilon}^E = \frac{\dot{\sigma}}{2G} + \left(\frac{1}{3K} - \frac{1}{2G} \right) \dot{\sigma} I \quad (7)$$

$$\dot{\epsilon}^I = A(\sigma, \bar{\sigma}, \epsilon, \bar{\epsilon}) \frac{\sigma'}{\bar{\sigma}} + B(\sigma, \bar{\sigma}, \epsilon, \bar{\epsilon}) I \quad (8)$$

where, $\dot{\epsilon}^E$ denotes the elastic strain rate, $\dot{\epsilon}^I$ the irreversible (viscoplastic), σ is the Cauchy stress tensor, σ' the stress deviator, and I the second order identity tensor, $\sigma = \frac{tr \sigma}{3}$ and

$\bar{\sigma} = \sqrt{\frac{3}{2} \text{tr}(\sigma')^2}$ are the first and second stress invariants while $\varepsilon = \frac{\text{tr} \varepsilon}{3}$ and $\bar{\varepsilon} = \sqrt{\frac{2}{3} \text{tr}(\varepsilon')^2}$ are the first and second strain invariants, and tr stands for the trace operator.

Elastic behavior is expressed in terms of a non-linear Hooke's law (7) and requires expressions for the shear modulus G and bulk modulus K (or similar moduli). The onset of irreversible behavior and the law of evolution of the irreversible strain should be described by the constitutive functions $A(\sigma, \bar{\sigma}, \varepsilon, \bar{\varepsilon})$ and $B(\sigma, \bar{\sigma}, \varepsilon, \bar{\varepsilon})$, respectively.

Further, creep phenomena observed when the load is held constant or relaxation, which occurs when strain is held constant, should also be accounted for. To this end, suitable stabilization surfaces should be specified. The stabilization surface is defined as the geometrical locus of points in the stress space at which the deformation by creep has stopped. For the determination of the stabilization surface and the specific mathematical expressions of the constitutive functions we follow the approach proposed by Cristescu (1989).

From triaxial compression tests with stepwise increase of loading followed by creep, the stabilization curves in the plane $\sigma_1 - \varepsilon_1$ (axial stress- axial strain) and $\sigma_1 - \varepsilon_3$ (axial stress-radial strain) can be determined. Denote, $\varepsilon_1 = f_1(\sigma_1, \sigma_3)$ and $\varepsilon_3 = f_3(\sigma_1, \sigma_3)$, the stabilization curves for the axial strain, and radial strain respectively (σ_1 stands for the axial stress, while σ_3 stands for the lateral confining pressure). Thus, the material response under axisymmetric triaxial conditions can be described as

$$\dot{\varepsilon}_1 = \left(\frac{1}{3G} + \frac{1}{9K} \right) \dot{\sigma}_1 + \left(-\frac{1}{3G} + \frac{2}{9K} \right) \dot{\sigma}_3 + h_1 \langle f_1(\sigma_1, \sigma_3) - \varepsilon_1 \rangle, \quad (9)$$

$$\dot{\varepsilon}_3 = \left(-\frac{1}{6G} + \frac{1}{9K} \right) \dot{\sigma}_1 + \left(\frac{1}{6G} + \frac{2}{9K} \right) \dot{\sigma}_3 + h_3 \langle f_3(\sigma_1, \sigma_3) - \varepsilon_3 \rangle, \quad (10)$$

where, $\dot{\varepsilon}_1$ and $\dot{\varepsilon}_3$ are the axial strain rate and transversal strain rate, respectively; $\langle \rangle$ is the Macauley bracket which defines the positive part of any expression,

i.e. $\langle A \rangle = \frac{1}{2}(A + |A|)$ while h_1 and h_3 are viscosity parameters.

Next, to identify $A(\sigma, \bar{\sigma}, \varepsilon, \bar{\varepsilon})$ and $B(\sigma, \bar{\sigma}, \varepsilon, \bar{\varepsilon})$, respectively we express (9) and (10) in terms of stress and strain invariants. Indeed, note that for axisymmetric conditions the stress are expressed as:

$$\sigma = \frac{\sigma_1 + 2\sigma_3}{3}, \quad \bar{\sigma} = \sigma_1 - \sigma_3, \quad \bar{\varepsilon} = \frac{2}{3}(\varepsilon_1 - \varepsilon_3) \quad \text{and} \quad \varepsilon = \frac{1}{3}(\varepsilon_1 + 2\varepsilon_3). \quad (11)$$

Substituting (11) in (9) and (10) we obtain:

$$\dot{\varepsilon}_1 = \frac{\dot{\sigma}_1}{2G} + \left\{ h_1 \left\langle f_1 \left(\sigma + \frac{2\bar{\sigma}}{3}, \sigma - \frac{\bar{\sigma}}{3} \right) - \varepsilon - \bar{\varepsilon} \right\rangle \right\} \frac{\sigma'_1}{\bar{\sigma}}, \quad (9')$$

$$\dot{\varepsilon}_3 = \frac{\dot{\sigma}_1}{2G} + \left\{ h_3 \left\langle f_2 \left(\sigma + \frac{2\bar{\sigma}}{3}, \sigma - \frac{\bar{\sigma}}{3} \right) - \varepsilon + \frac{\bar{\varepsilon}}{2} \right\rangle \right\} \frac{\sigma'_1}{\bar{\sigma}} \quad (10')$$

Further, we form the combinations $\dot{\varepsilon}_1 - \dot{\varepsilon}_3$ and $\dot{\varepsilon}_1 + 2\dot{\varepsilon}_3$ and use the expression (9)' and (10)' to get

$$A(\sigma, \bar{\sigma}, \varepsilon, \bar{\varepsilon}) = \left\{ h_1 \left\langle f_1 \left(\sigma + \frac{2\bar{\sigma}}{3}, \sigma - \frac{\bar{\sigma}}{3} \right) - \varepsilon - \bar{\varepsilon} \right\rangle - h_3 \left\langle f_3 \left(\sigma + \frac{2\bar{\sigma}}{3}, \sigma - \frac{\bar{\sigma}}{3} \right) - \varepsilon + \frac{\bar{\varepsilon}}{2} \right\rangle \right\} \quad (11)$$

$$B(\sigma, \bar{\sigma}, \varepsilon, \bar{\varepsilon}) = \frac{1}{3} \left\{ h_1 \left\langle f_1 \left(\sigma + \frac{2\bar{\sigma}}{3}, \sigma - \frac{\bar{\sigma}}{3} \right) - \varepsilon - \bar{\varepsilon} \right\rangle + 2h_3 \left\langle f_3 \left(\sigma + \frac{2\bar{\sigma}}{3}, \sigma - \frac{\bar{\sigma}}{3} \right) - \varepsilon + \frac{\bar{\varepsilon}}{2} \right\rangle \right\} \quad (12)$$

Although, the specific expressions of the stabilization curves $f_1(\sigma_1, \sigma_3)$ and $f_3(\sigma_1, \sigma_3)$ are most accurately determined from creep tests, data obtained in quasistatic compression at strain rate of

the order of $10^{-6}/s$ can provide a good approximation of these functions. For concrete, we approximate the stabilization boundaries by the following functions :

$$f_1(\sigma_1, \sigma_3) = a_1 \cdot (\sigma_1 - \sigma_3) + G(m, n, p, \sigma_3) \cdot (\sigma_1 - \sigma_3)^4, \quad (13)$$

$$f_3(\sigma_1, \sigma_3) = b_1 \cdot (\sigma_1 - \sigma_3) + G(r, s, t, \sigma_3) \cdot (\sigma_1 - \sigma_3)^8 \quad (14)$$

$$\text{and } G(\alpha, \beta, \gamma, \sigma_3) = \alpha + (\beta - \alpha) \cdot \exp(-\sigma_3 / \gamma). \quad (15)$$

where $a_1, b_1, m, n, p, r, s, t$ are material parameters. To determine those parameters and describe correctly the influence of the confining pressure on the behavior, data obtained in tests under at least six different confining pressures should be used. As pointed out in the discussion of the available experimental results, the data at low confining pressures do not correlate with the data at very high confining pressures (WES tests data). Thus, for the fitting of the G function it was decided to use the GERC data and guess values of the axial and radial strain for confining pressures of 300 MPa, and 450 MPa respectively (at $\sigma_3 = 300$ MPa and $\sigma_1 = 380$ MPa we took $\varepsilon_1 = 0.00172$, $\varepsilon_3 = -3.8 \cdot 10^{-4}$; at $\sigma_3 = 450$ MPa and the same deviator, we took $\varepsilon_1 = 0.0017$, $\varepsilon_3 = -3.6 \cdot 10^{-4}$). The obtained values are: $a_1 = 2.8 \cdot 10^{-5}$, $m = 1.017 \cdot 10^{-12}$, $n = 3.3 \cdot 10^{-11}$, $p = 109.57$, $b_1 = -3.4 \cdot 10^{-6}$, $r = -5.1 \cdot 10^{-20}$, $s = -0.82 \cdot 10^{-18}$ and $t = 74.6$. An average value of 60 GPa was considered for the dynamic Young modulus $E = 60$ GPa and a Poisson's coefficient $\nu = 0.22$. The viscosity coefficient h_1 was determined using data obtained in unconfined dynamic tests DCCU3 and DCCU5; in DCCU3 test, the strain rate was $\dot{\varepsilon}^{(1)} = 52/s$ and the loading rate was $\dot{\sigma}_1^{(1)} = 1 \cdot 10^6$ MPa/s while in DCCU5 test the strain rate was of $\dot{\varepsilon}^{(2)} = 107/s$ and the loading rates of $\dot{\sigma}_1^{(2)} = 2.77 \cdot 10^6$ MPa/s. Indeed, if

$\sigma_1^{(1)}$ and $\sigma_1^{(2)}$ are the stress levels corresponding to the same value of the axial strain ε_1 in DCCU3 and DCCU5, respectively then from (9) follows that:

$$h_1 = \frac{(\dot{\varepsilon}_1^{(1)} - \dot{\varepsilon}_1^{(2)}) - \left(\frac{\dot{\sigma}_1^{(1)} - \dot{\sigma}_1^{(2)}}{E} \right)}{f_1(\sigma_1^{(1)}, 0) - f_1(\sigma_1^{(2)}, 0)} \quad (16)$$

For $\sigma_1^{(1)} = 91.2$ MPa, $\sigma_1^{(2)} = 105$ MPa, we get $h_1 = 5.67 \cdot 10^3 \text{ s}^{-1}$. A formula similar to (16) can be used to derive $h_3 = 20 \cdot 10^3 \text{ s}^{-1}$.

d. Comparison of the theoretical predictions with experimental data

First, we present a comparison between the model predictions and unconfined quasistatic data QSC-1 (Figure 38). The comparison is very good on the whole. Figures 39-40 shows the theoretical $\sigma_1 - \varepsilon_1$ and $\sigma_1 - \varepsilon_3$ curves obtained for $\dot{\sigma}_1 = 1 \cdot 10^6$ MPa/s and $\sigma_3 = 0$, the experimental curve obtained in the unconfined dynamic compression test DCCU3 (average loading rate of $1 \cdot 10^6$ MPa/s, strain rate of 52/s), and the elastic response. The lower part of the experimental dynamic stress- strain curves present concavities, which are not due to rate effects but rather result from other phenomena such as the crushing of asperities at the ends of the specimen. Figures 41-42 show the theoretical $\sigma_1 - \varepsilon_1$ and $\sigma_1 - \varepsilon_3$ curves obtained for $\dot{\sigma}_1 = 2.77 \cdot 10^6$ MPa/s and $\sigma_3 = 0$, the experimental curve obtained in the unconfined dynamic compression test DCCU5 (average loading rate of $2.77 \cdot 10^6$ MPa/s, strain rate of 107/s), and the elastic response. It is to be noted that the trends observed experimentally are well simulated for high values of the axial stress (the slope of experimental curve is close to the slope of the theoretical curve for stresses beyond 80 MPa). The difference between the experiment and simulation is within the scatter of the experimental data.

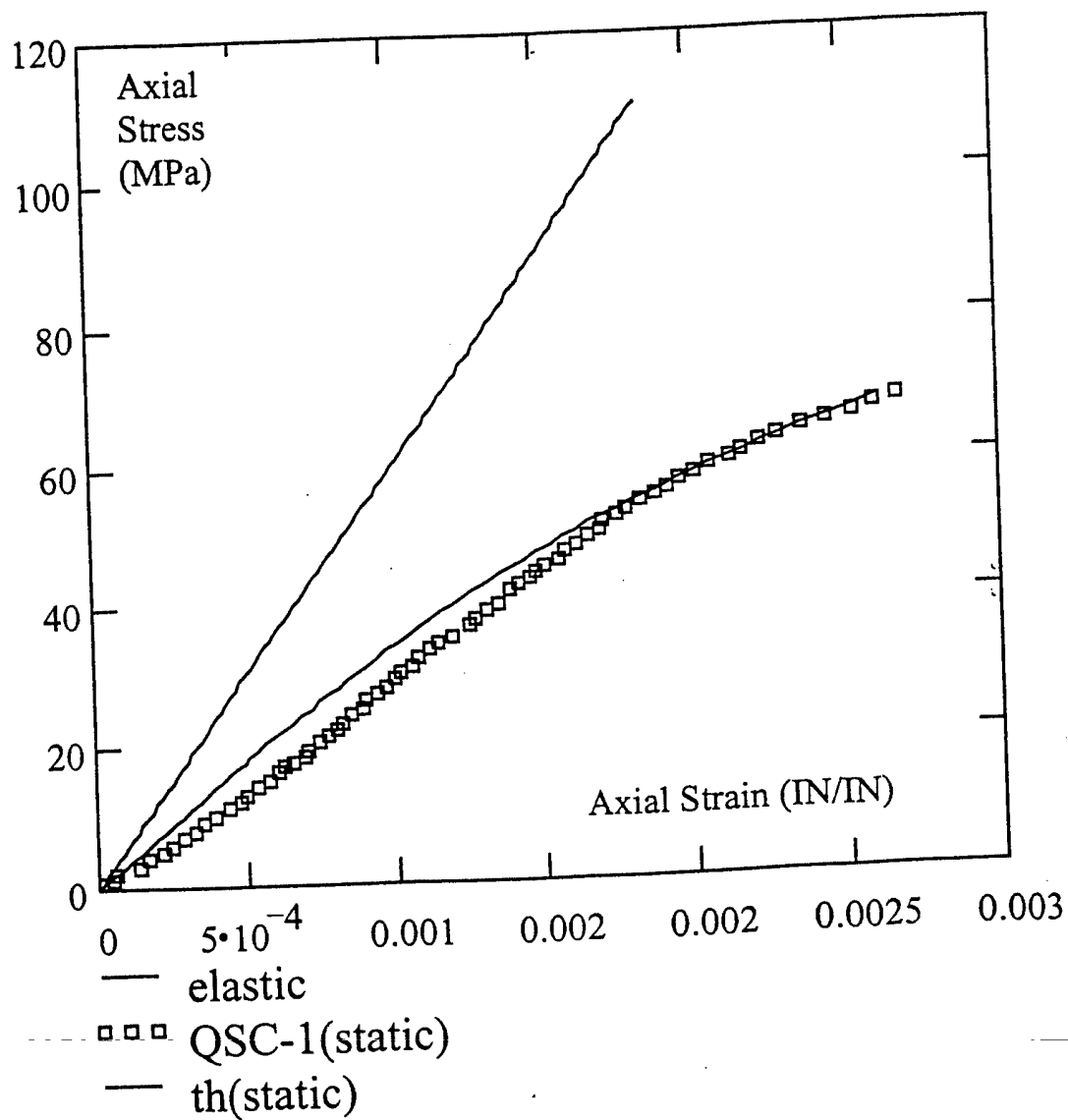


Figure 38. Comparison between the theoretical $\sigma_1 - \varepsilon_1$ curve, elastic curve, and data in the unconfined quasi-static test QSC-1.

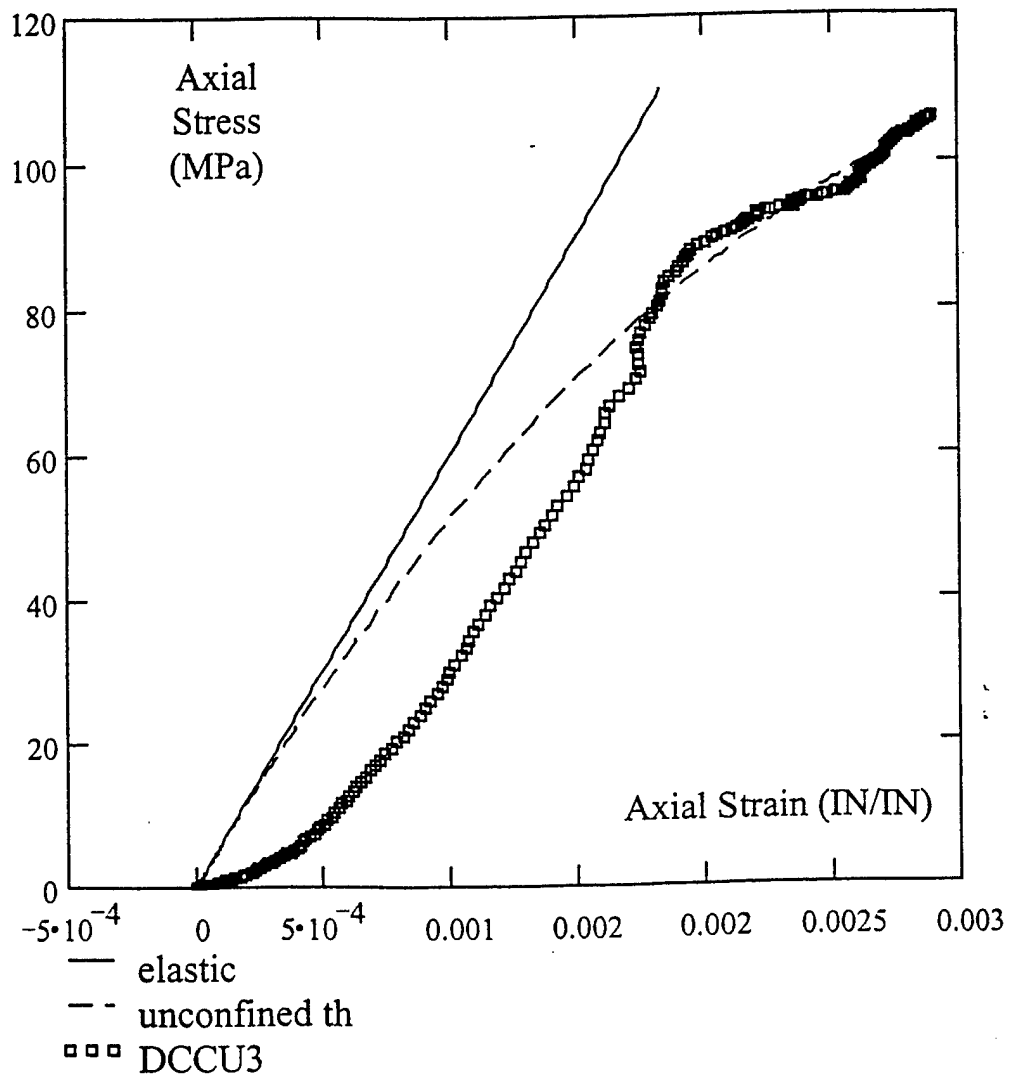


Figure 39. Comparison between the theoretical $\sigma_1 - \varepsilon_1$ curve, elastic curve, and data in the unconfined dynamic test DCCU3 conducted at a strain rate of 52/s.

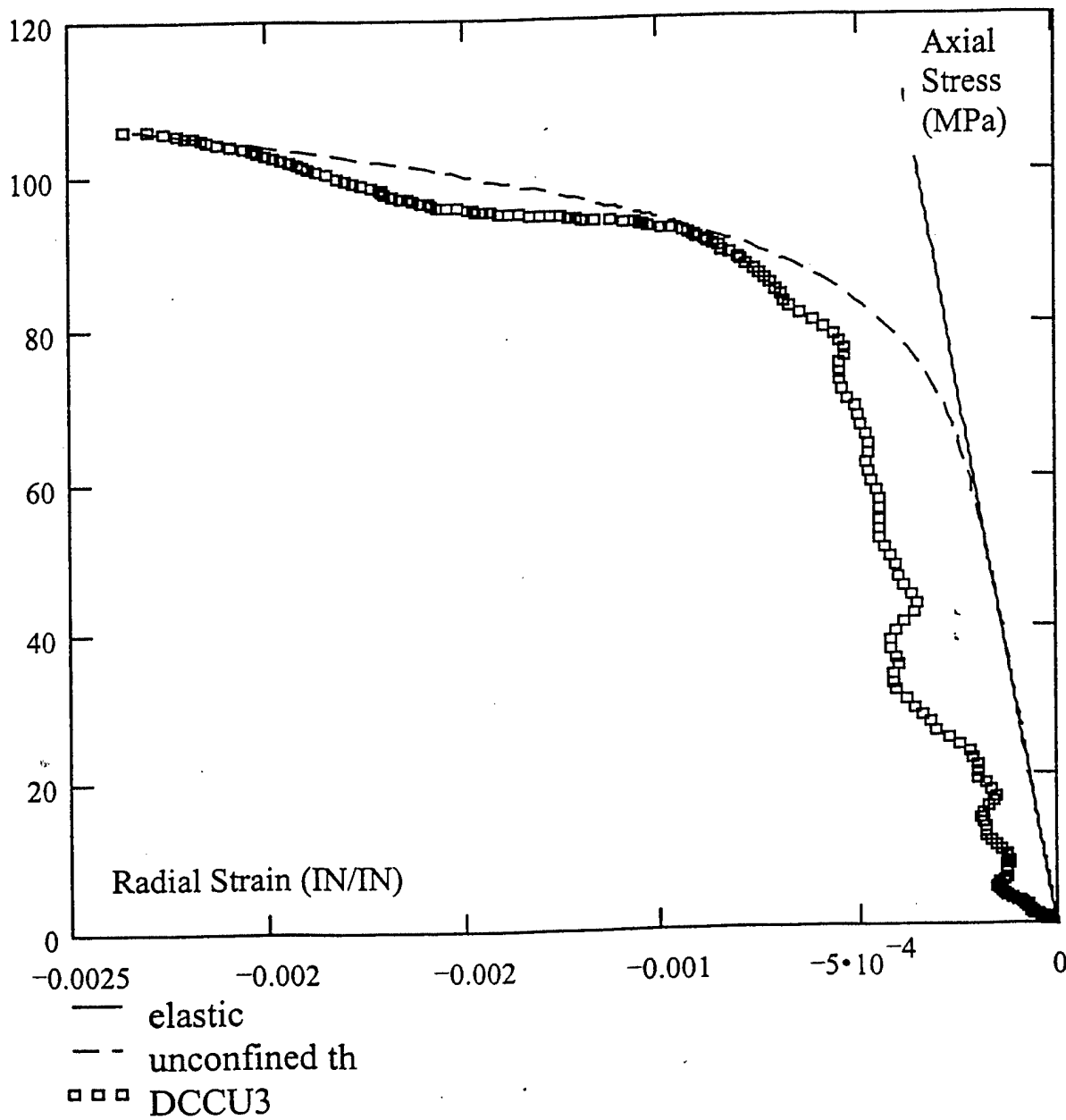


Figure 40. Comparison between the theoretical $\sigma_1 - \varepsilon_3$ curve, elastic curve, and data in the unconfined dynamic test DCCU3 conducted at a strain rate of 52/s.

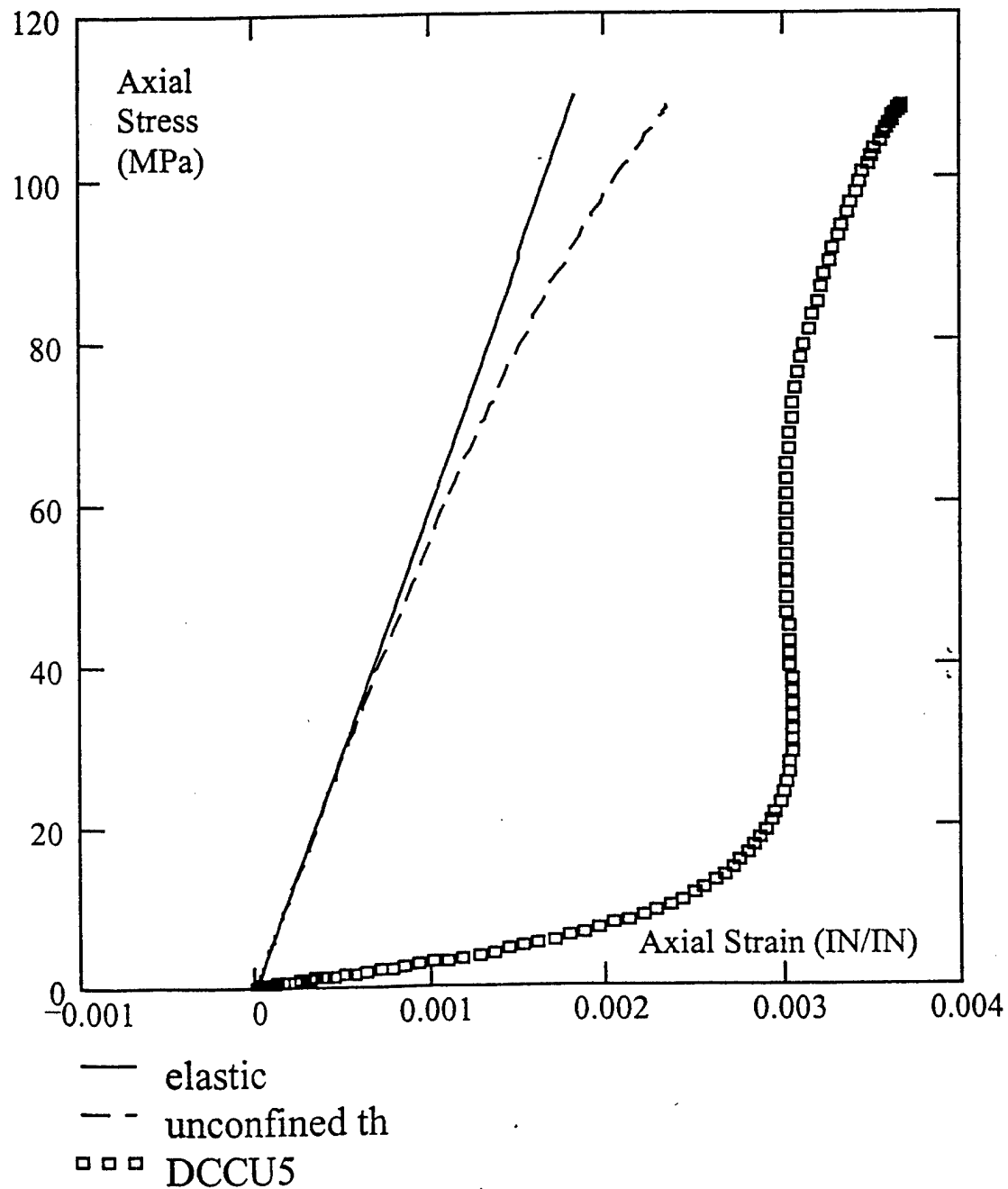


Figure 41. Comparison between the theoretical $\sigma_1 - \varepsilon_1$ curve, elastic curve, and data in the unconfined dynamic test DCCU5 conducted at a strain rate of 107/s.

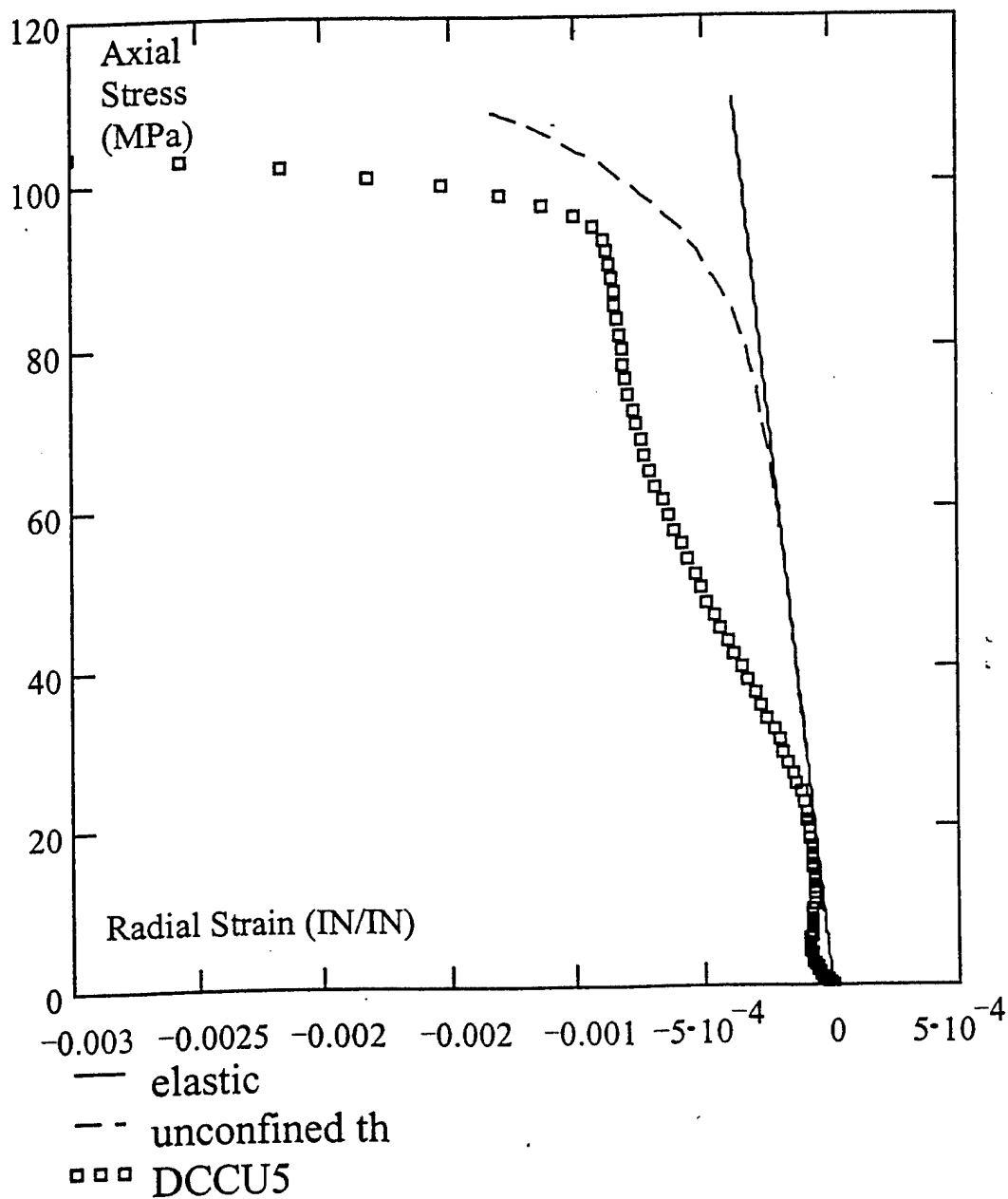


Figure 42. Comparison between the theoretical $\sigma_1 - \varepsilon_3$ curve, elastic curve, and data in the unconfined dynamic test DCCU3 conducted at a strain rate of 107/s.

Figures 43-44 shows a comparison between the theoretical quasistatic response, elastic, and data obtained in the quasi-static GERC test at 3.45 MPa confining pressure(QSCC-1). The static stress-strain curves are well reproduced by the model.

Figures 45-46 show a comparison between the model predictions and data obtained in the confined dynamic test DCC4 conducted at a strain rate of 53/s under a lateral confining pressure of 3.57 MPa. The model reproduces qualitatively the observed behavior.is within the scatter of the data.

It can be noted that the rate influence and confining pressure influence are correctly described The theoretical curves correspond to a constant loading rate (the average loading rate in the test) while in the tests the loading rate was not constant. Therefore, we cannot expect a perfect agreement between the model and data. However, the general trends of the data are reproduced and for higher values of the stress the comparison is within the natural scatter of the data.

e. Conclusions

The model presented was developed in the framework of non-associated viscoplasticity theory in order to simulate the non-linear stress-dependent and rate-dependent behavior of concrete. The model captures the basic features of the material behavior such as strain-hardening, confining pressure, rate influence, creep and relaxation phenomena. Instantaneous response is modeled as being linear elastic although a stress dependence of the elastic moduli has been experimentally observed. Although, the model developed is applicable to fully 3-D stress conditions, all the parameters involved can be determined from the results of a few quasistatic and dynamic tests. The agreement between model prediction and data obtained in unconfined dynamic tests is rather good, the degree of accuracy being within the natural scatter of the data.

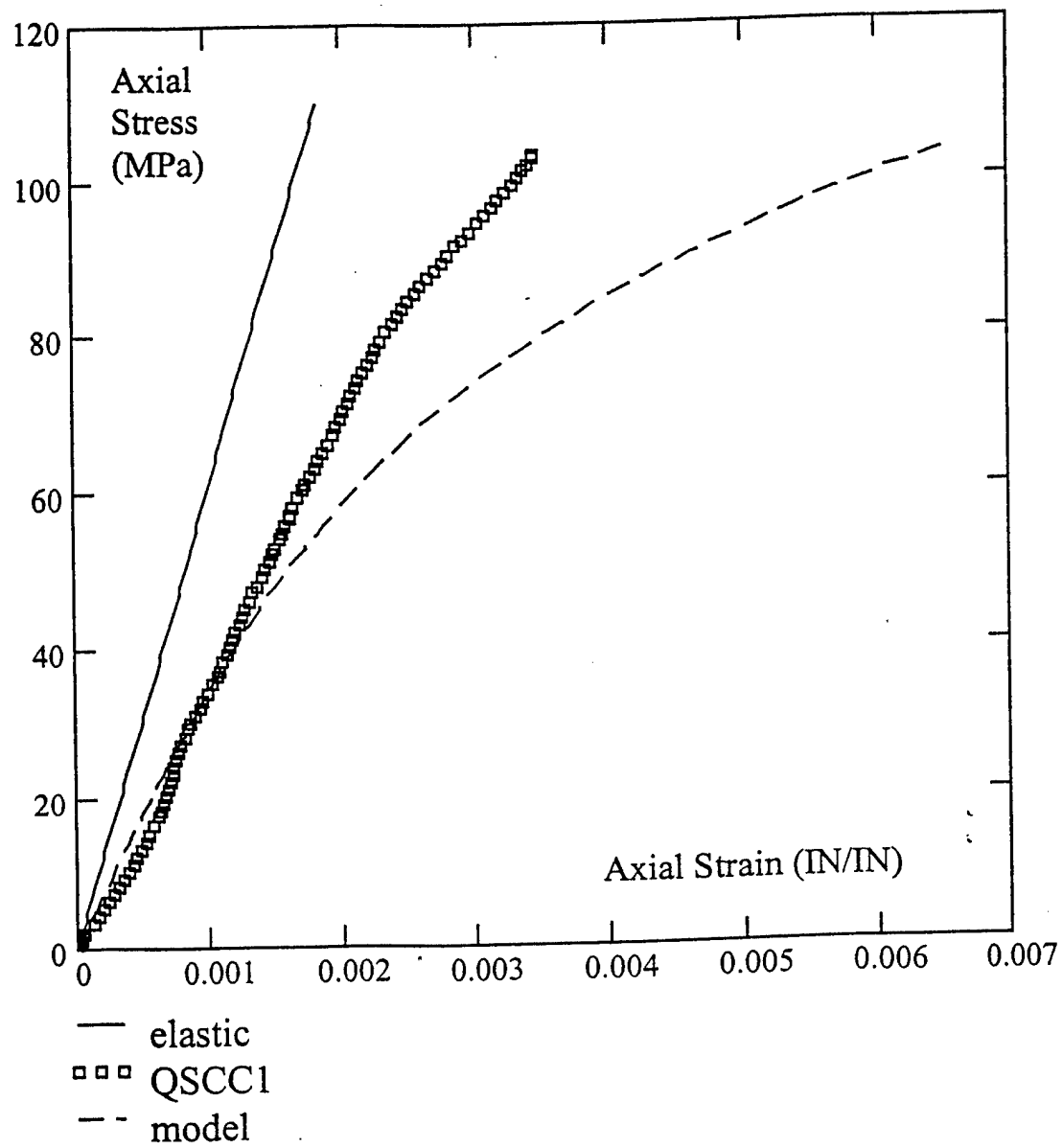


Figure 43. Comparison between the theoretical $\sigma_1 - \varepsilon_1$ curve, elastic curve, and data in the confined quasi-static test QSCC-1 ($\sigma_3 = 3.45$ MPa).

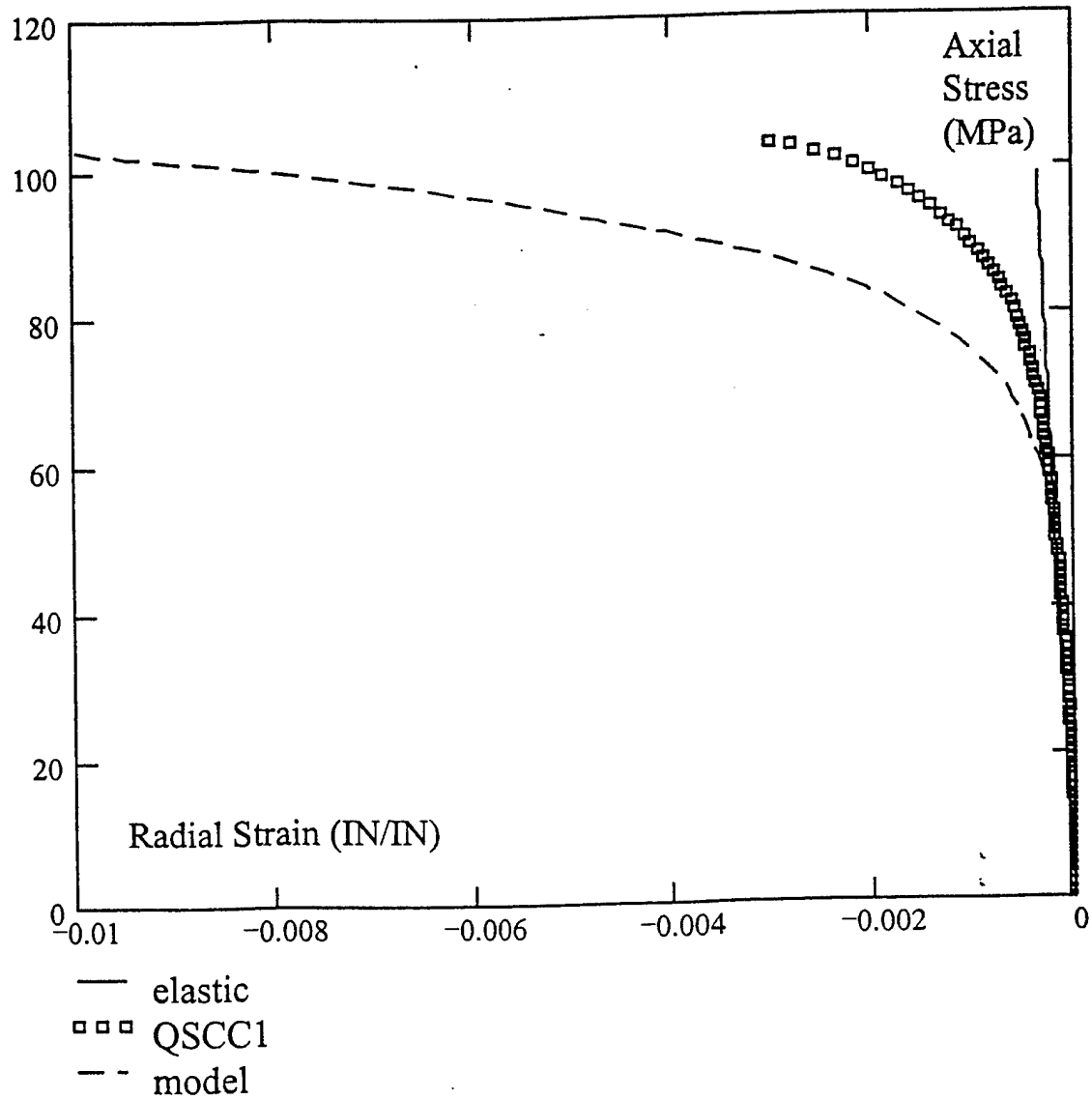


Figure 44. Comparison between the theoretical $\sigma_1 - \varepsilon_3$ curve, elastic curve, and data in the confined quasi-static test QSCC1 ($\sigma_3 = 3.45$ MPa).

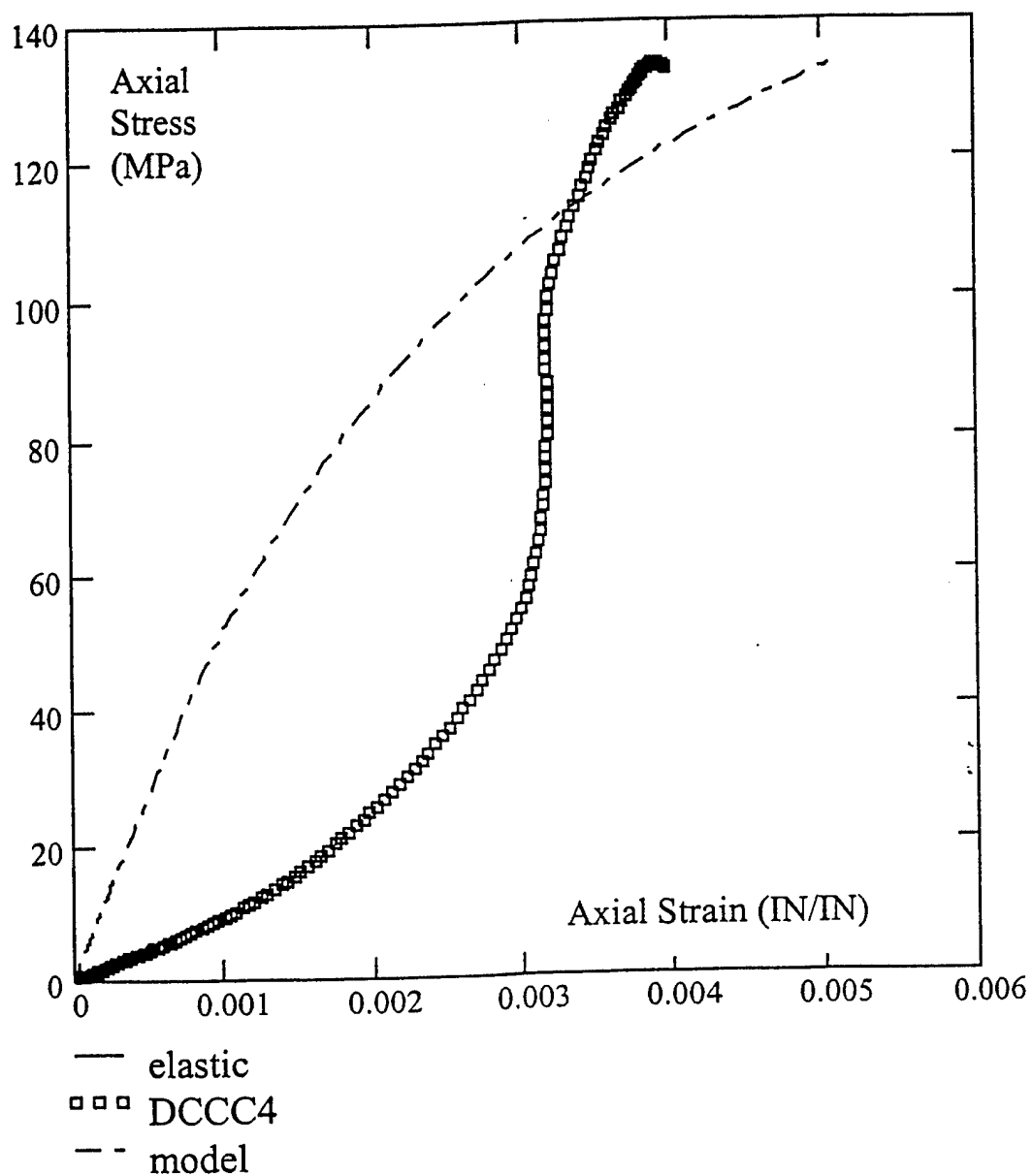


Figure 45. Comparison between the theoretical $\sigma_1 - \varepsilon_1$ curve, elastic curve, and data in the confined dynamic test DCCC4 conducted at a strain rate of 53/s, confining pressure 3.57 MPa.

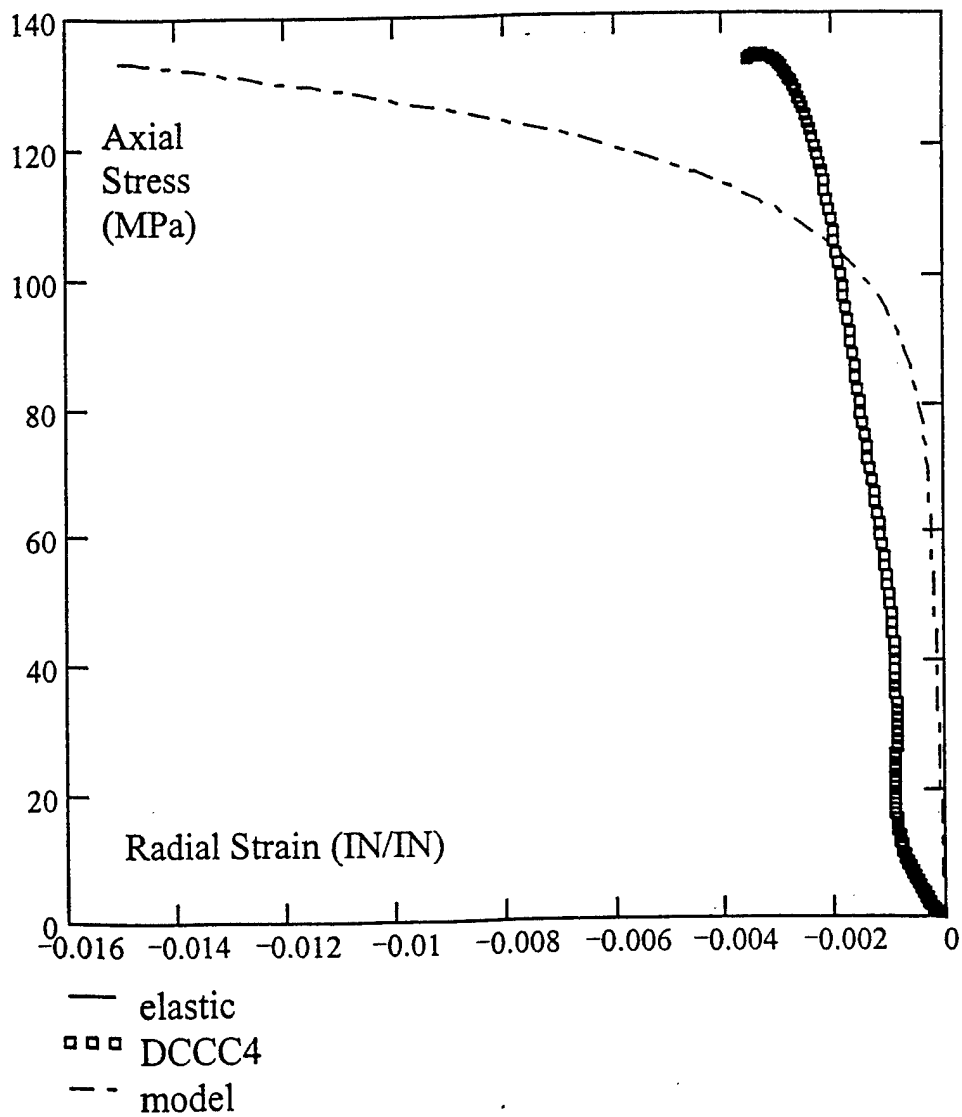


Figure 46. Comparison between the theoretical $\sigma_1 - \varepsilon_3$ curve, elastic curve, and data in the confined dynamic test DCCC4 conducted at a strain rate of 53/s, confining pressure 3.57 MPa.

References

1. Watstein, D. and Boresi, A. P., "The Effect of Loading Rate on the Compressive Strength and Elastic Properties of Plain Concrete," US National Bureau of Standards, Report 1523, Washington, DC, 1952.
2. Reinhardt, H. W., "Simple relations for the strain rate influence in concrete", Darmstad Concrete, Vol. 2, pp.203-213, 1987.
3. Cowell, W. L., "Dynamic Properties of Plain Portland Cement Concrete," US Naval Civil Engineering Laboratory, Port Hueneme, CA 1996.
4. Malvern, L. E. and Ross, C. A., "Dynamic Response of Concrete and Concrete Structures," Two Annual Reports and a Final Report AFOSR Grant F49620-83-K007, AF Office of Scientific Research, Washington, DC, 1982 – 1986.
5. Ross, C.A., Thompson, P.Y. and Tedesco, J.W., Split-Hopkinson Pressure Bar Tests on Concrete and Mortar in Tension and Compression", ACI Material Journal, Vol. 86, No.5, pp 475-481, Sept. –Oct. 1989.
6. Ross, C.A., Tedesco, J.W. and Kuennen, S.T., "Effects of Strain Rates on Concrete Strength", ACI Materials Journal, Vol. 92, No. 1, pp. 37-47, Jan.-Feb. 1995.
7. Ross, C.A., Jerome, D.M., Tedesco, J.W. and Hughes, M.L., "Moisture and Strain Rate Effects on Concrete Strength", ACI Materials Journal, Vol. 93, No. 3, pp. 293-300, May-June, 1996.
8. Weerheijm, J., "Concrete under Impact Tensile Loading and Lateral Compression", *Ph. D. Thesis*, Technical University of Delft, 1992.
9. Osborn, J.J., "Loading on Penetrators in Concrete Slabs", Tech. Rept. AFATL-TR-82-9, Air Force Armament Lab, Eglin AFB, FL, Feb. 1982.
10. Osborn, J.J. and Matuska, D.A., "Dynamic Response of a Kinetic Energy Penetrator", Tech. Rept. AFATL-TR-78-24, Vol. II, Air Force Armament Lab, Eglin AFB, FL, Mar. 1978.
11. Derucher, K. N., Korfiatis, G. P., and Ezeldin, A. S., "Materials for Civil & Highway Engineers", Prentice Hall, Upper Saddle River, N.J., 1998.
12. Malvern, L.E. and Jenkins, D.A., "Dynamic Testing of Laterally Confined Concrete", Tech. Rept. ESL-TR-89-47 Air Force Engineering and Services Lab, Tyndall AFB, FL, 1990.
13. Cristescu, N., Rock Rheology, Kluwer Academic Pub., Netherlands, 1989.
14. Cristescu, N. and Hunsche, V., Time Effects in Rock Mechanics, J. Wiley & Sons, England, 1998.

15. Johnson, G.R. and Stryk, R.A., "Users Instructions for the 1992 Version of the EPIC Research Code", Allant Tech Systems, Inc., Brooklyn Park, MN, 1992.
16. Bell, R.L., et al, "CTH User's Manual and Input Instructions", Version 1.027, Sandia Nat. Lab, Albuquerque, NM, 1994.
17. Matuska, D.A., Osborn, J.J. and Pibun, E.W., "Hull Documentation, Vol. II Users Manual", Orlando Technology, Inc., Shalimar, FL, Aug., 1991.
18. Brace, W. F. and Bombolakis, E. G., "A note on brittle crack growth in compression". J. Geophys. Res. Vol. 68, 12, pp. 3709-3713.
19. Mindess, S. "The application of fracture mechanics to cement and concrete: A historical review." in Fracture Mechanics of Concrete, ed. F. H. Wittmann, Elsevier Science Publishers, B.V. Amsterdam, 1983.
20. Nemat-Nasser, S. and Horii, H. "Compresion-Induced Nonplanar Crack Extension with Application to Splitting", J. Geophys. Res., 87, pp 6805-6825, 1982.
21. Lemaitre, J and Chaboche, J.-L. "Mecanique des Materiaux Solides", Ed Dunod, 1984.
22. Mazars, J. " Mechanical damage and fracture of concrete structures", Proc. 5th International Symposium on Fracture, Cannes, 1980.
23. Krajcinovic, D. and Fonseka, G.U. " The continuous damage theory of brittle materials Part I: General Theory, Part II: Uniaxial and plane response modes", J. of Applied Mechanics, Vol. 48, pp. 809-815 and 816-824, 1981.
24. Chaboche, J. L "A continuum damage theory with anisotropic and unilateral damage", Recherche Aerospatiale, Vol. 2, pp. 139-147, 1995.
25. Halm, D. and Dragon, A. " A model of anisotropic damage by mesocrack growth; unilateral effect", Int. J. Damage Mech., Vol. 5, pp. 384-402.
26. Zaitsev, Y. " Simulation of behavior of light-weight concrete under load and its trial", In: Fracture toughness and fracture energy of concrete, ed. F. H. Wittmann, Elsevier Science Publishers, B.V. Amsterdam, 1986.
27. Schreyer, H. L. and Gao, J., "The Prediction of Axial Splitting Under Uniaxial Compression as a Discontinious Bifurcation," Thirteenth U. S. National Congress of Applied Mechanics (Book of Abstracts) University of Florida, Gainesville, FL, pp TA8-9, June 1998

28. Malvern, L. E., Jenkins, D. A., and Dehoff, R. T., Rate and Confinement Effects on Cracking and Failure in Uniaxial Compression of Concrete," AFOSR-93-0071 (AD-A261164) AF Office of Scientific Research AFOSR/NA Bolling AFB, DC, Nov. 1992.
29. Ross, C. A., "Crack Patterns Resulting from High Strain-Rate Tests on Concrete," ESL-TR-92-08, AF Eng. & Ser. Cent., Eng. & Ser. Lab., Tyndall AFB, FL, 32403, March 1992.
30. Krajcinovic, D., "Continuous Damage Mechanics," Appl. Mech. Rev., 37(1), pp 1-6, 1984.
31. Budiansky, B. and O'Connell, R. J., "Elastic Moduli of a Cracked Solid," J. Solids and Structures, 12, pp 81-97, 1976.
32. Taylor, L. M., Chen, En-P., and Kuszmaul, J. S., Microcrack-Induced Damage Accumulation in Brittle Rock Under Dynamic Loading," Comp. Meth. In Appl. Mech. And Eng., 55, pp 301-320, 1986.
33. Ross, C. A. "The Effects of Dynamic Pre-Compression on the Dynamic Tensile Strength of Concrete and Mortar," ASMF Conf. PVP-Vol. 361, Structures Under Extreme Loading Conditions-1998, Eds. Zukas, Jerome and Shin, San Diego, CA, pp 31-36, 1998.
34. Ross, C. A., "Split Hopkinson Pressure Bar Tests," ESL TR-88-62, HQ AFESC/RDCM, HQ AF Engineering & Services Center, Tyndall AFB, FL, 1989.
35. Ahrens, T. J., "Penetration into Concrete," AF Office Scientific Research Review Meeting, San Diego, CA, June 1998.
36. Nadai, A. Theory of Flow and Fracture of Solids, Vol. 1, McGraw-Hill Book Co, New York, 1950.
37. Nadai, A. Theory of Flow and Fracture of Solids, Vol. 1, McGraw-Hill Book Co, New York, 1963.
38. Bell, J. F. The Experimental Foundation of Solid Mechanics . Handbuck der Physik, Vol VI a/1, Springer Verlag, Berlin, 1973.
39. Bridgman, P. W. "Volume changes in the plastic stage of simple compression". J. Applied. Physics, Vol. 20, pp. 1241-1251, 1949.
40. Brace, W. F, Paulding, B.W. Jr., and Scholz, C. "Dilatancy in the fracture of crystalline rocks". J. Geophys. Res. Vol. 71, 16, pp.3939-3953, 1966.
41. Bieniawski, Z. T. "Mechanics of brittle fracture of rock. Part I-Theory of the fracture process; Part II-Experimental studies; Part III-Fracture in tension and under long-term loading" . Int. J. Rock. Mech. Min. Sci. , Vol. 4, pp. 365-430, 1967.

42. Schofield, A. and Wroth, P. Critical State Soil Mechanics. McGraw-Hill Book Co. New York, 1968.
43. Wood, D. M. Soil Behavior and Critical State Soil Mechanics, Cambridge University Press, Cambridge, 1990.

APPENDIX A
Miscellaneous Figures

QUASISTATIC CONFINED MORTAR TEST

QSMC-5, CONFINING PRESSURE = 1.72 MPa, STRAIN RATE = 1.25E-6/SEC

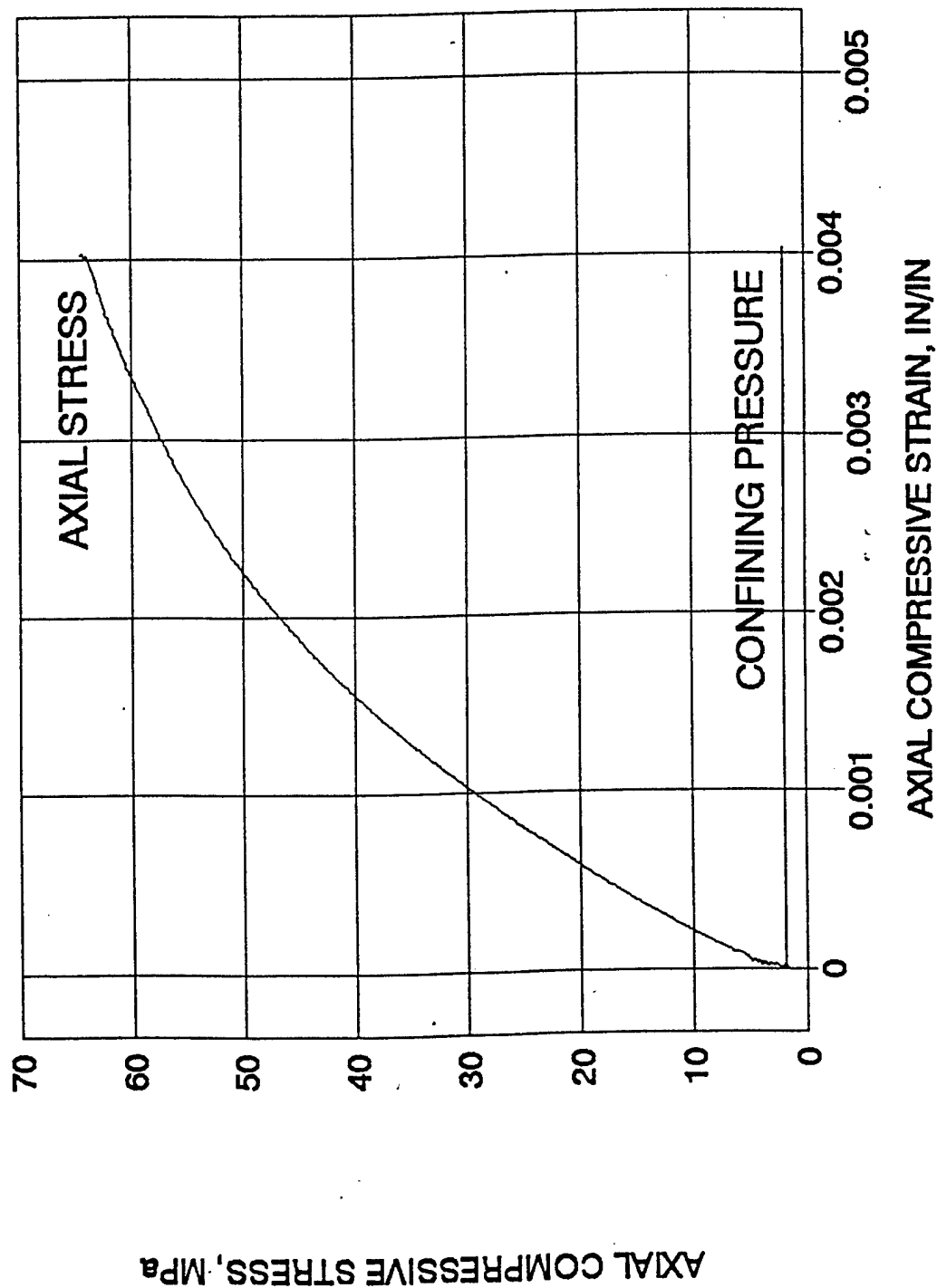


Figure A-1. Stress-strain curve for quasistatic confined mortar test.

QUASISTATIC CONFINED MORTAR TEST

QSMC-5, CONFINING PRESSURE = 1.72 MPa, STRAIN RATE = 1.25E-6/SEC

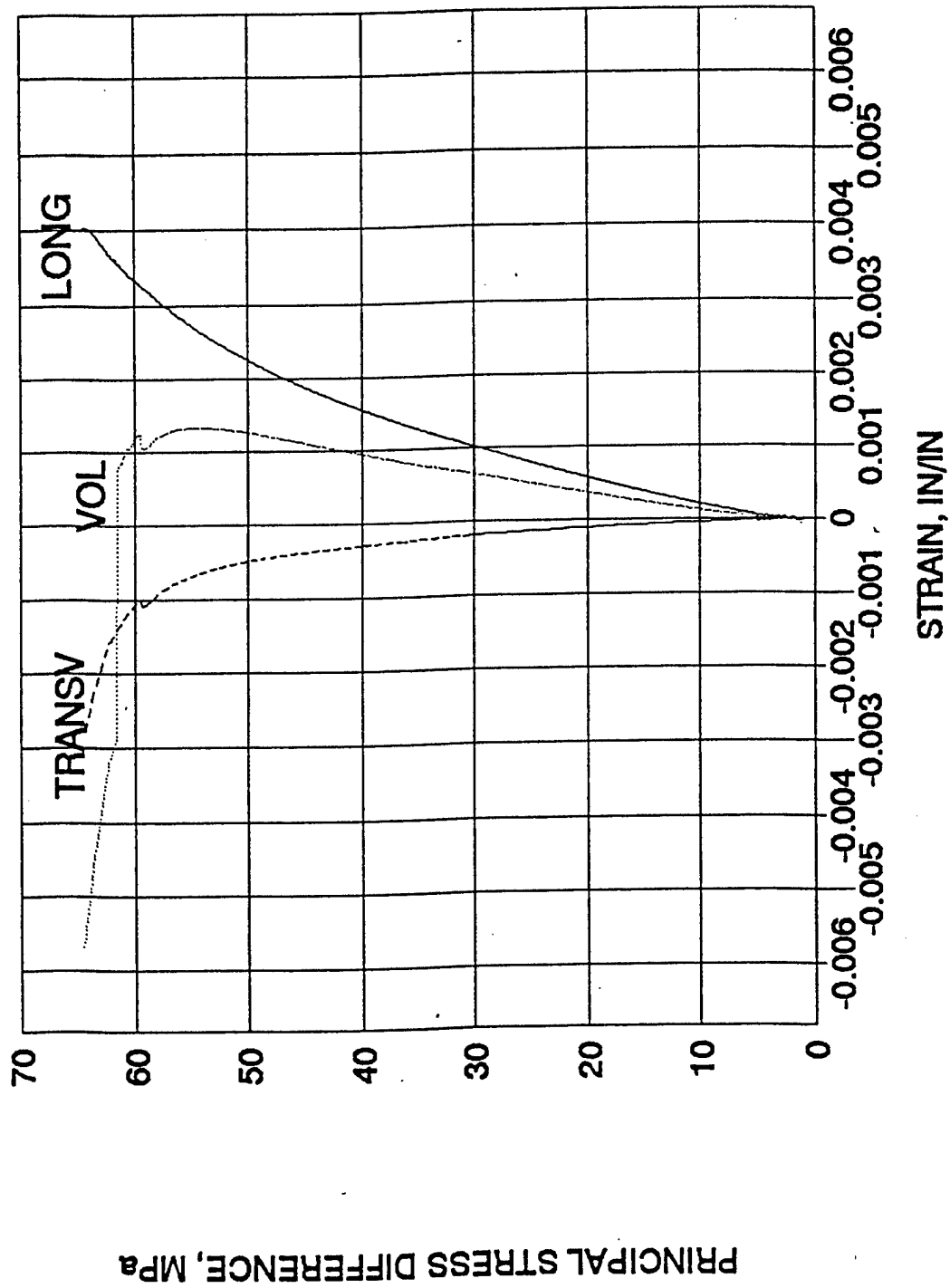


Figure A-2. Longitudinal, transverse and volumetric strain for quastatic confined mortar test.

QUASISTATIC CONFINED MORTAR TEST

QSMC-4, CONFINING PRESSURE = 3.45 MPa, STRAIN RATE = 1.25×10^{-6} /SEC

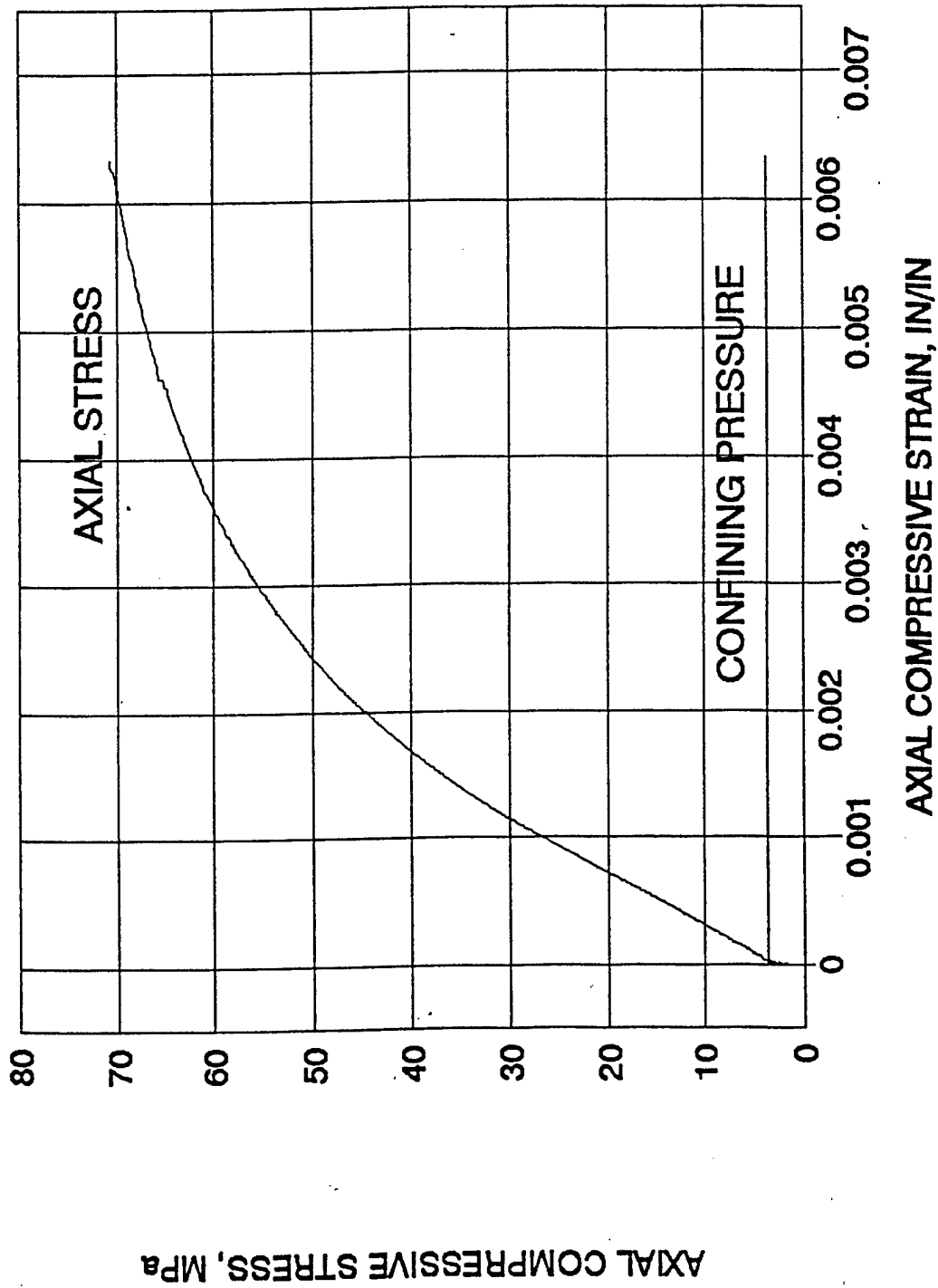


Figure A-3. Stress-strain curve for quasistatic confined mortar test.

QUASISTATIC CONFINED MORTAR TEST

QSMC-4, CONFINING PRESSURE = 3.45 MPa, STRAIN RATE = 1.25E-6/SEC

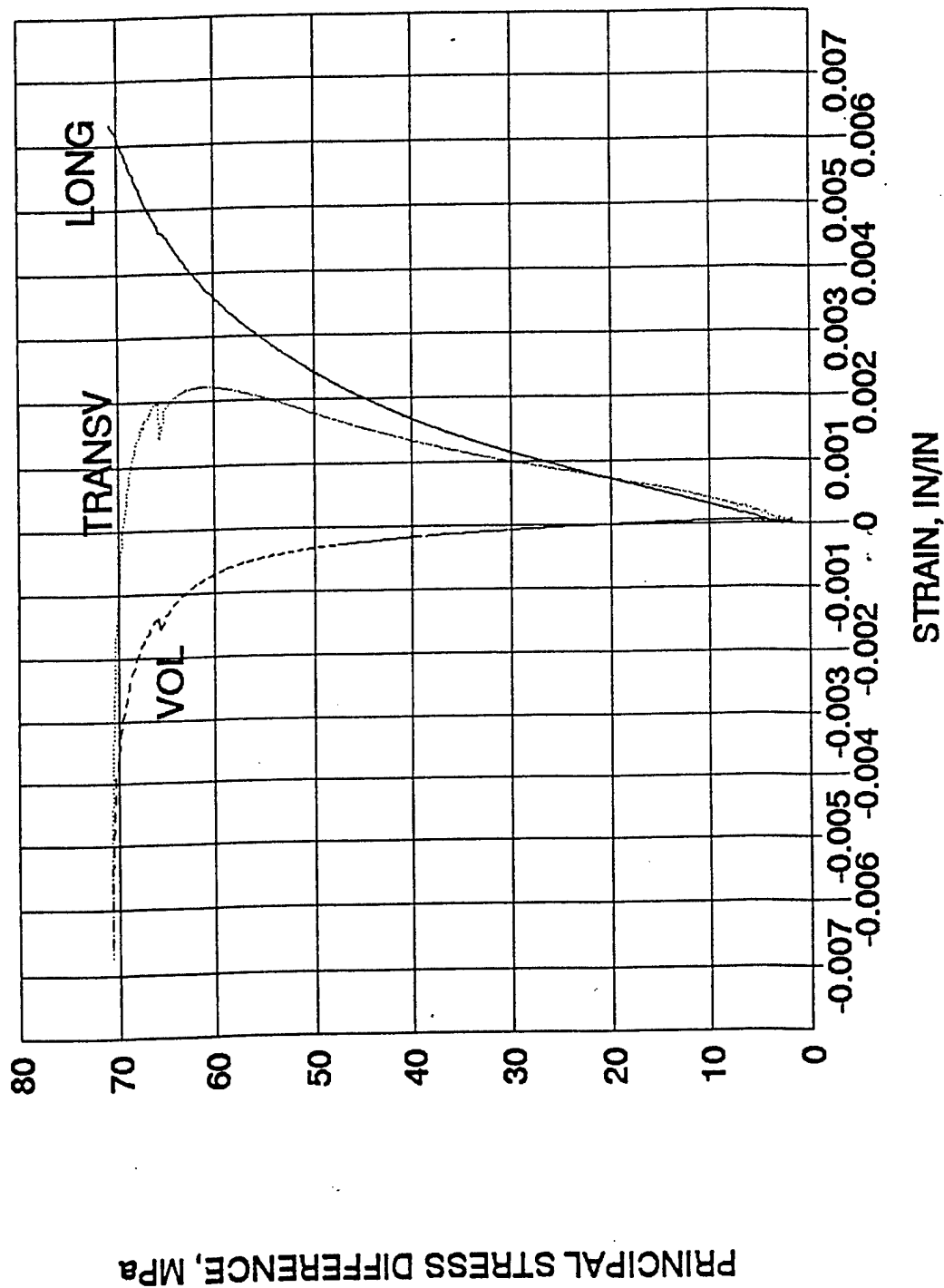


Figure A-4. Longitudinal, transverse and volumetric strain for quastatic confined mortar test

QUASISTATIC CONFINED MORTAR TEST

QSMC-9, CONFINING PRESSURE = 6.90 MPa, STRAIN RATE = 1.25E-6/SEC

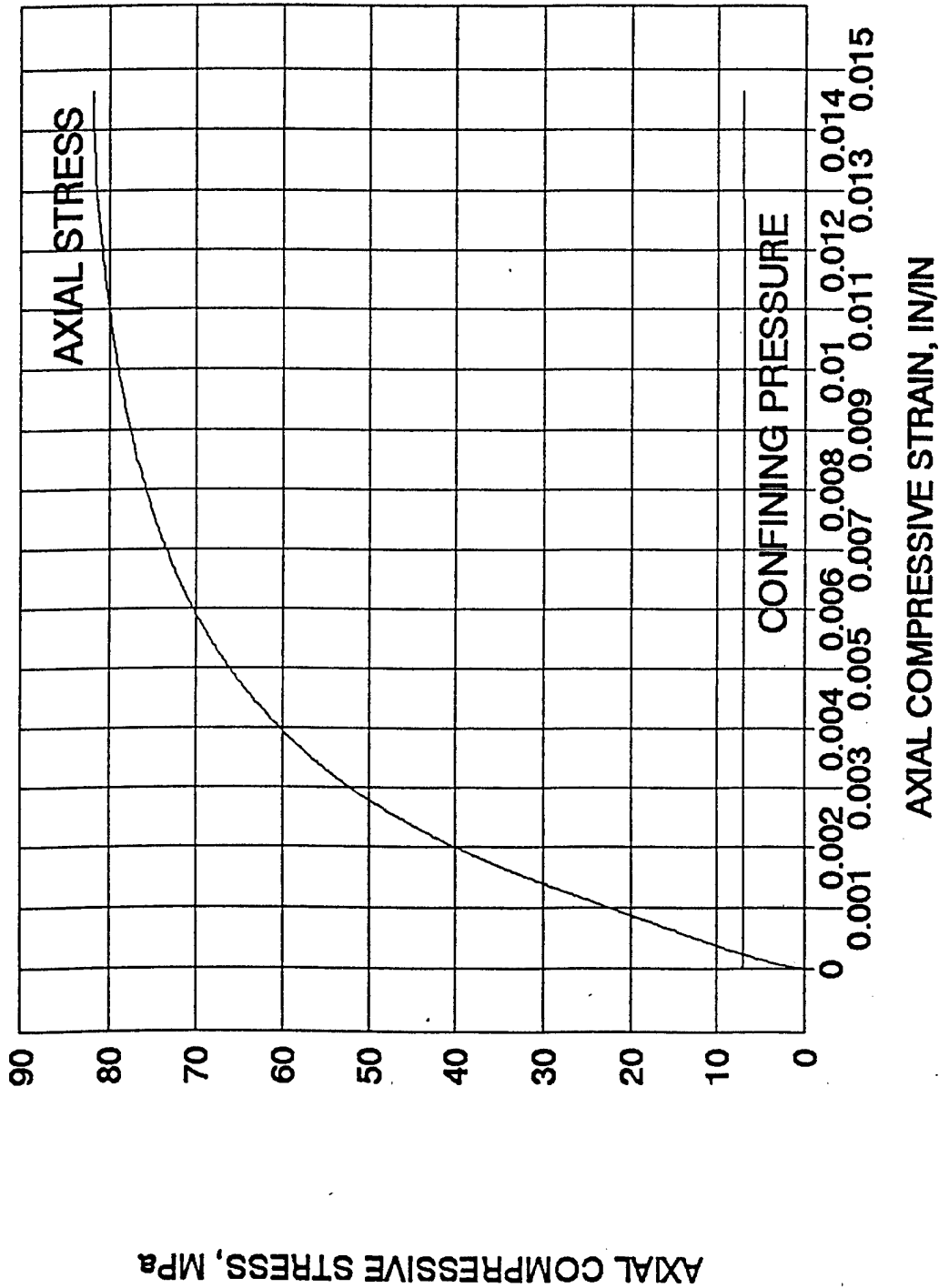


Figure A-5. Stress-strain curve for quasistatic confined mortar test.

QUASISTATIC CONFINED MORTAR TEST

QSMC-9, CONFINING PRESSURE = 6.90 MPa, STRAIN RATE = 1.25E-6/SEC

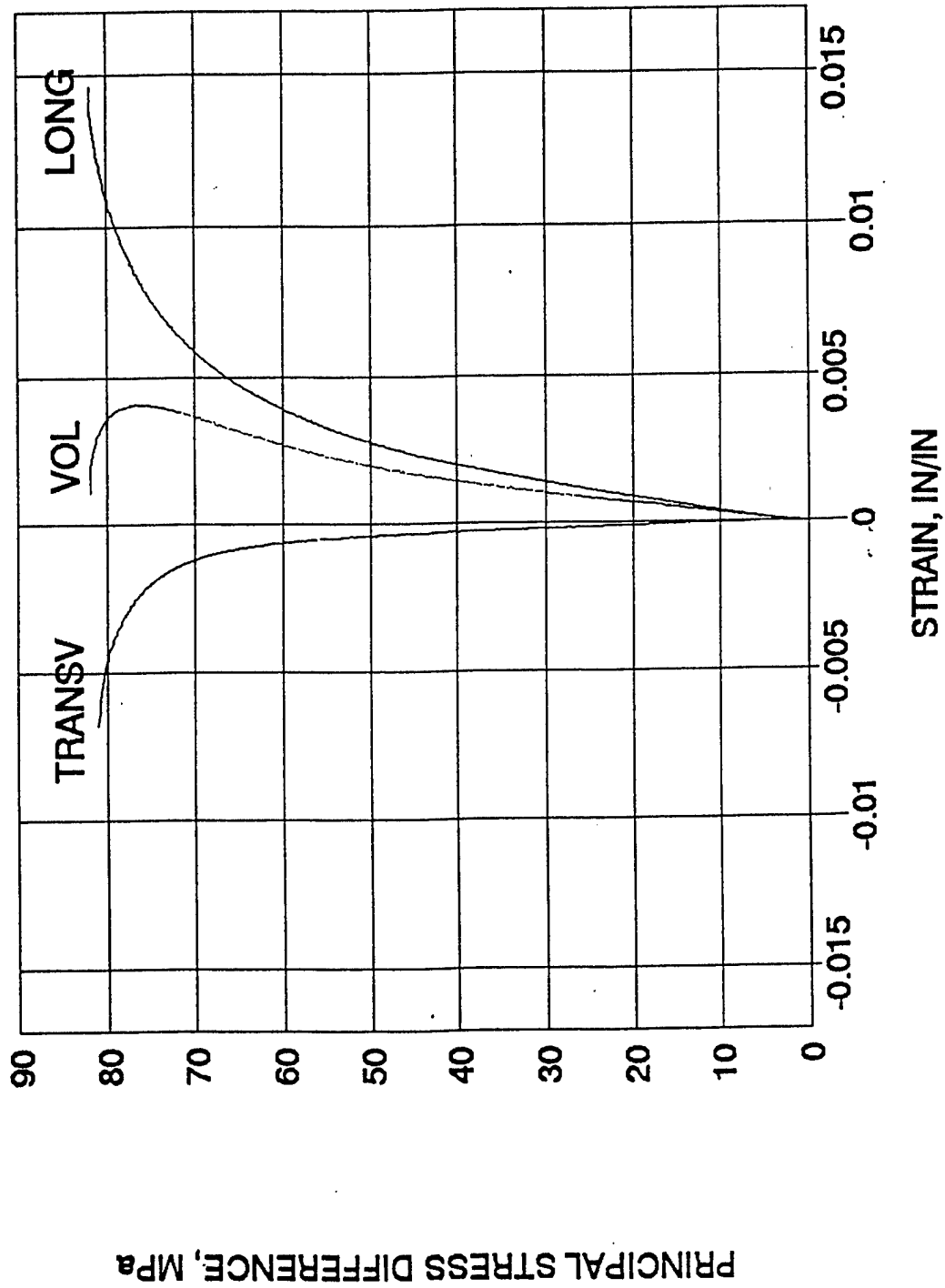


Figure A-6. Longitudinal, transverse and volumetric strain for quasistatic confined mortar test.

QUASISTATIC CONFINED MORTAR TEST

QSMC-7, CONFINING PRESSURE = 6.90 MPa, STRAIN RATE = 1.25×10^{-6} /SEC

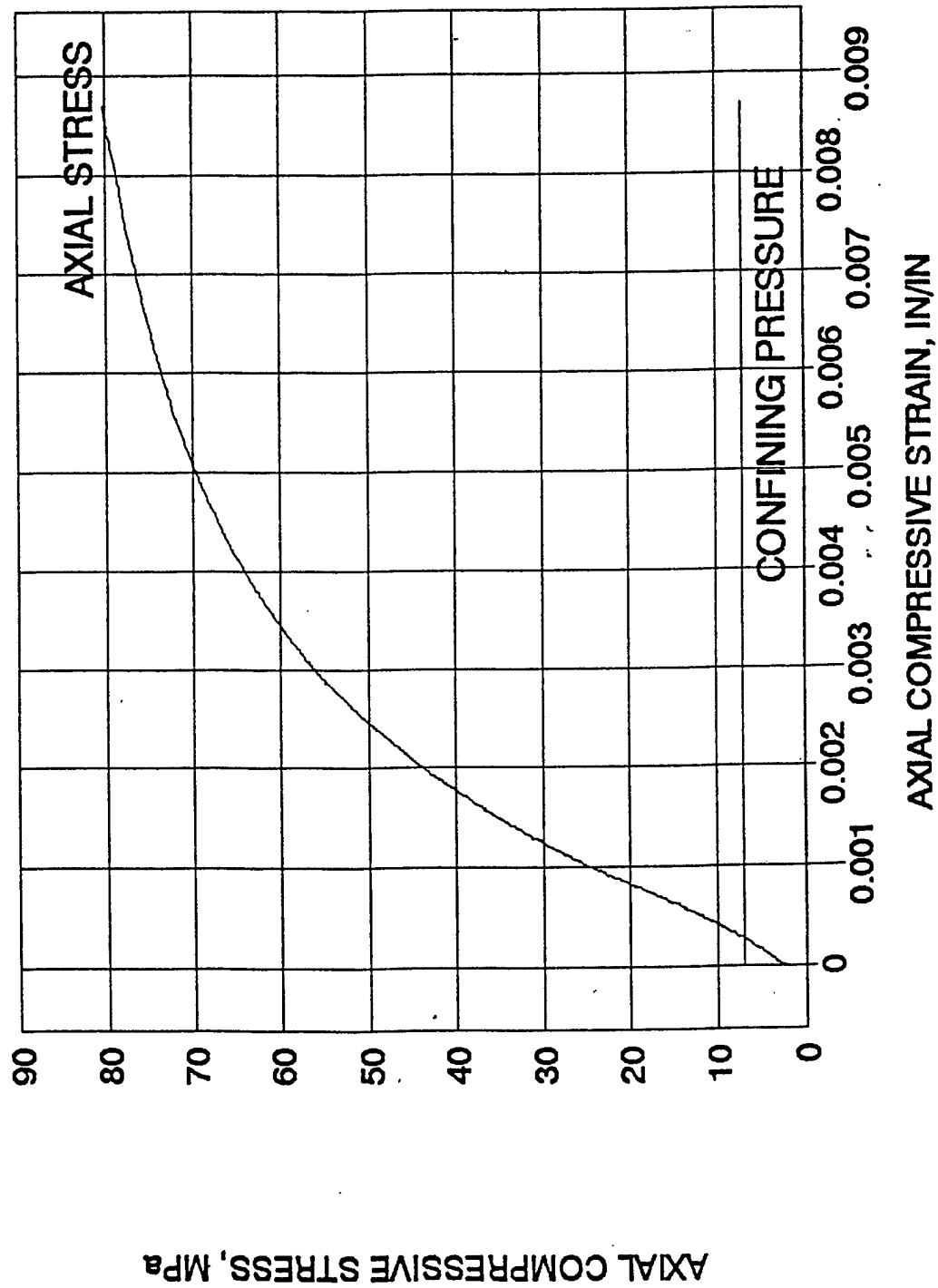


Figure A-7. Stress-strain curve for quasistatic confined mortar test.

QUASISTATIC CONFINED MORTAR TEST

QSMC-7, CONFINING PRESSURE = 6.90 MPa, STRAIN RATE = 1.25E-6/SEC

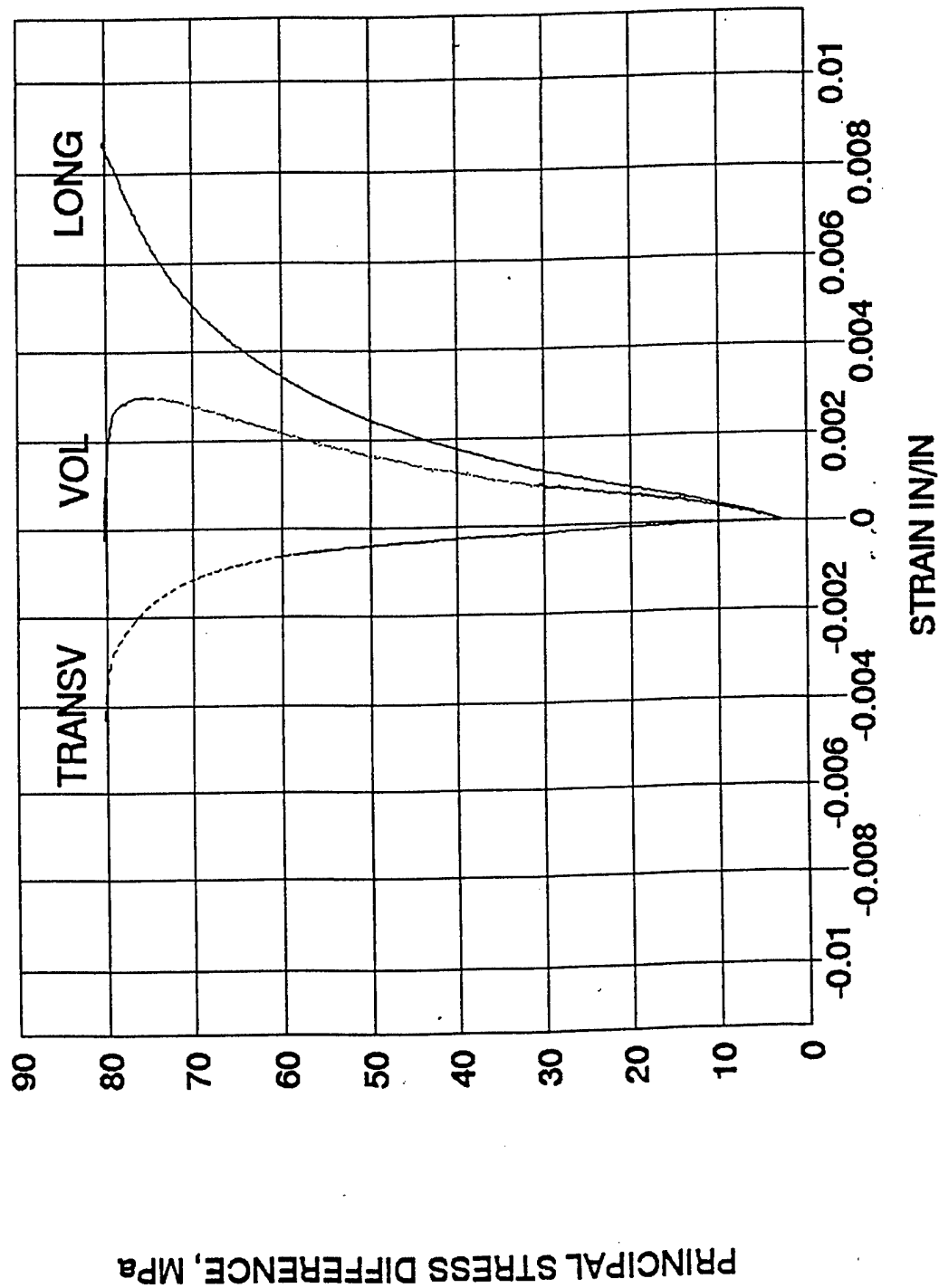


Figure A-8. Longitudinal, transverse and volumetric strain for quasistatic confined mortar test.

DYNAMIC CONFINED TEST OF MORTAR

DCMC-27, CONFINING PRESSURE = 1.72 MPa, STRAIN RATE = 140/SEC

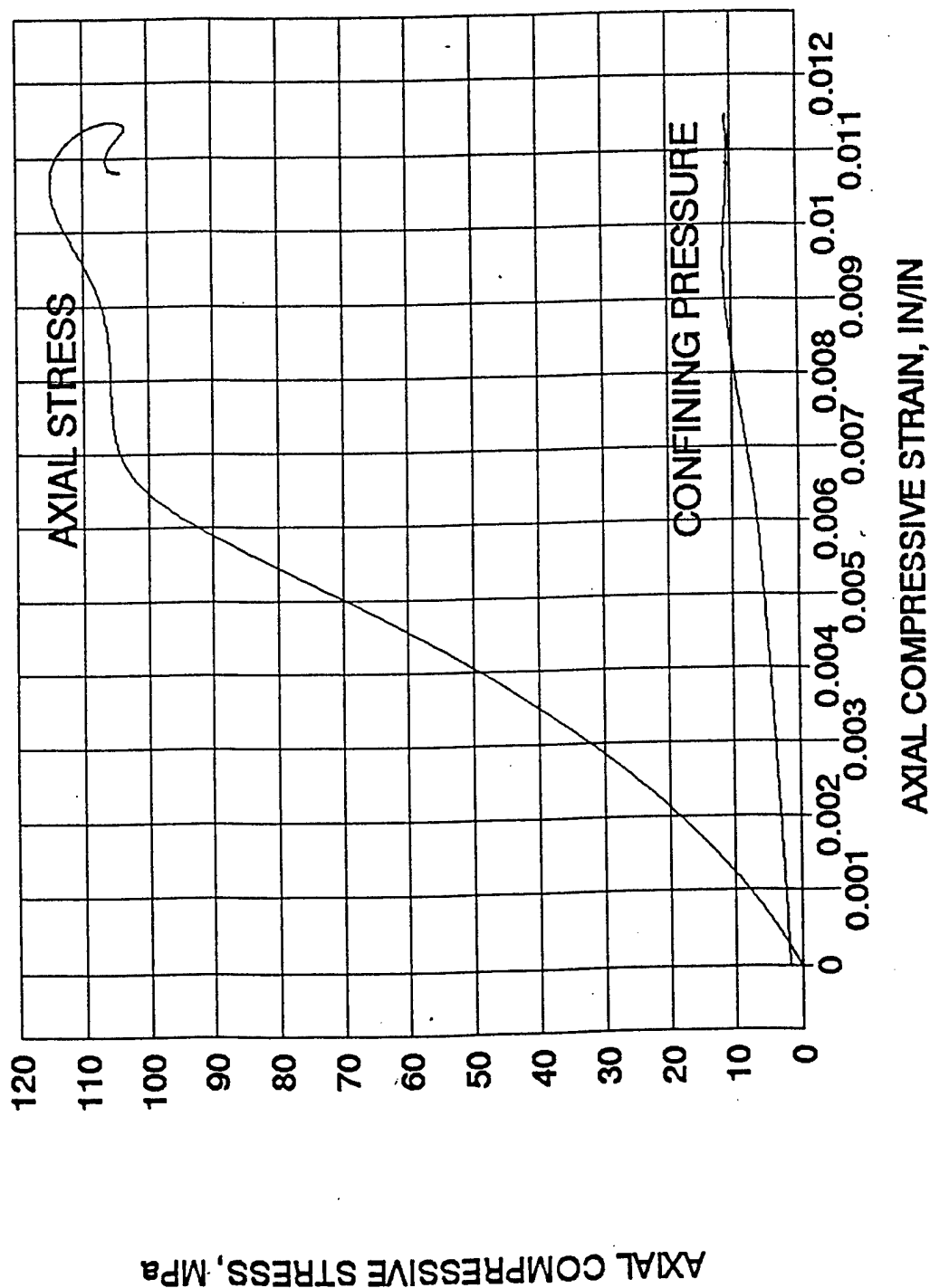


Figure A-9. Stress-strain curve and confining pressure for dynamic confined mortar test.

DYNAMIC CONFINED TEST OF MORTAR

DCMC-27, CONFINING PRESSURE = 1.72 MPa, STRAIN RATE = 140/SEC

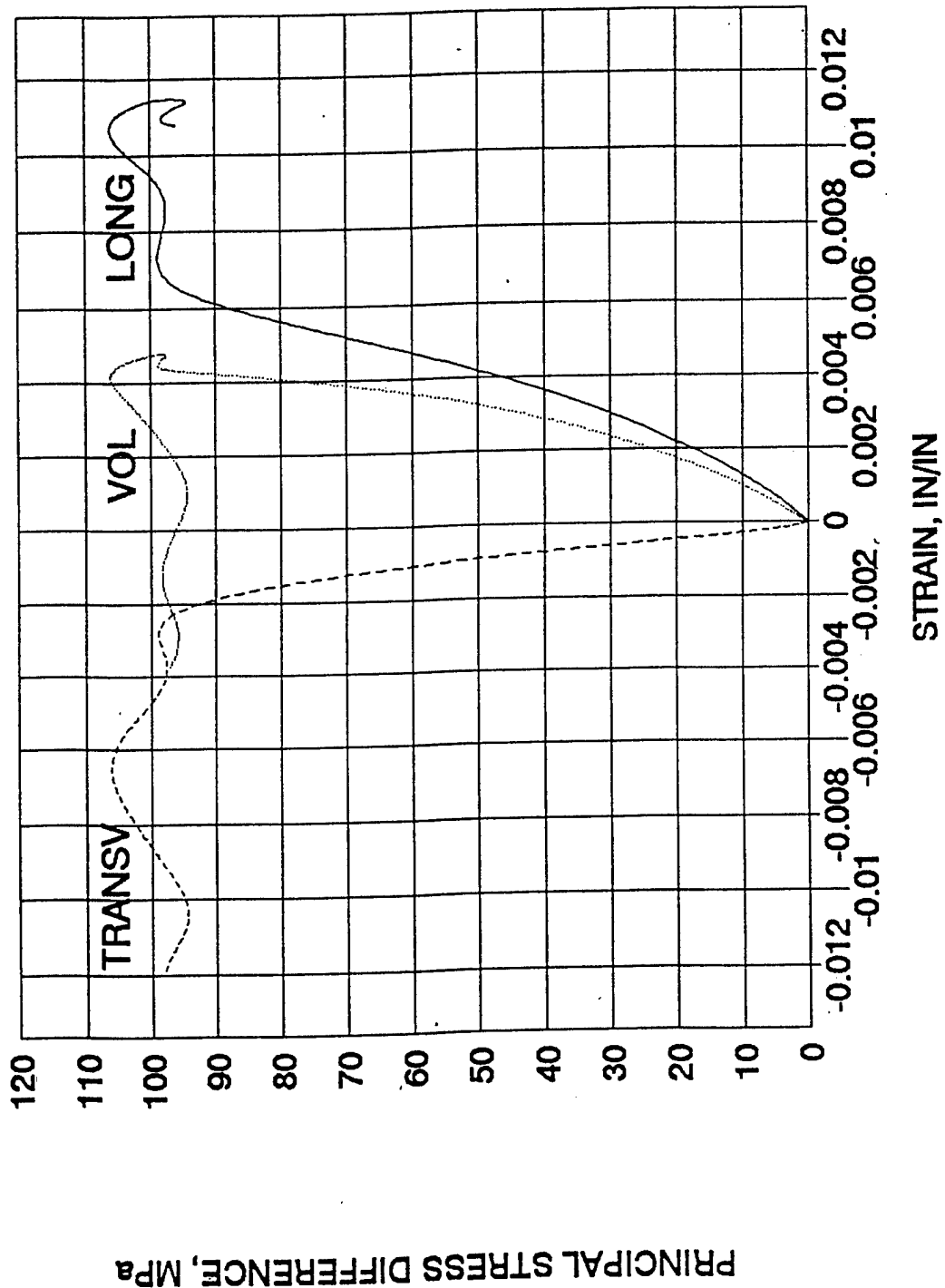


Figure A-10. Longitudinal, transverse and volumetric strain for dynamic confined mortar test.

DYNAMIC CONFINED TEST OF MORTAR

DCMC-20, CONFINING PRESSURE = 3.45 MPa, STRAIN RATE = 80/SEC

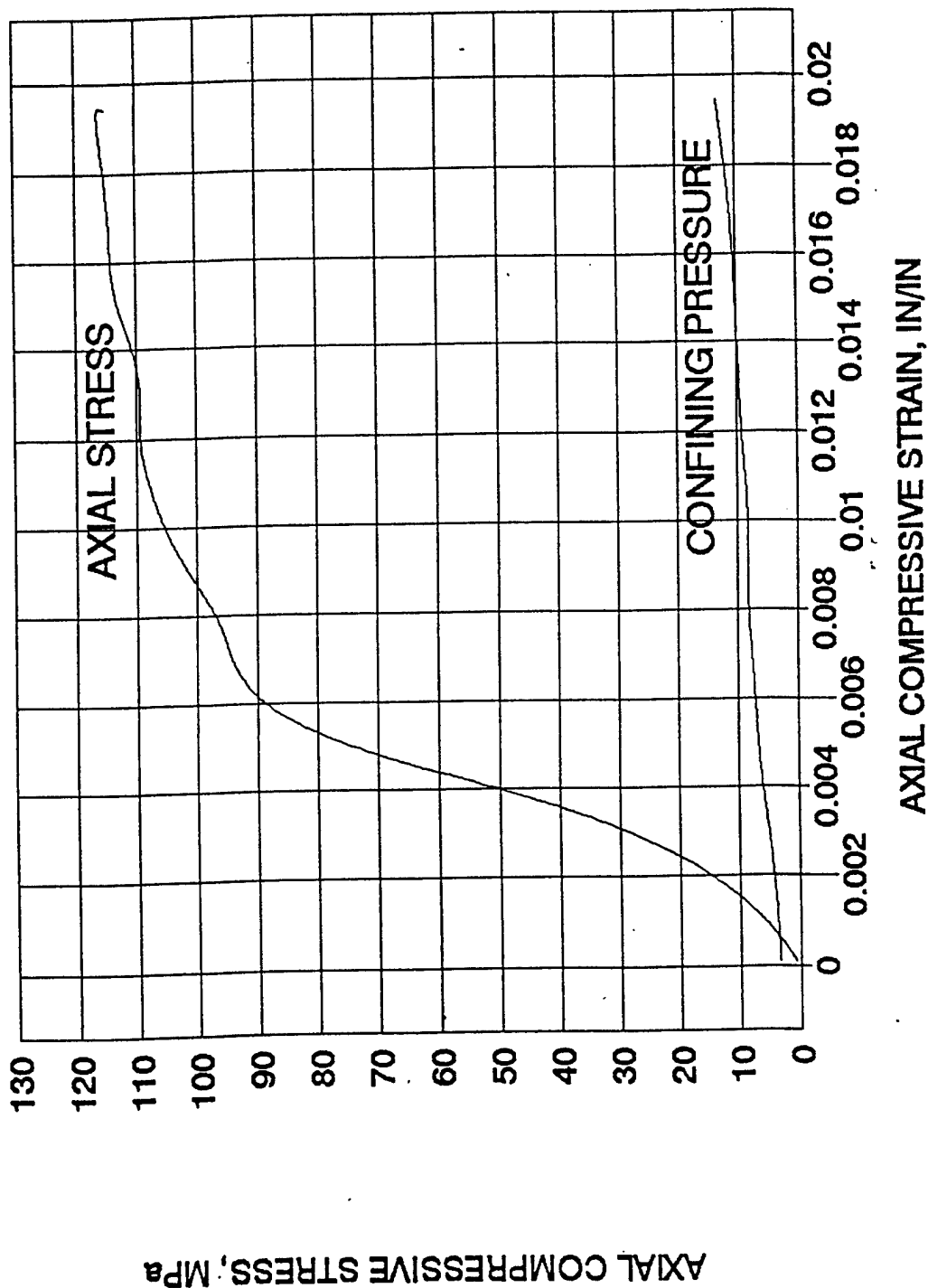


Figure A-11. Stress-strain curve and confining pressure for dynamic confined mortar test.

DYNAMIC CONFINED TEST OF MORTAR

DCMC-20, CONFINING PRESSURE = 3.45 MPa, STRAIN RATE = 80/SEC

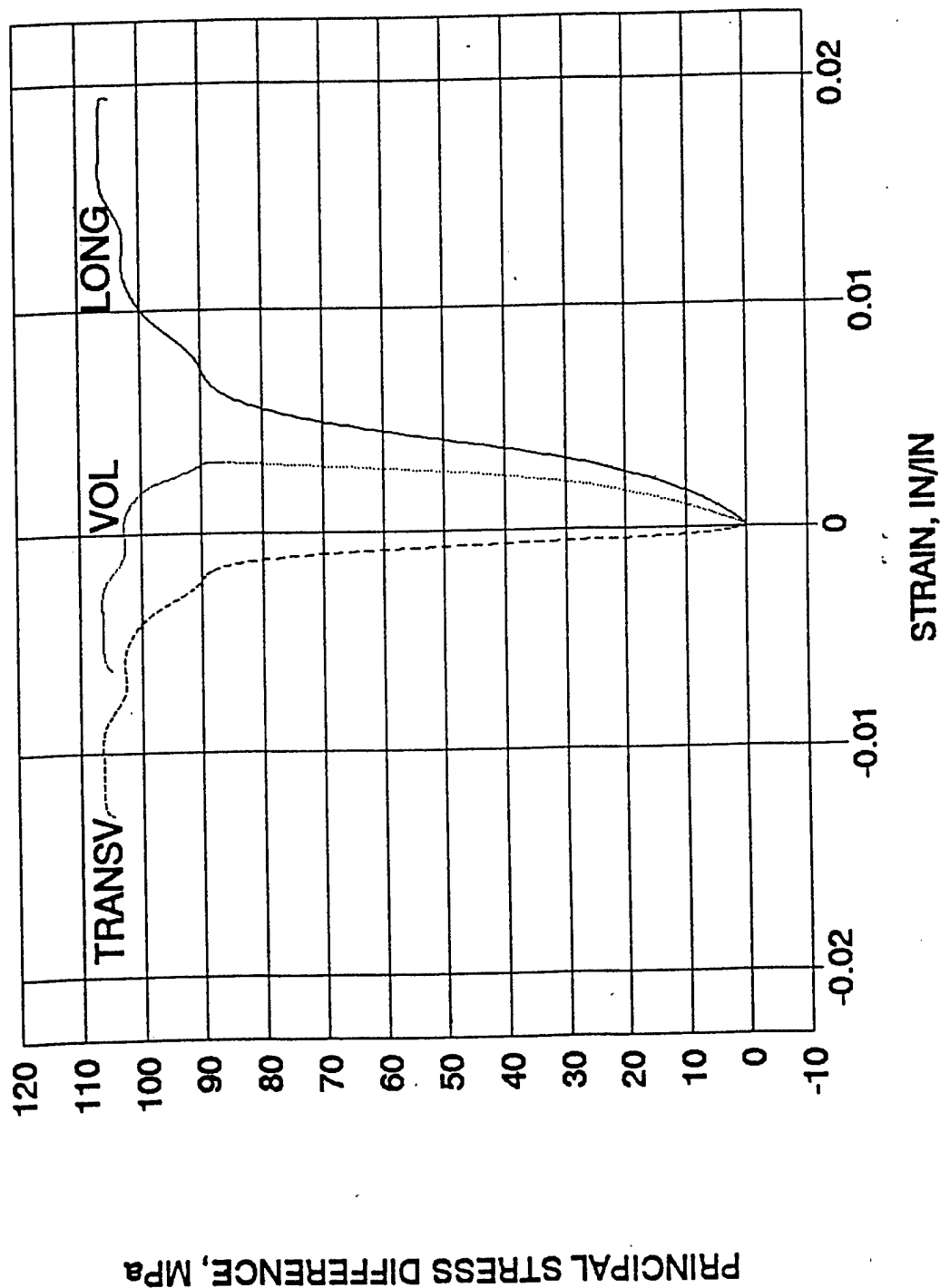


Figure A-12. Longitudinal, transverse and volumetric strain for dynamic confined mortar test.

DYNAMIC CONFINED TEST OF MORTAR

DCMC-30, CONFINING PRESSURE = 6.90 MPa, STRAIN RATE = 52/SEC

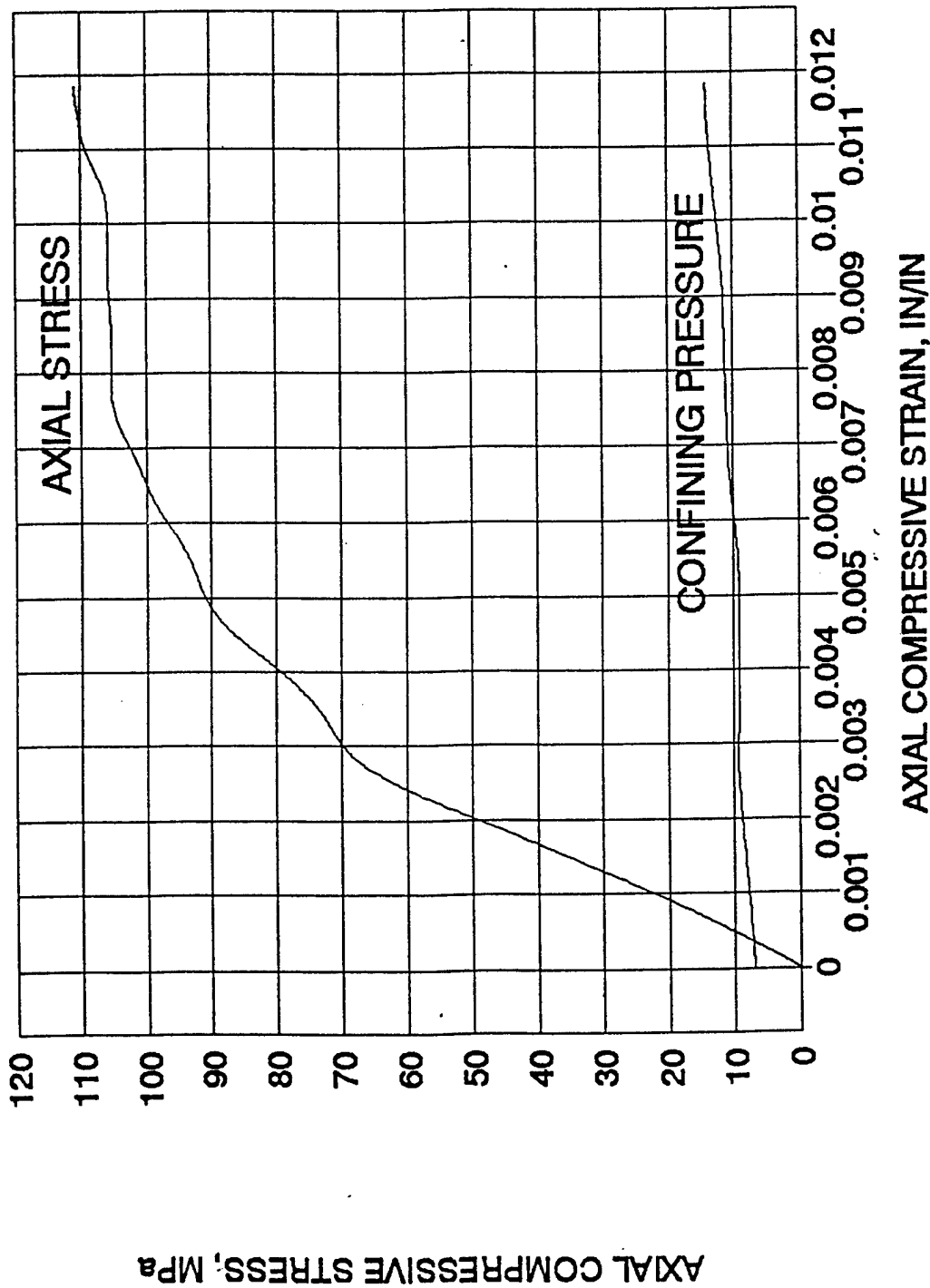


Figure A-13. Stress-strain curve and confining pressure for dynamic confined test of mortar.

DYNAMIC CONFINED TEST OF MORTAR

DCMC-30, CONFINING PRESSURE = 6.90 MPa, STRAIN RATE = 52/SEC

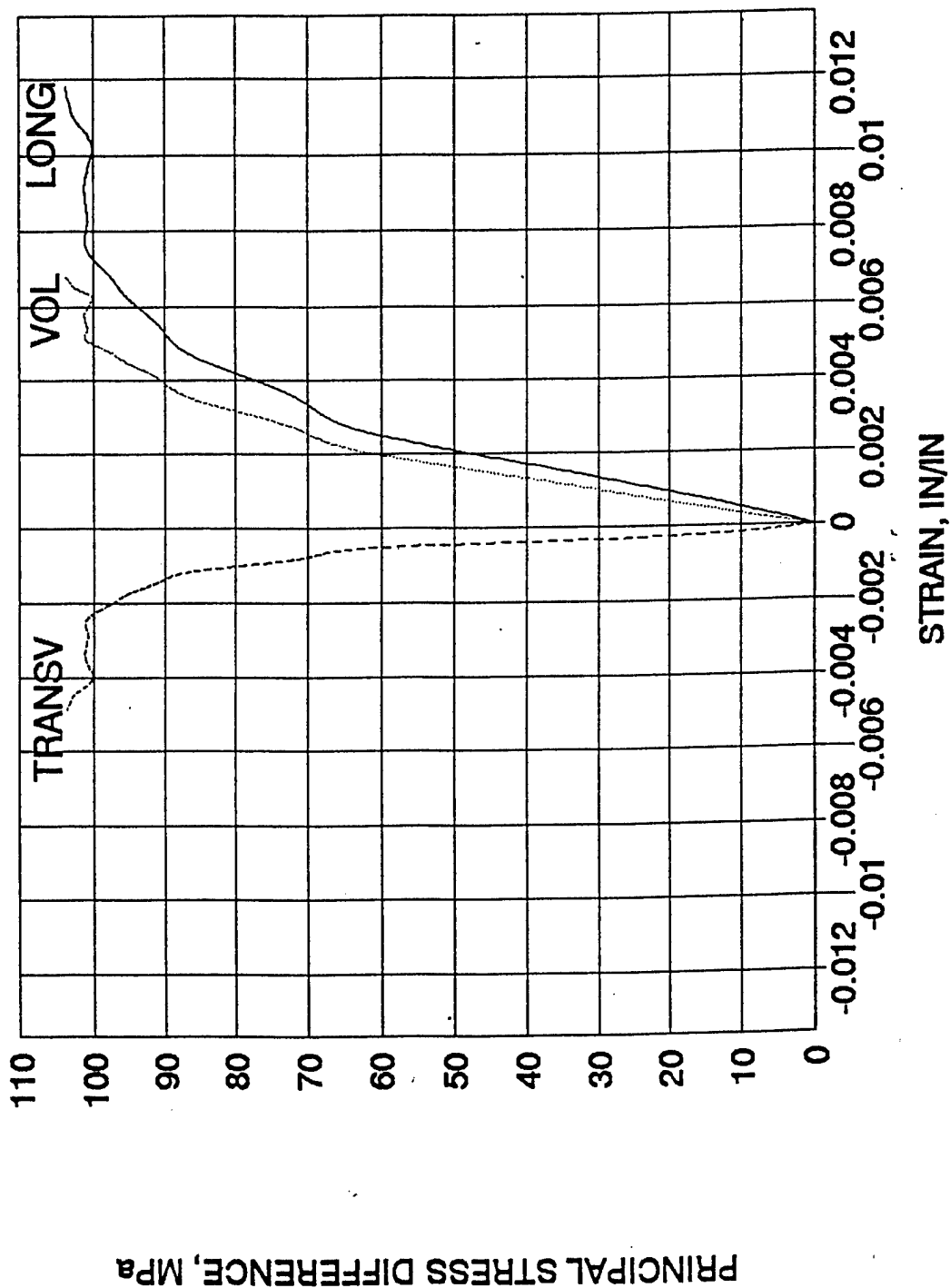


Figure A-14. Longitudinal, transverse and volumetric strain for dynamic confined mortar test.

DYNAMIC CONFINED TEST OF MORTAR

DCMC-24, CONFINING PRESSURE = 6.90 MPa, STRAIN RATE = 67/SEC

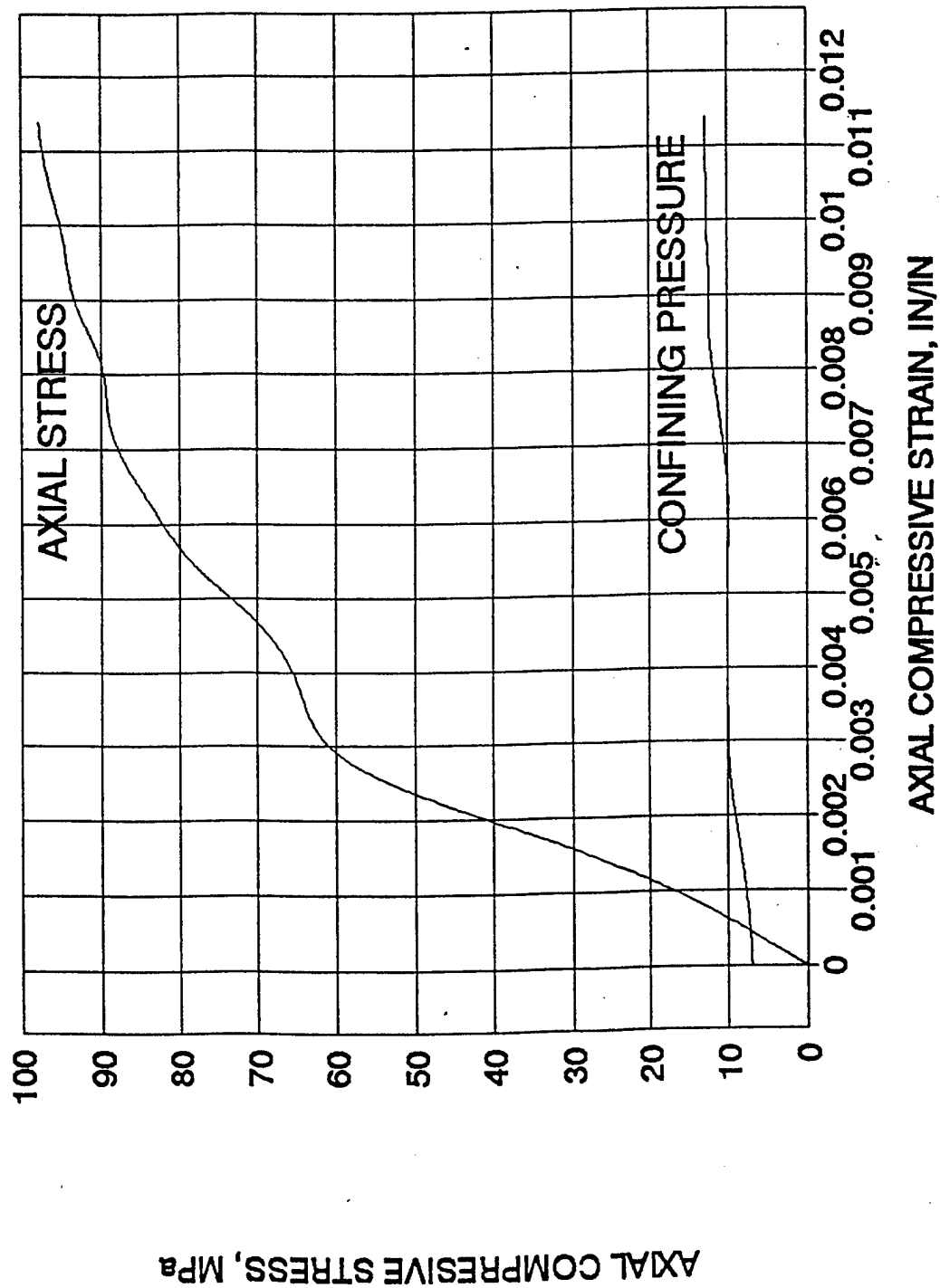


Figure A-15. Stress-strain curve and confining pressure for dynamic confined mortar test.

DYNAMIC CONFINED TEST OF MORTAR

DCMC-24, CONFINING PRESSURE = 6.90 MPa, STRAIN RATE = 67/SEC

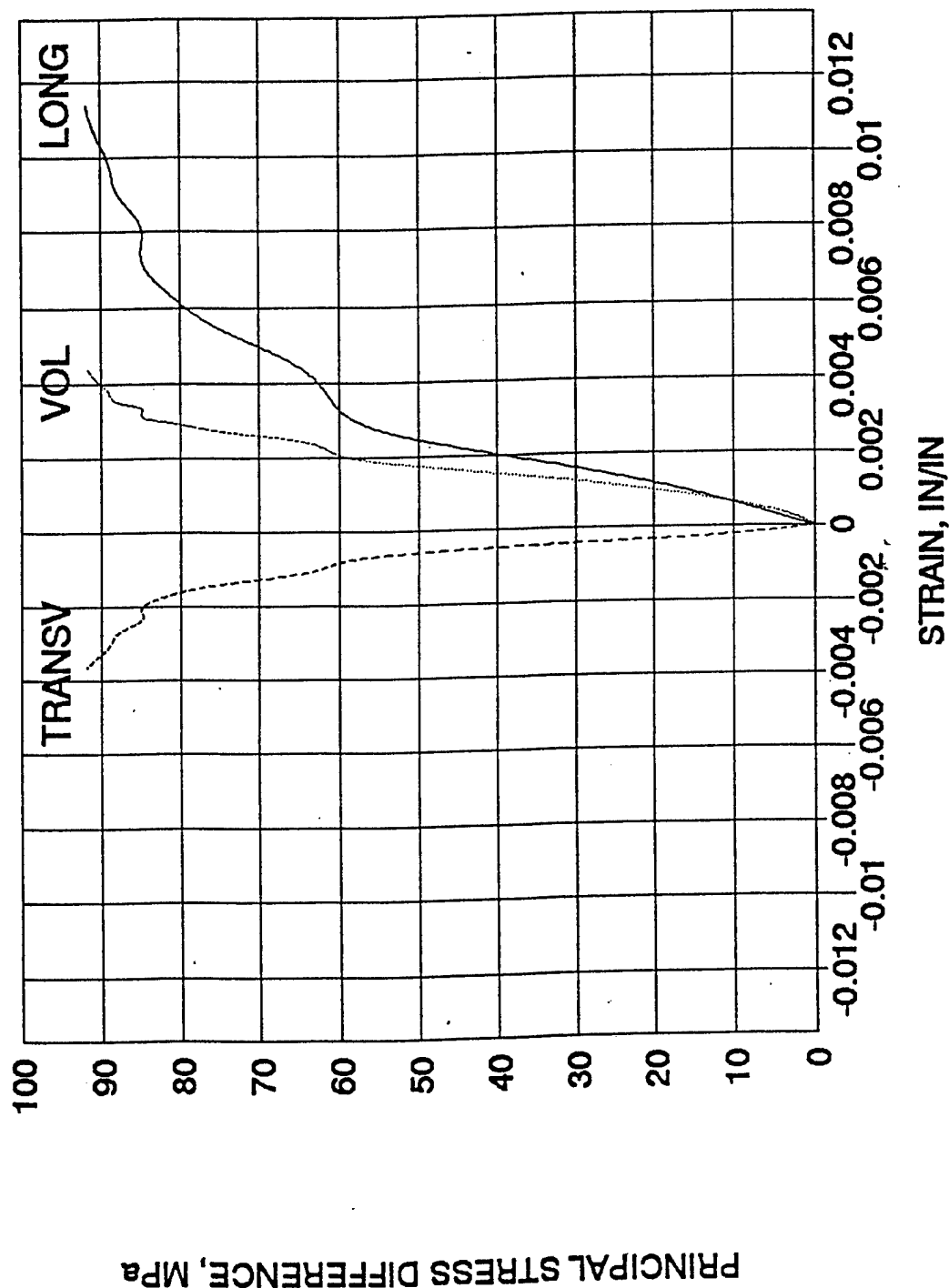


Figure A-16. Longitudinal, transverse and volumetric strain for dynamic confined mortar test.

DYNAMIC CONFINED TEST OF MORTAR

DCMC-25, CONFINING PRESSURE = 6.90 MPa, STRAIN RATE = 123/SEC

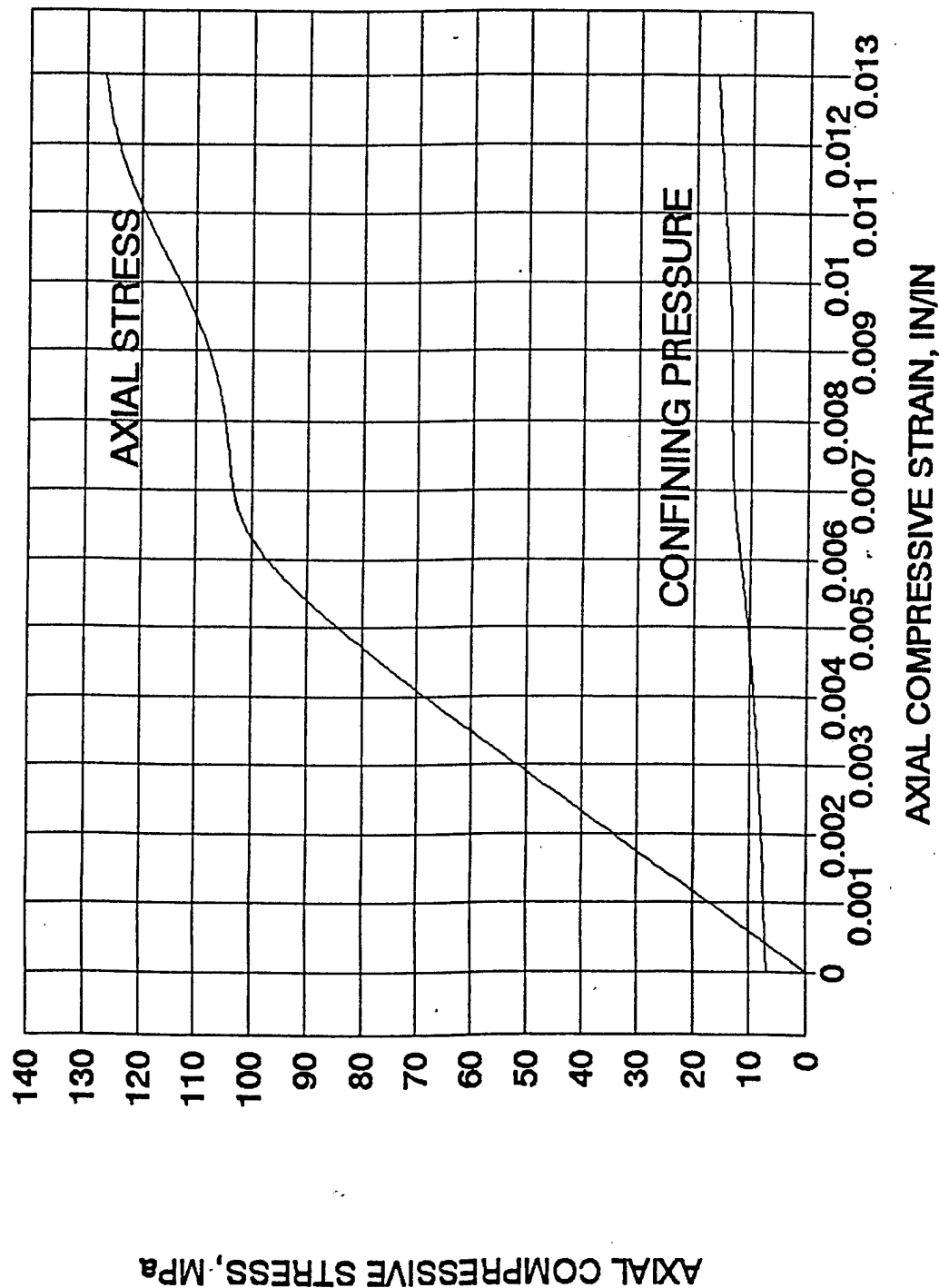


Figure A-17. Stress-strain curve and confining pressure for dynamic confined mortar test.

DYNAMIC CONFINED TEST OF MORTAR

DCMC-25, CONFINING PRESSURE = 6.90 MPa, STRAIN RATE = 123/SEC

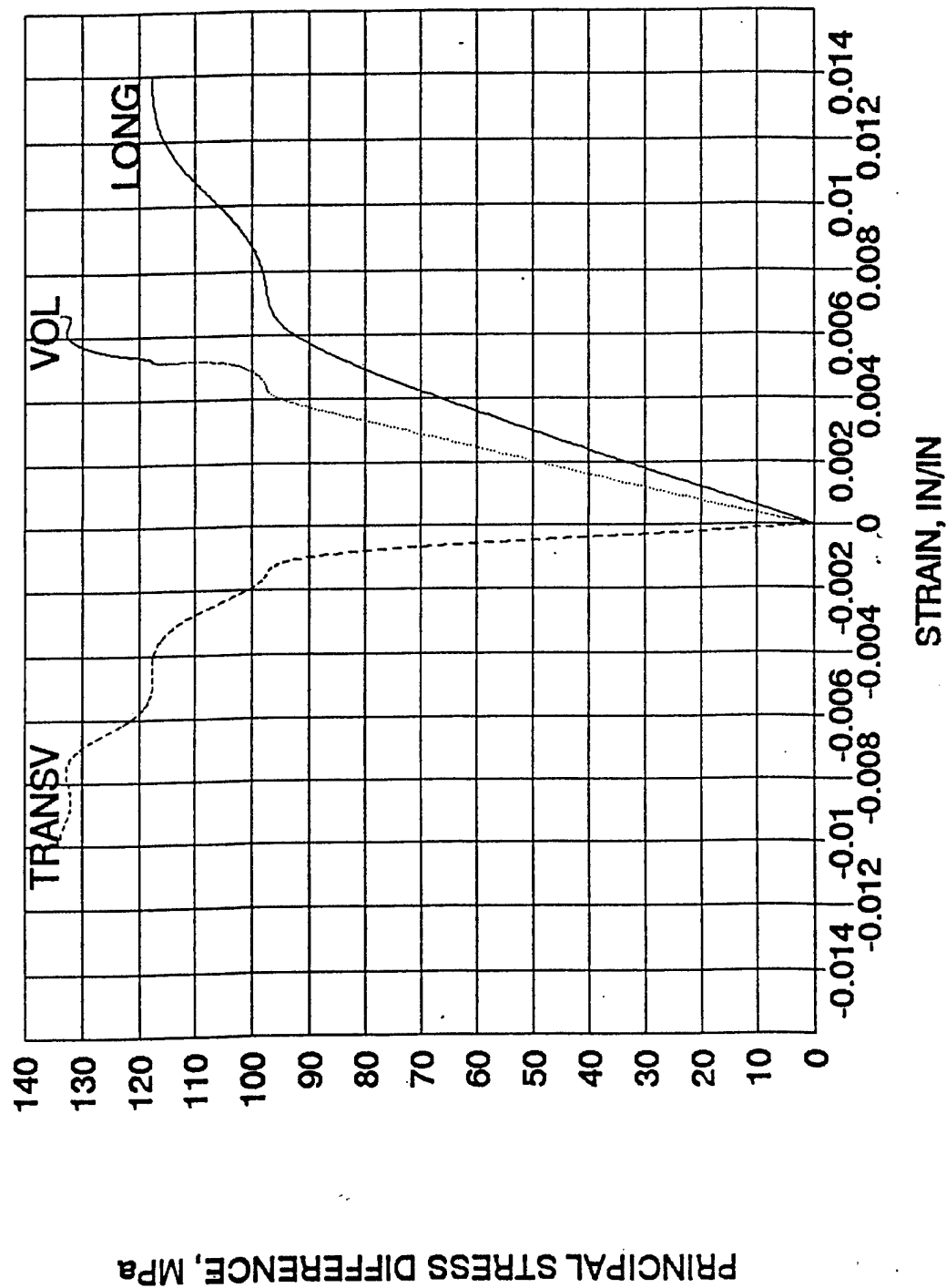


Figure A-18. Longitudinal, transverse and volumetric strain for dynamic confined mortar test.

QUASISTATIC MODULUS TEST FOR CONCRETE

QSC-1, STRAIN RATE = $0.77\text{E-}6/\text{SEC}$

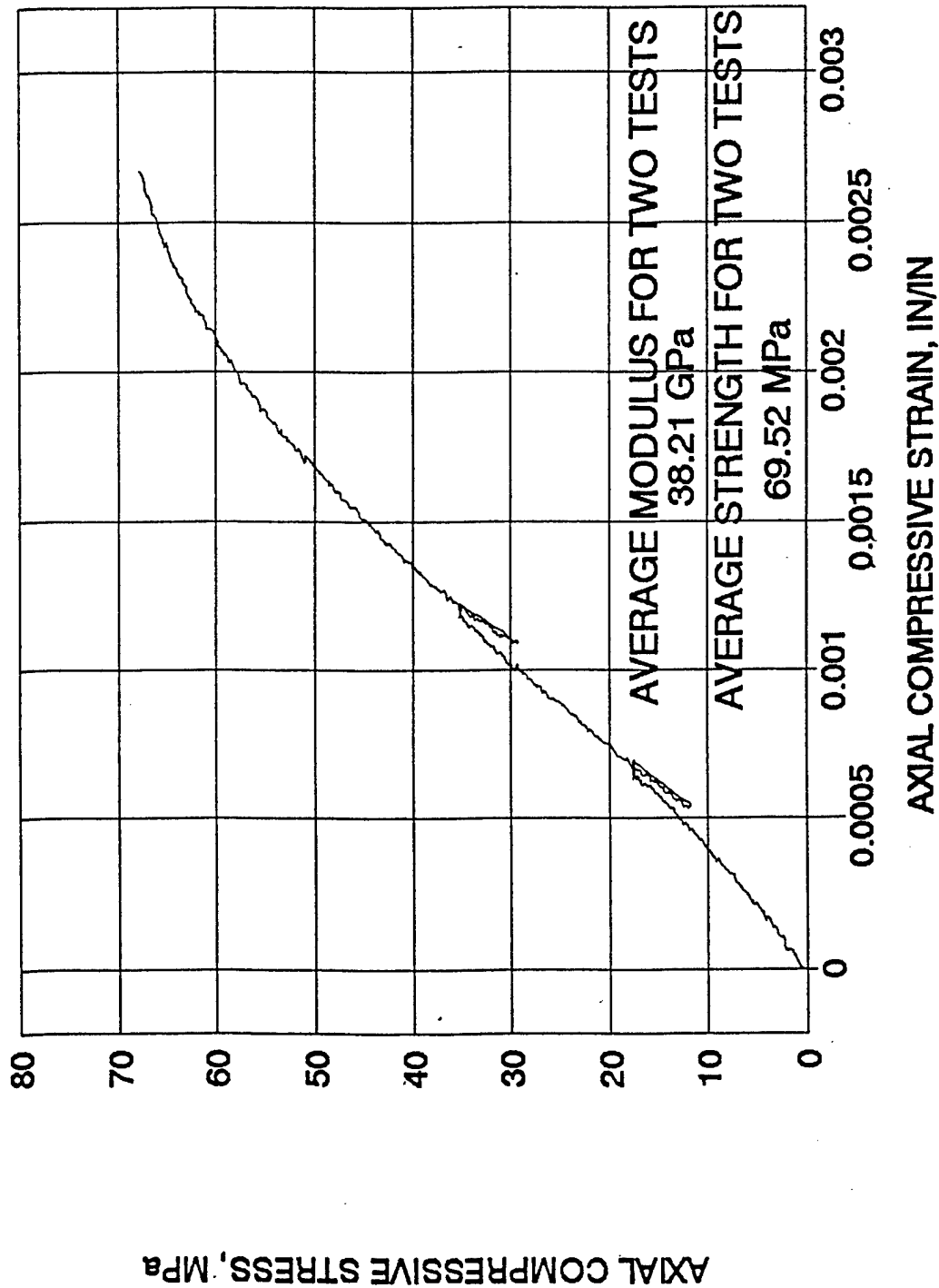


Figure A-19. Stress-strain curve for modulus test of concrete.

QUASISTATIC MODULUS TEST FOR CONCRETE

QSC-1, STRAIN RATE = $0.77E-6/SEC$

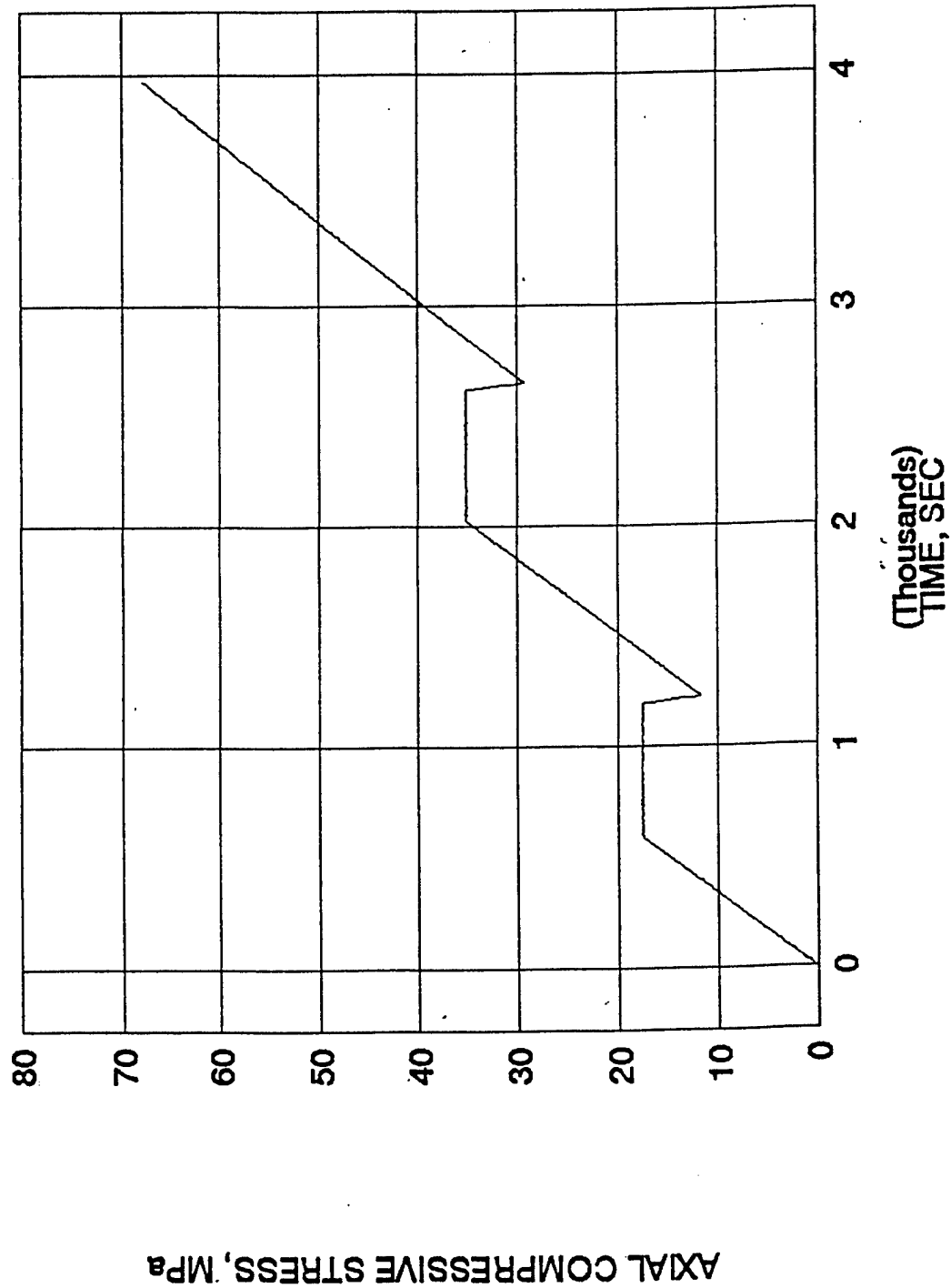


Figure A-20. Modulus test for quasistatic concrete.

QUASISTATIC CONFINED CONCRETE TEST

QSCC-1, CONFINING PRESSURE = 3.45 MPa, STRAIN RATE = 0.77E-6/SEC

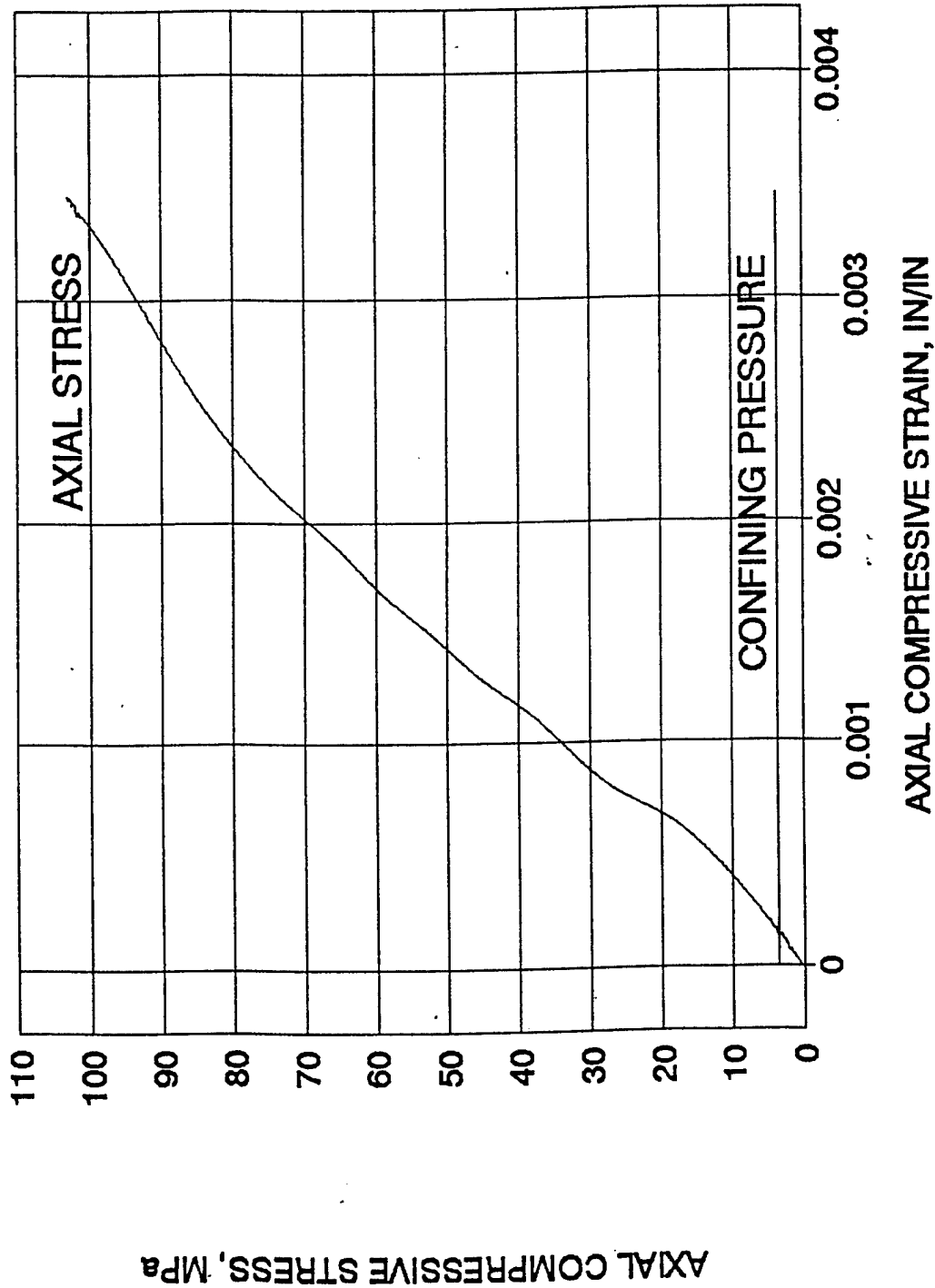


Figure A-21. Stress-strain curve and confining pressure for quastatic confined concrete test.

QUASISTATIC CONFINED CONCRETE TEST

QSCC-1, CONFINING PRESSURE = 3.45 MPa, STRAIN RATE = 0.77E-6/SEC

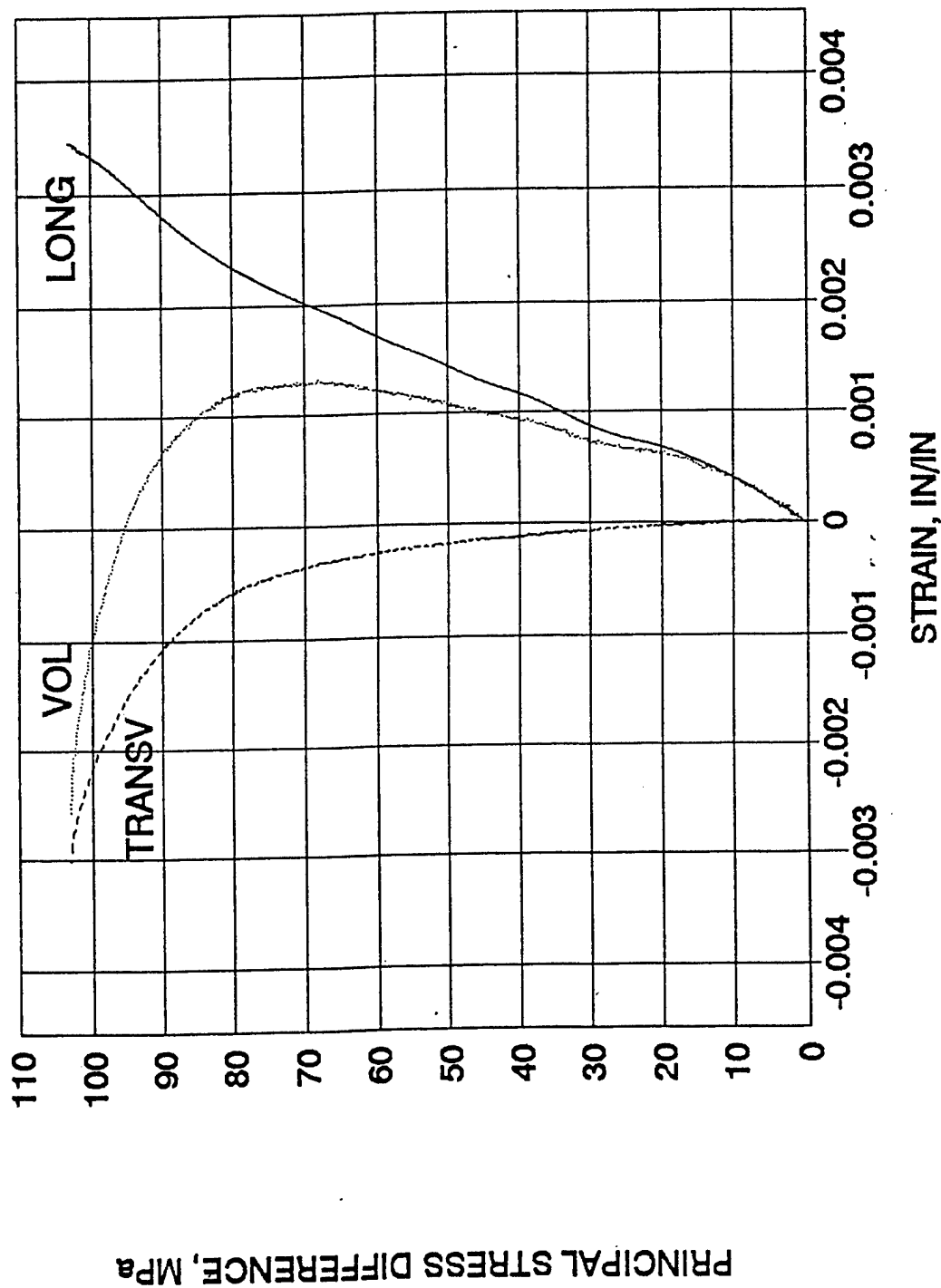


Figure A-22. Longitudinal, transverse and volumetric strain for quasistatic confined concrete test.

QUASISTATIC CONFINED CONCRETE TEST

QSCC-6, CONFINING PRESSURE = 6.90 MPa, STRAIN RATE = $0.77\text{E-}6/\text{SEC}$

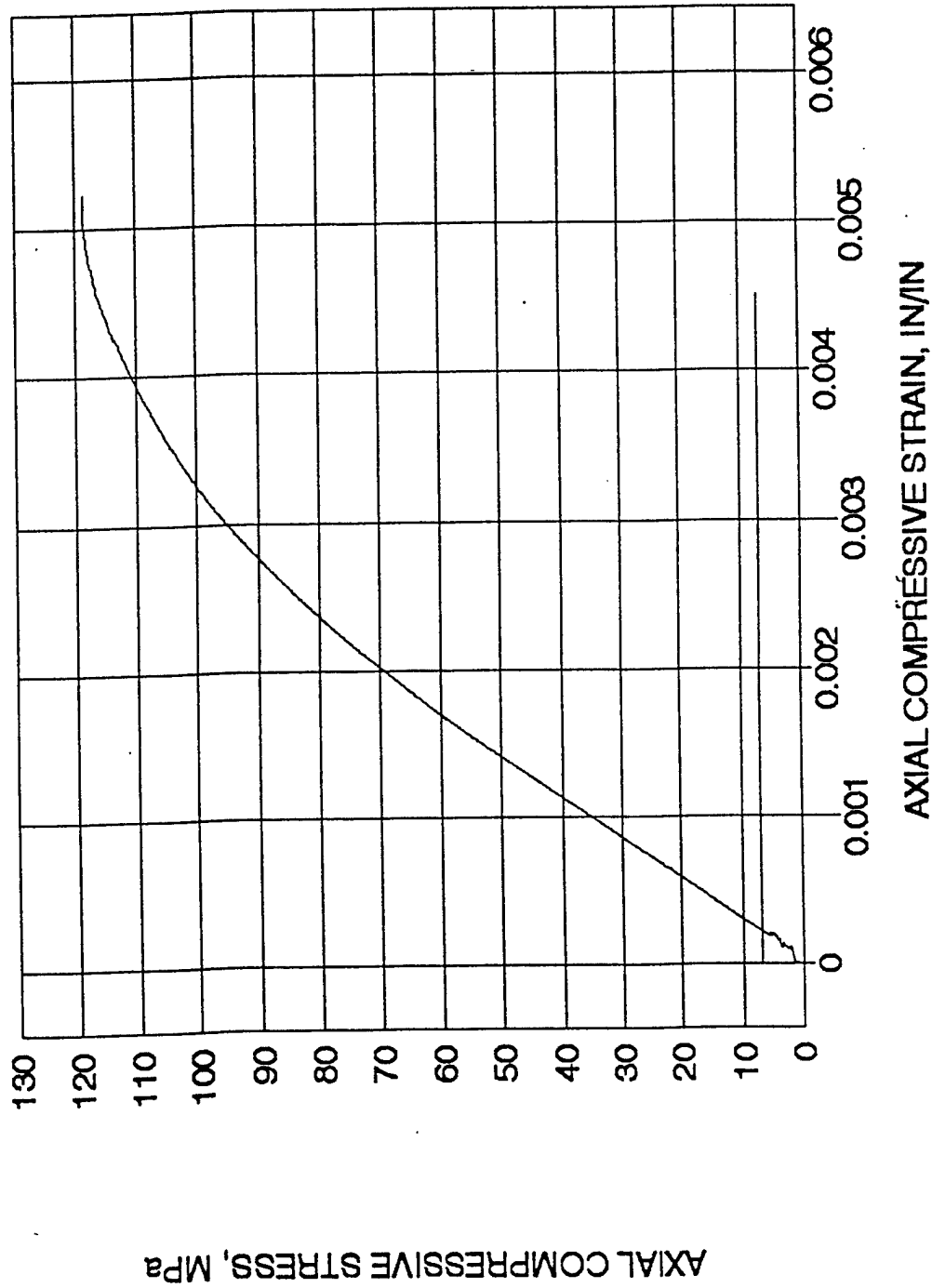


Figure A-23. Stress-strain curve and confining pressure for quasistatic confined concrete test.

QUASISTATIC CONFINED CONCRETE TEST

QSCC-6, CONFINING PRESSURE = 6.90 MPa, STRAIN RATE = 0.77E-6/SEC

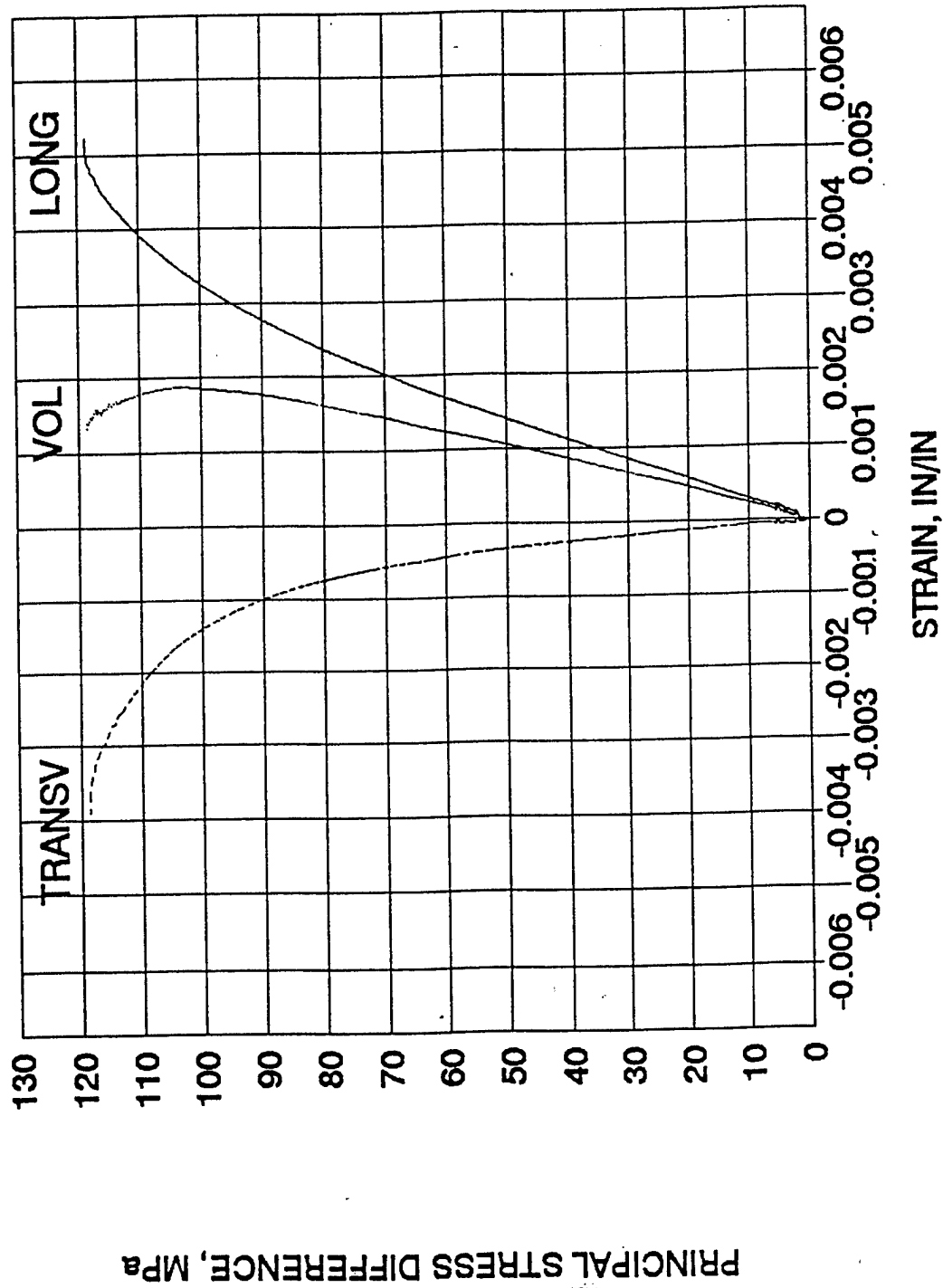


Figure A-24. Longitudinal, transverse and volumetric strain for quastatic confined concrete test.

QUASISTATIC CONFINED CONCRETE TEST

QSCC-12, CONFINING PRESSURE = 1.81 MPa, STRAIN RATE = 0.77E-6/SEC

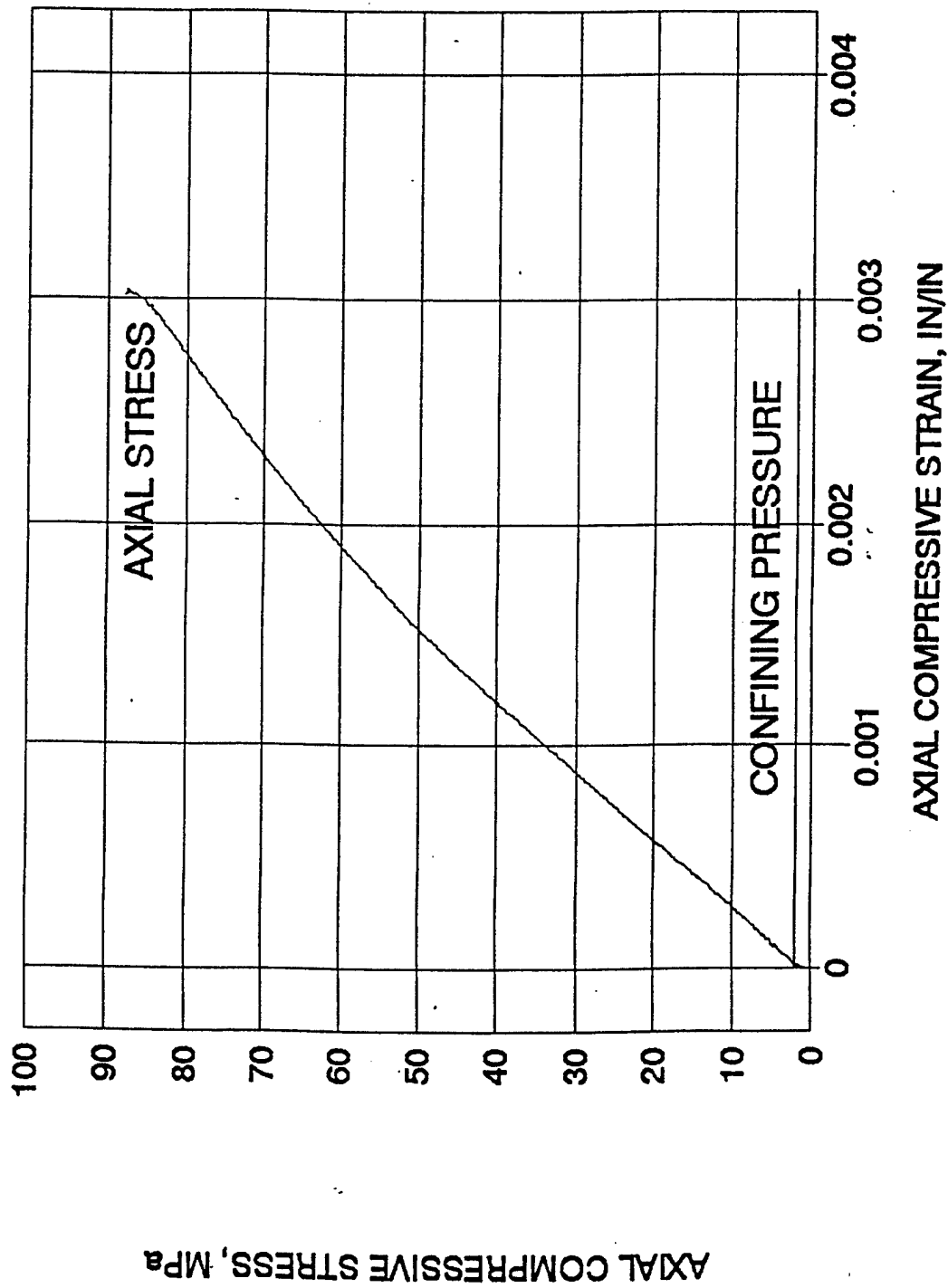


Figure A-25. Stress-strain curve and confining pressure for quastatic confined concrete test.

QUASISTATIC CONFINED CONCRETE TEST

QSCC-12, CONFINING PRESSURE = 1.81 MPa, STRAIN RATE = $0.77\text{E-}6/\text{SEC}$

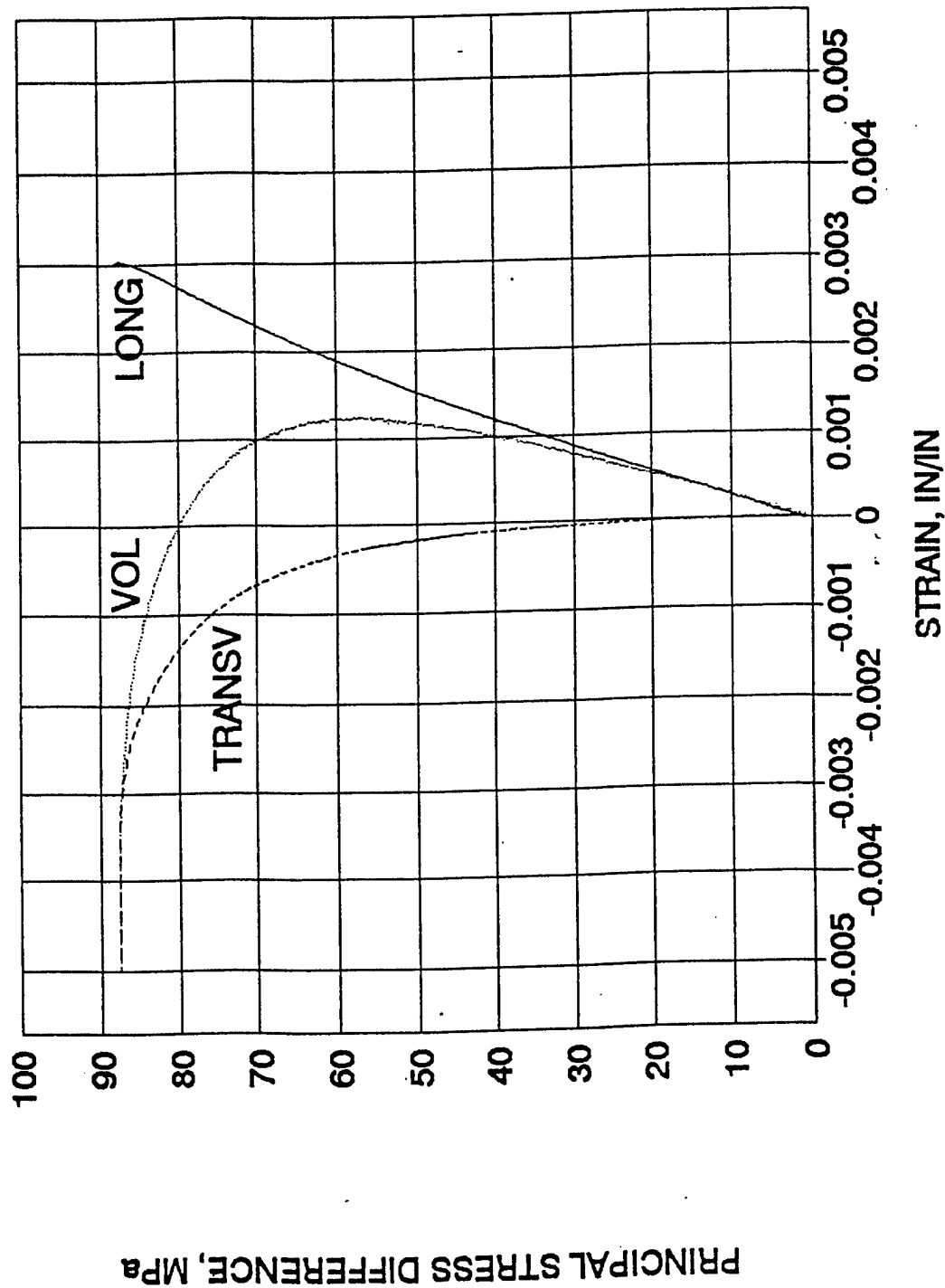


Figure A-26. Longitudinal, transverse and volumetric strain for quasistatic confined concrete test.

DYNAMIC UNCONFINED CONCRETE TEST

DCCU-2, STRAIN RATE = 64/SEC

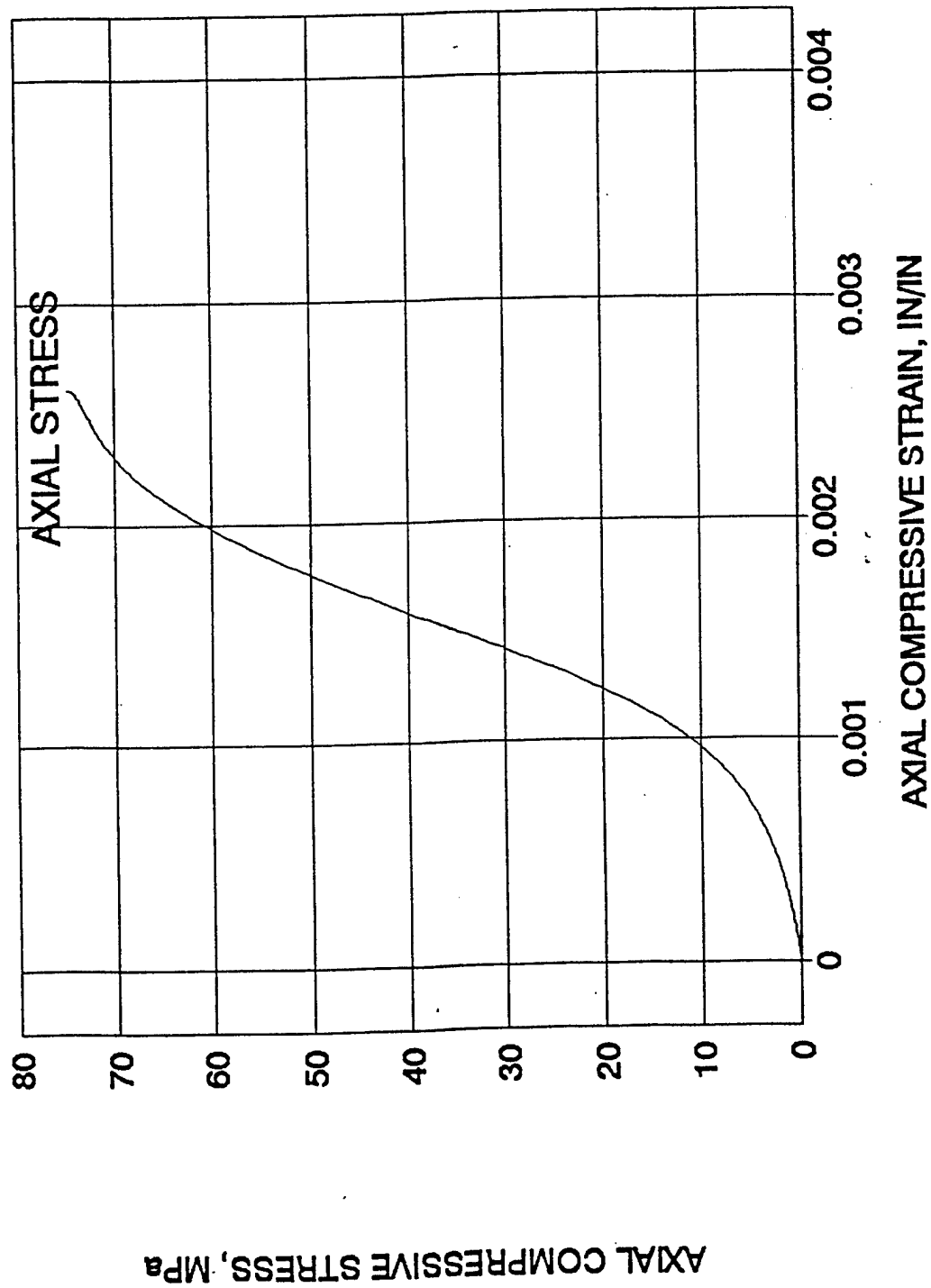


Figure A-27. Stress-strain curve for dynamic unconfined concrete test.

DYNAMIC UNCONFINED CONCRETE TEST

DCCU-2, STRAIN RATE = 64/SEC

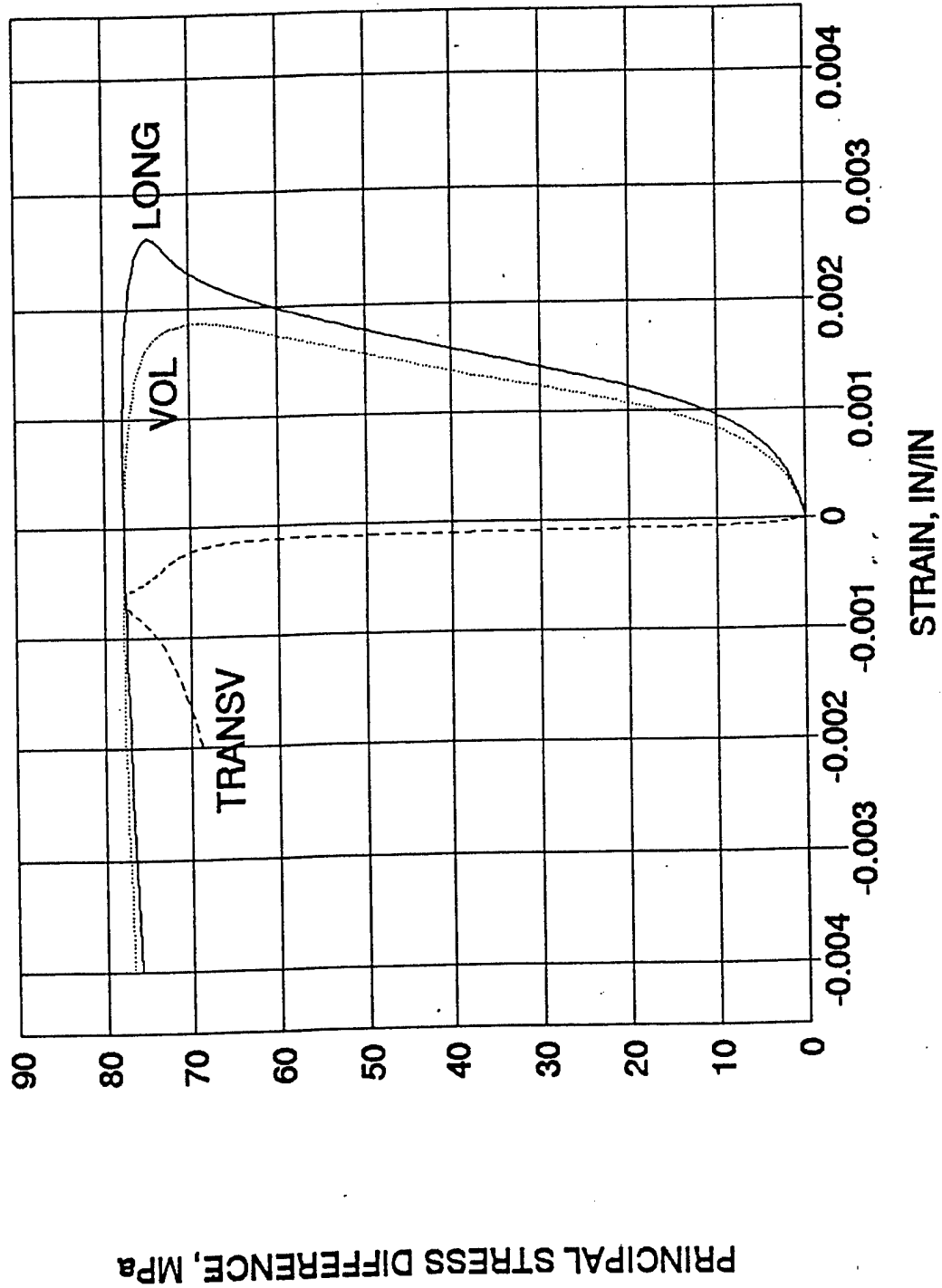


Figure A-28. Longitudinal, transverse and volumetric strain for dynamic unconfined concrete test.

DYNAMIC UNCONFINED CONCRETE TEST

DCCU-3, STRAIN RATE = 52/SEC

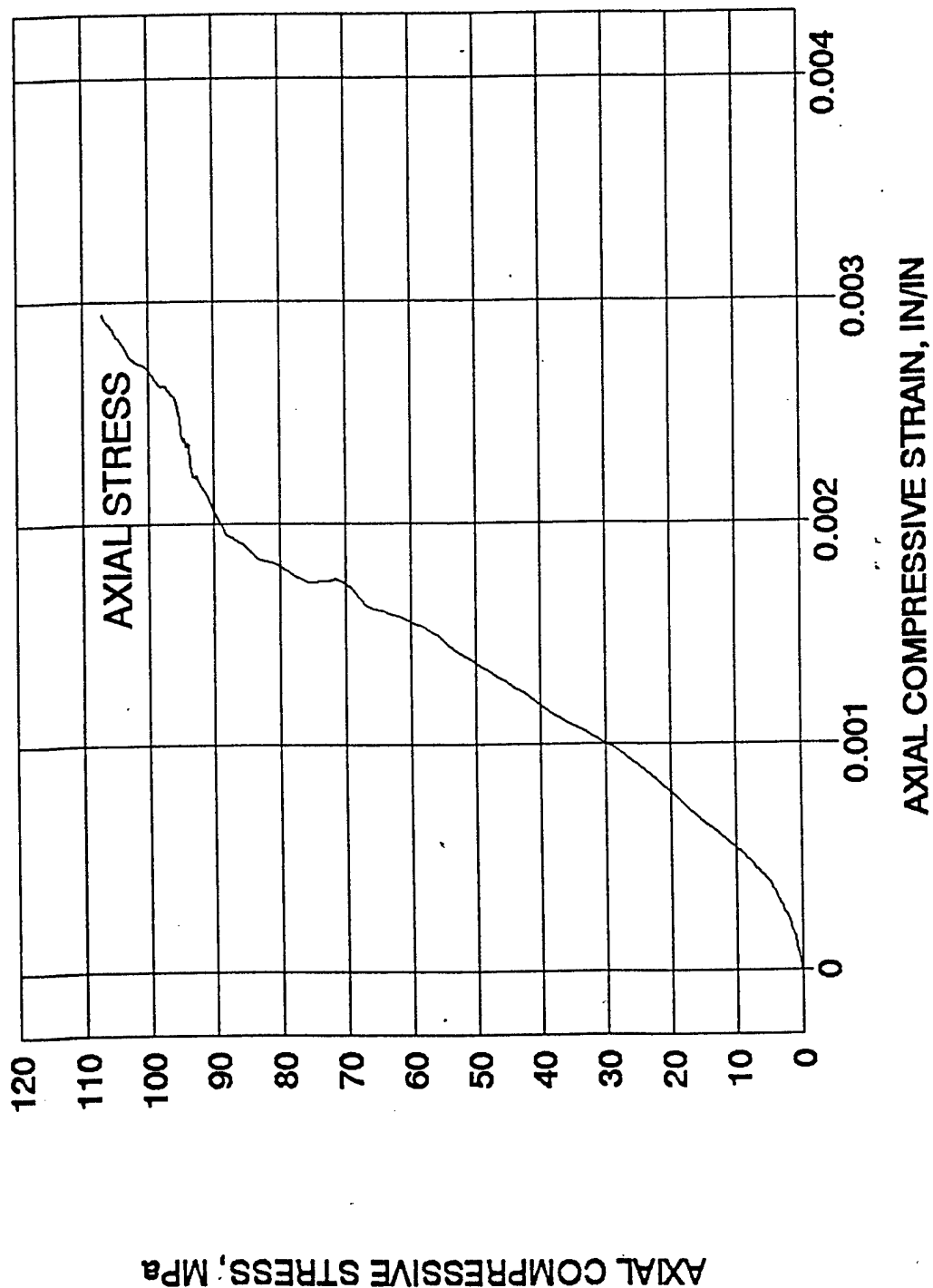


Figure A-29. Stress-strain curve for dynamic unconfined concrete test.

DYNAMIC UNCONFINED CONCRETE TEST

DCCU-3, STRAIN RATE = 52/SEC

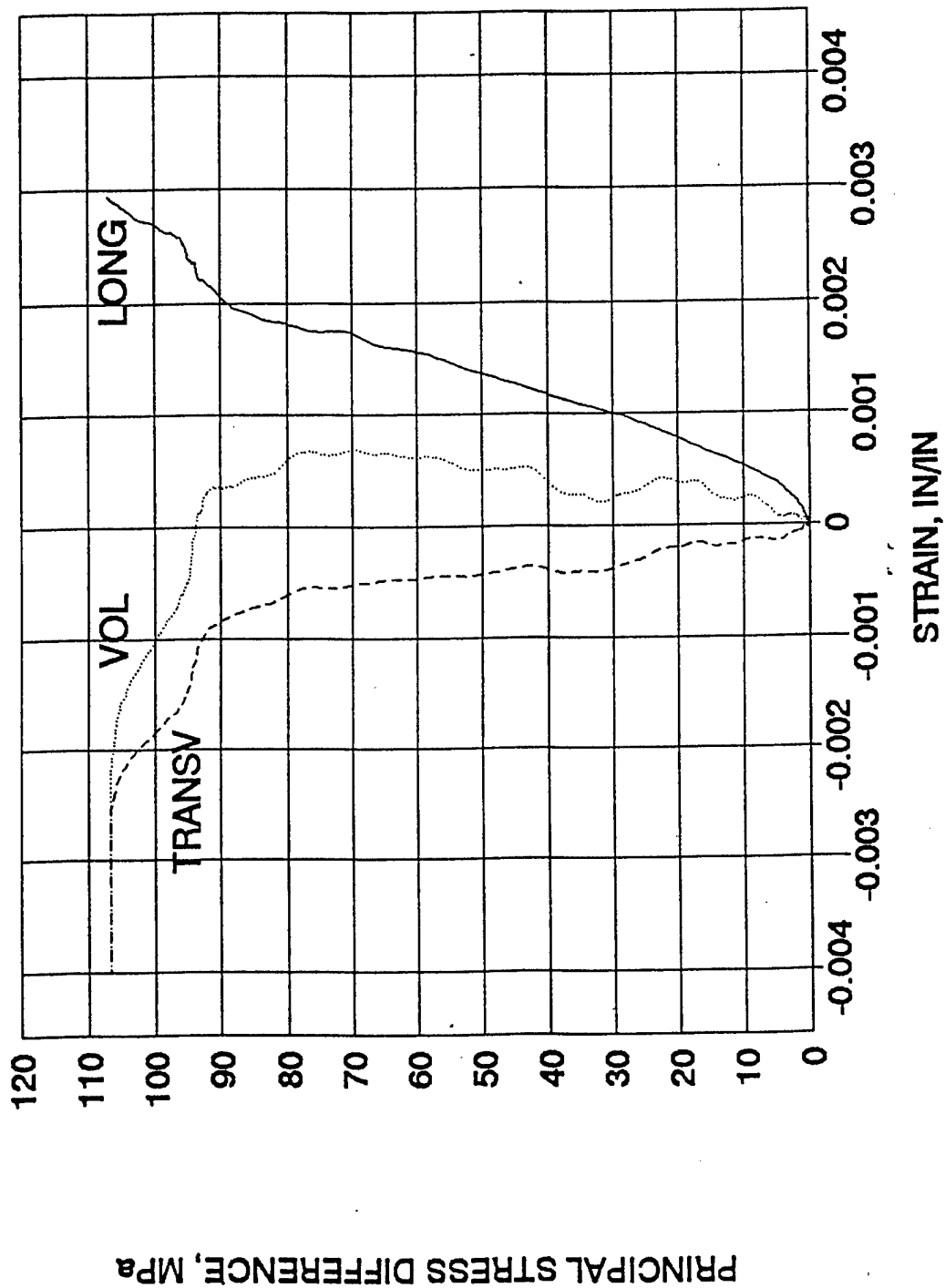


Figure A-30. Longitudinal, transverse and volumetric strain for dynamic unconfined concrete test.

DYNAMIC UNCONFINED CONCRETE TEST

DCCU-5, STRAIN RATE = 107/SEC

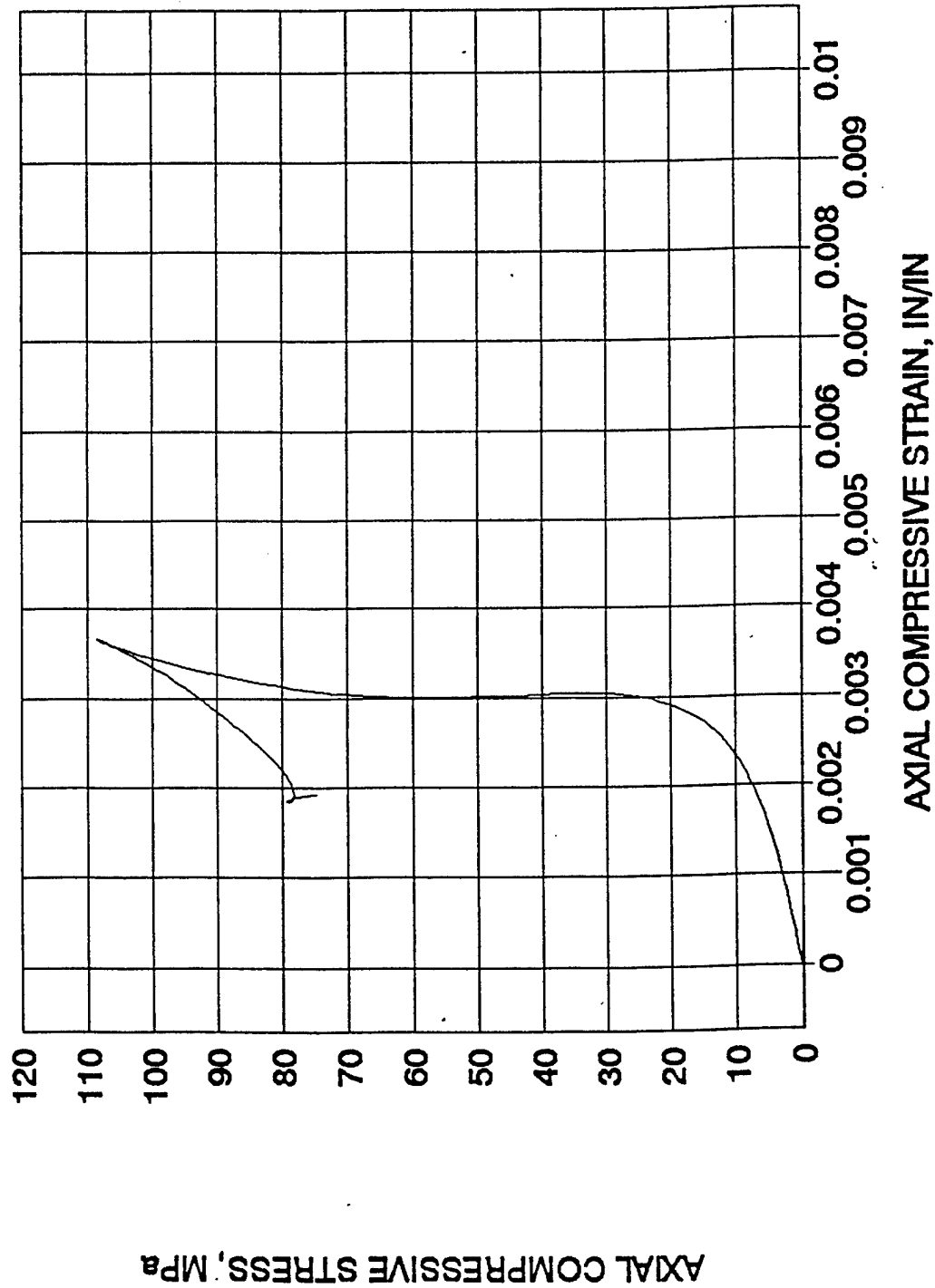


Figure A-31. Stress-strain curve for dynamic unconfined concrete test.

DYNAMIC UNCONFINED CONCRETE TEST

DCCU-5, STRAIN RATE = 107/SEC

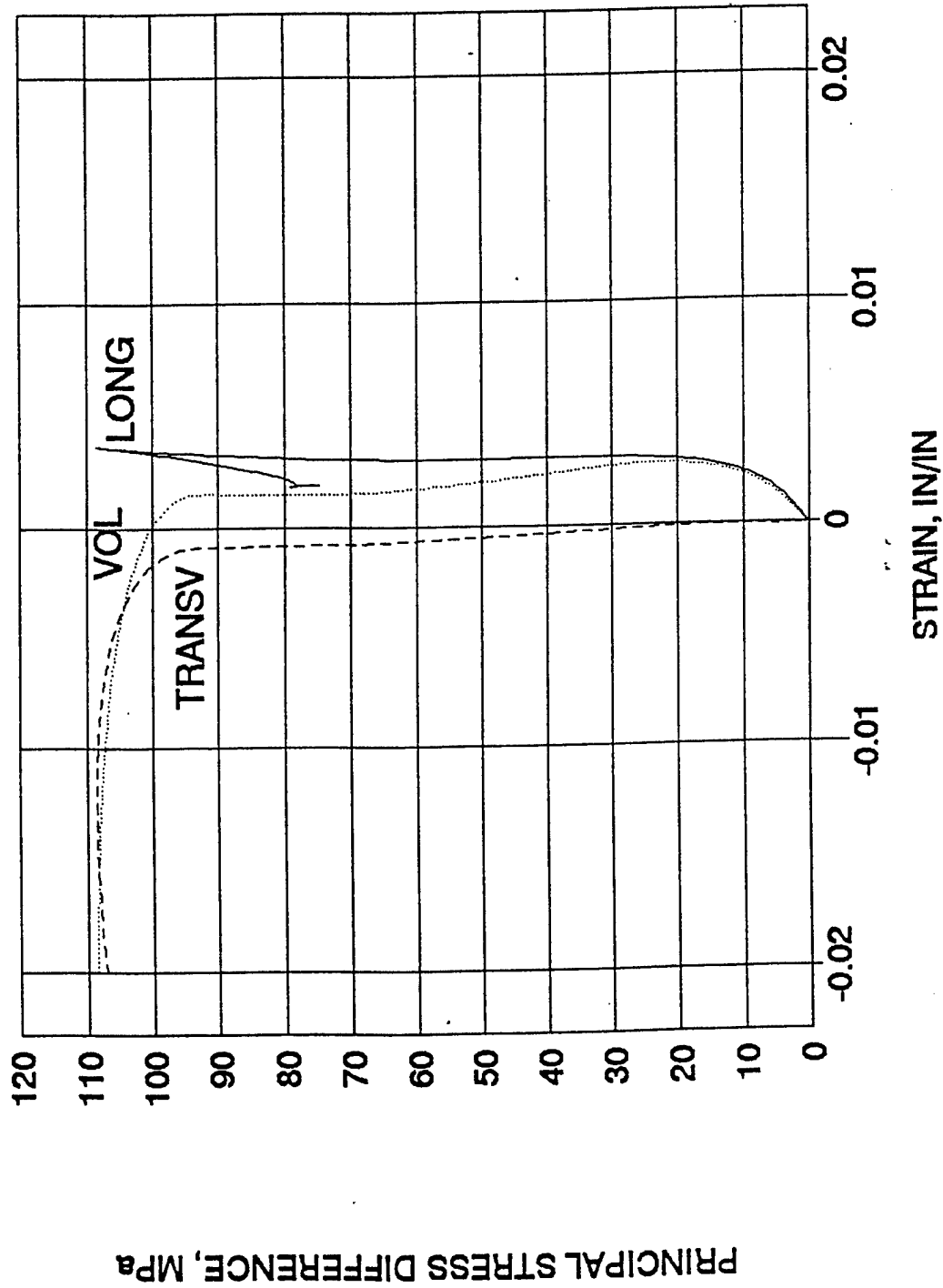


Figure A-32. Longitudinal, transverse and volumetric strain for dynamic unconfined concrete test.

DYNAMIC CONFINED CONCRETE TEST

DCCC-3, CONFINING PRESSURE = 3.40 MPa, STRAIN RATE = 47/SEC

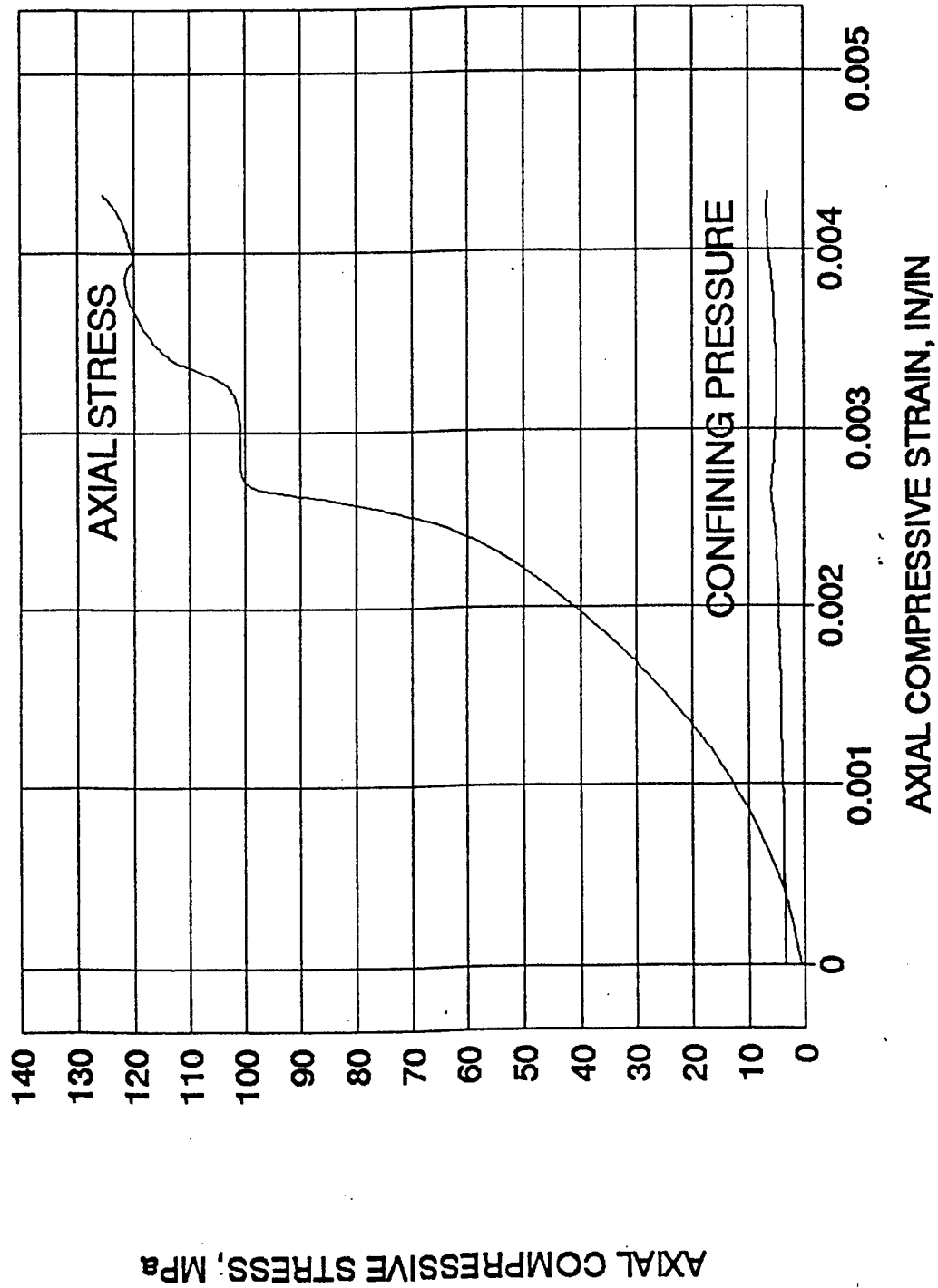


Figure A-33. Stress-strain curve and confining pressure for dynamic confined concrete test.

DYNAMIC CONFINED CONCRETE TEST

DCCC-3, CONFINING PRESSURE = 3.40 MPa, STRAIN RATE = 47/SEC

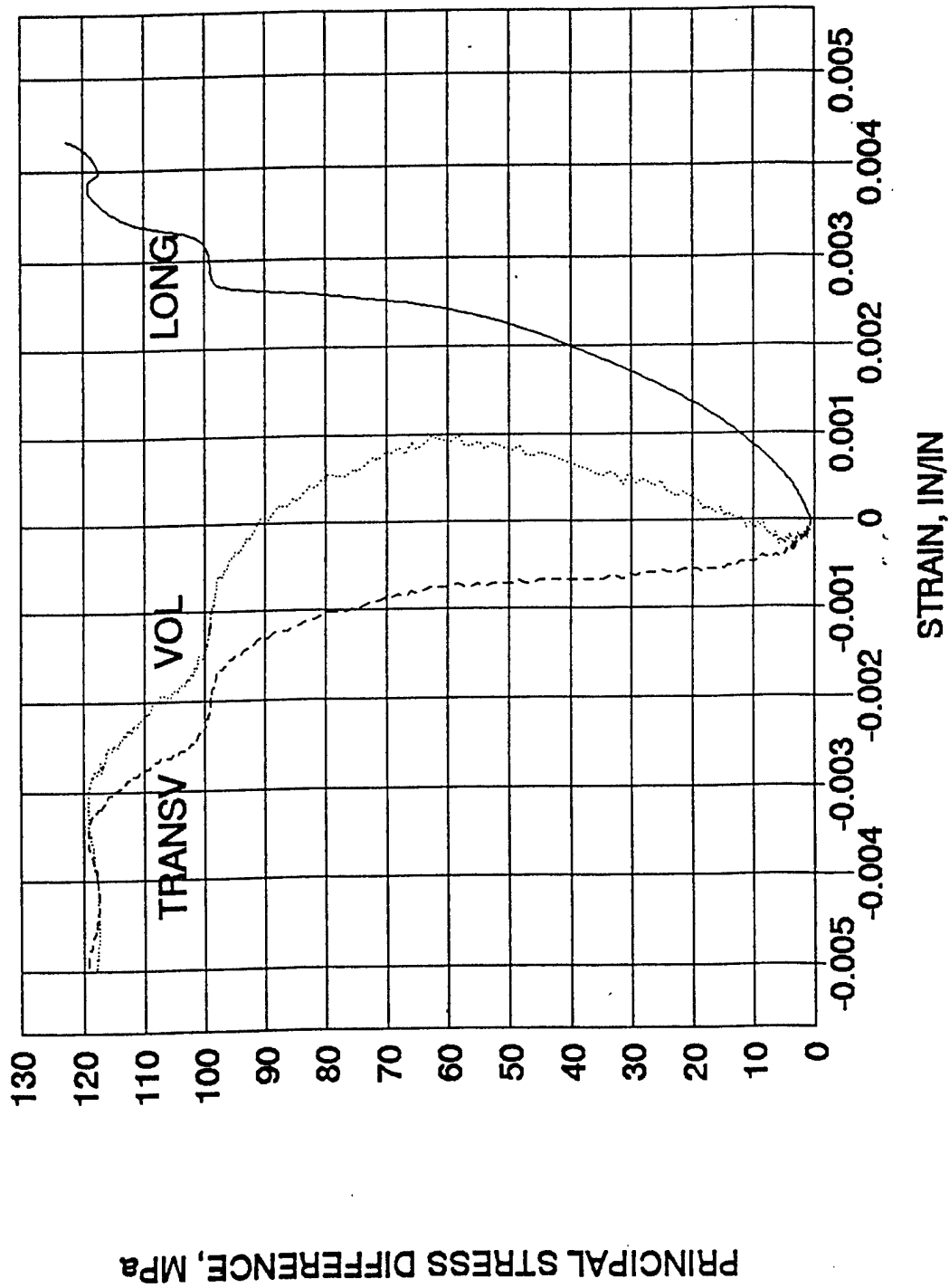


Figure A-34. Longitudinal, transverse and volumetric strain for dynamic confined concrete test.

DYNAMIC CONFINED CONCRETE TEST

DCCC-4, CONFINING PRESSURE = 3.57 MPa, STRAIN RATE = 53/SEC

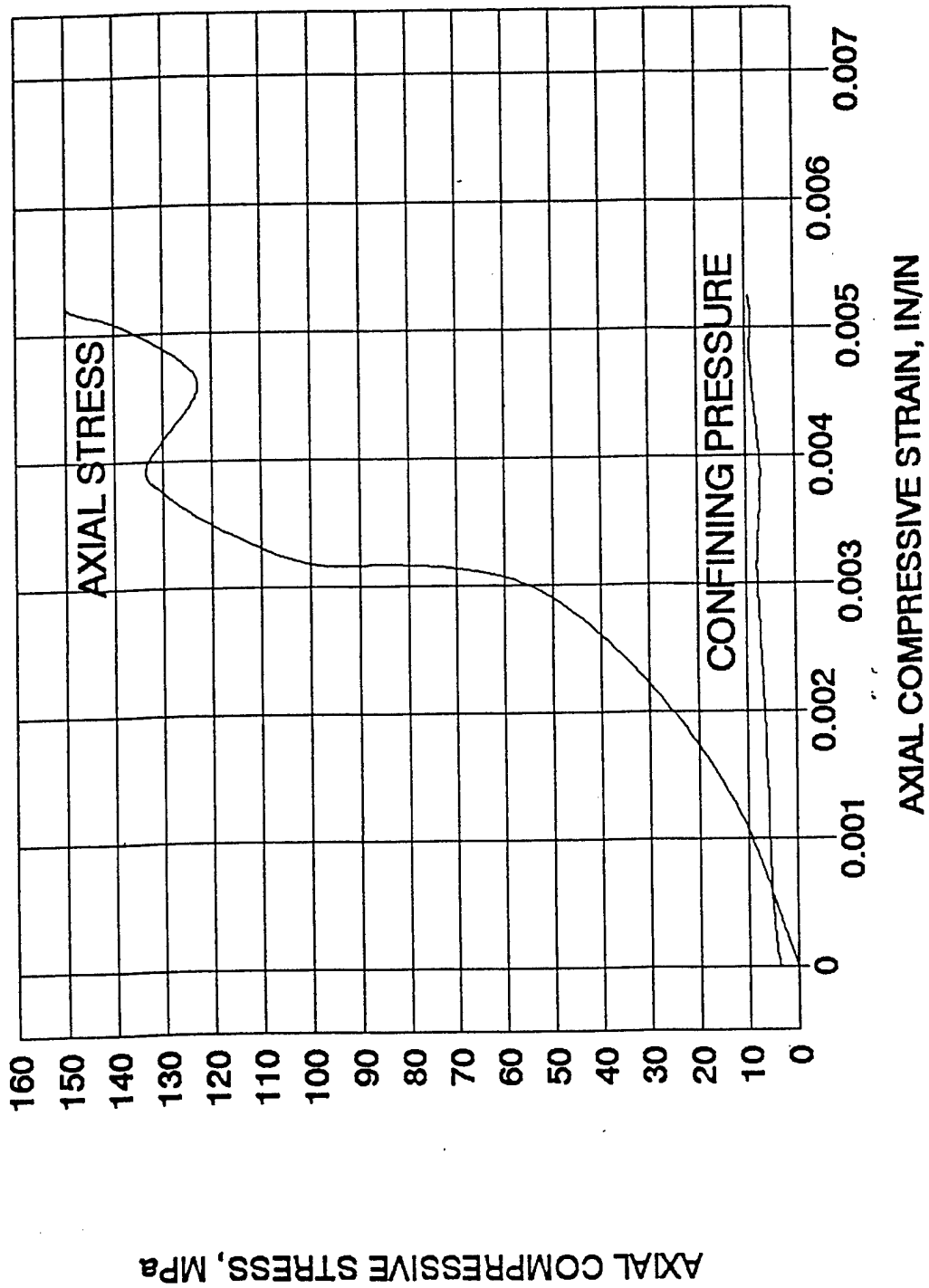


Figure A-35. Stress-strain curve and confining pressure for dynamic confined concrete test.

DYNAMIC CONFINED CONCRETE TEST

DCCC-4, CONFINING PRESSURE = 3.57 MPa, STRAIN RATE = 53/SEC

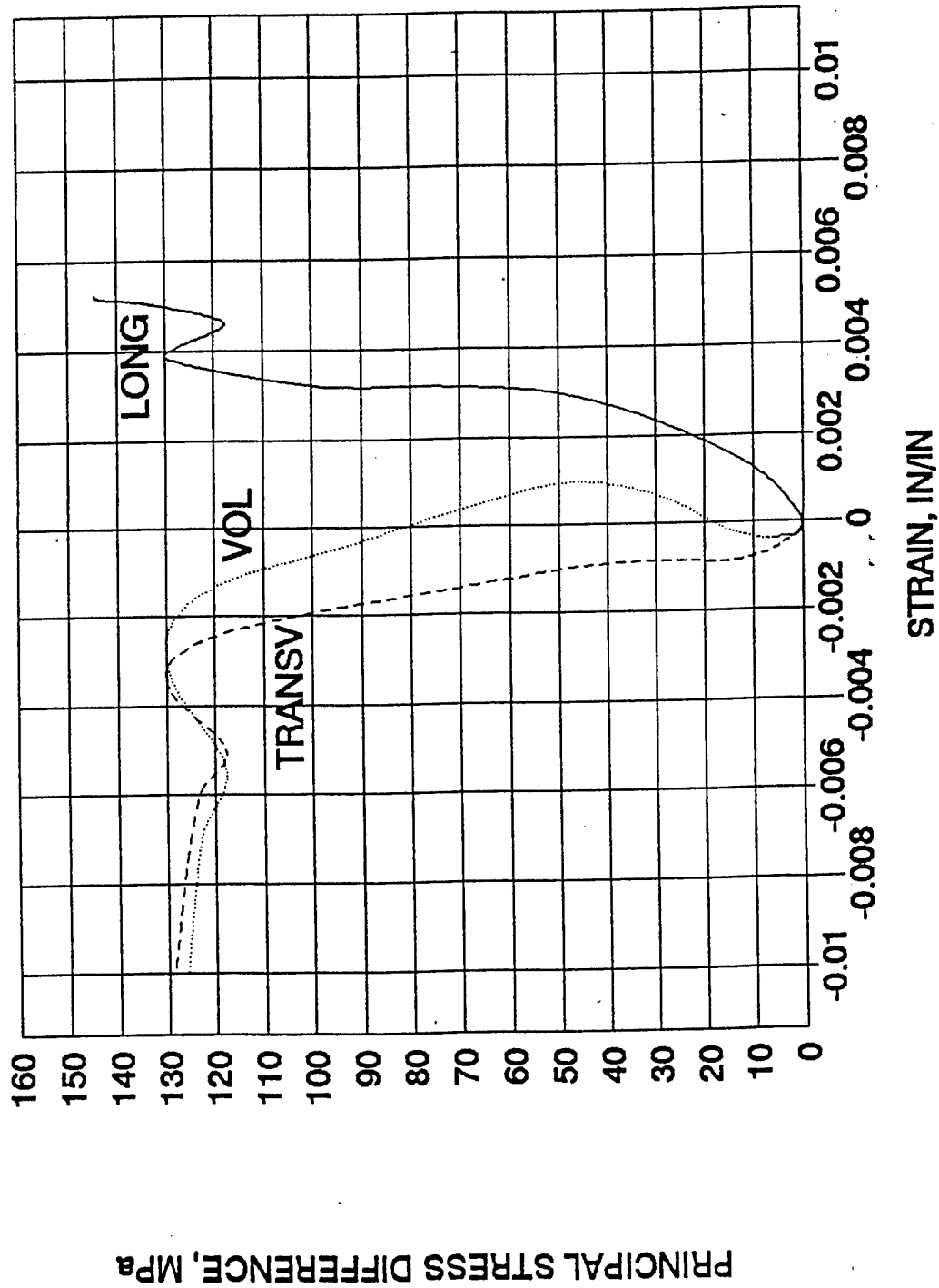


Figure A-36. Longitudinal, transverse and volumetric strain for dynamic confined concrete test.

DYNAMIC UNCONFINED TEST OF GRANITE

DCGU-2, STRAIN RATE = 40/SEC

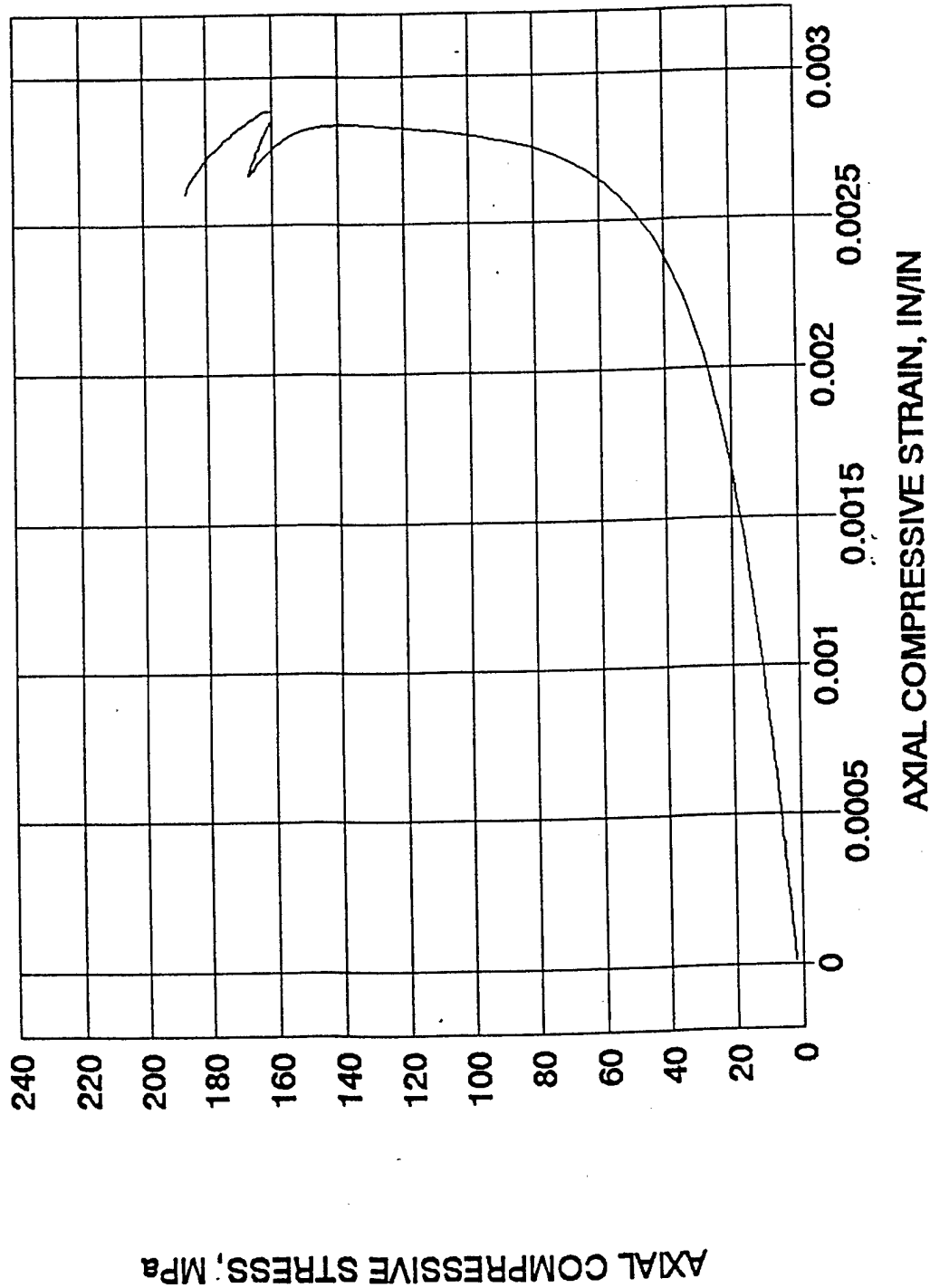


Figure A-37. Stress-strain curve for dynamic unconfined granite test.

DYNAMIC UNCONFINED TEST OF GRANITE

DCGU-2, STRAIN RATE = 40/SEC

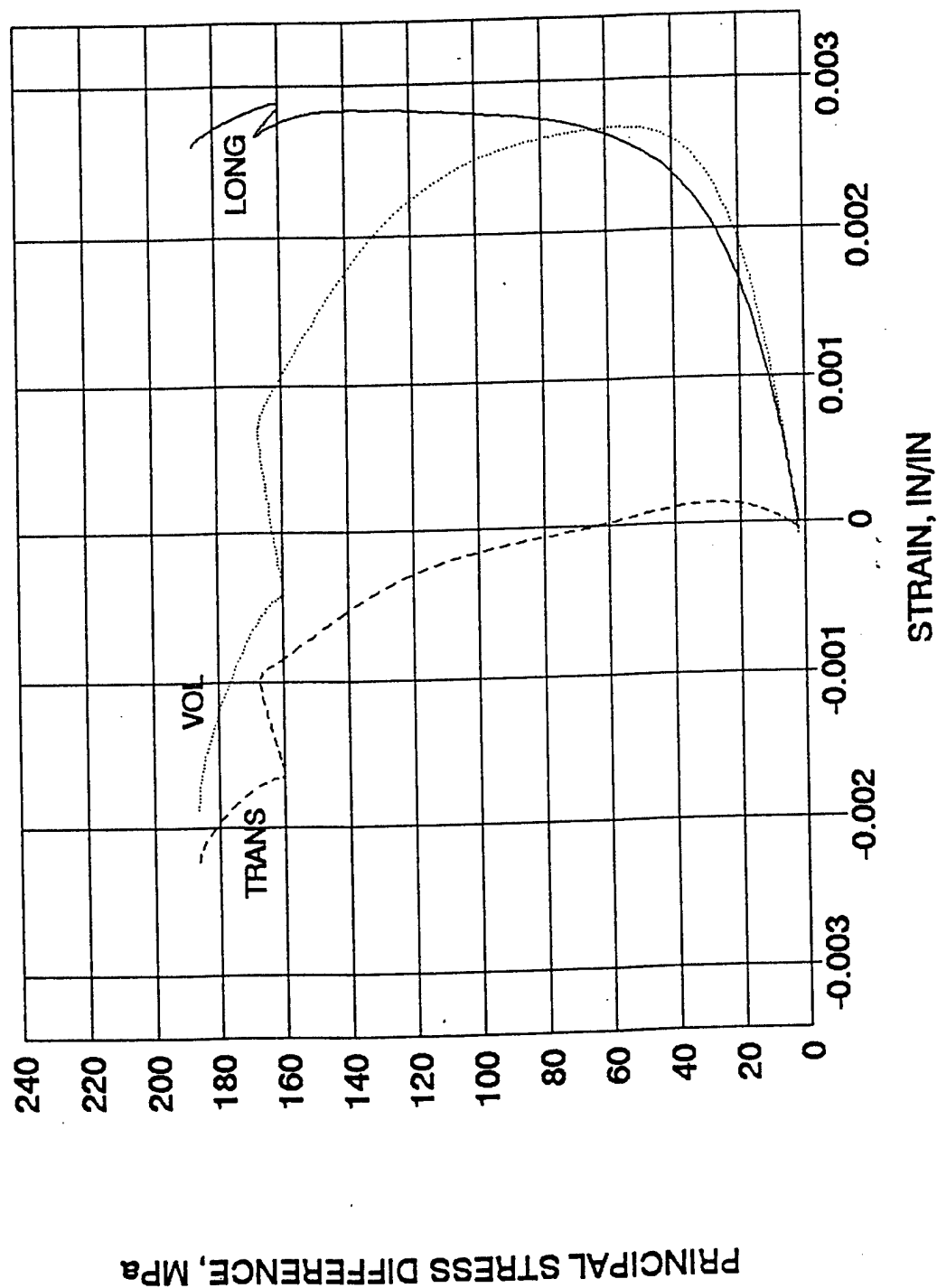


Figure A-38. Longitudinal, transverse and volumetric strain for dynamic unconfined granite test.

DYNAMIC UNCONFINED GRANITE TEST

DCGU-3, STRAIN RATE = 24/SEC

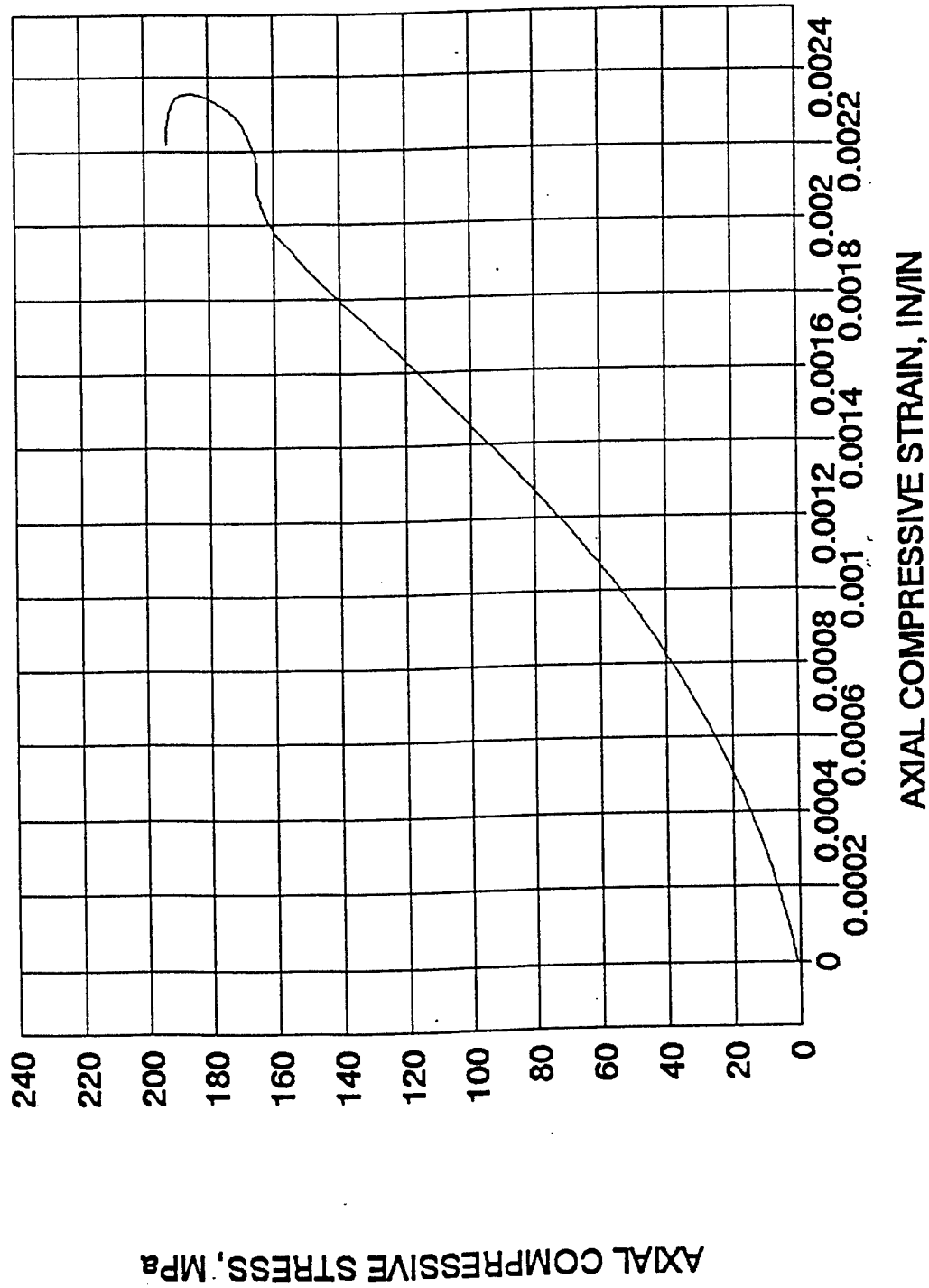


Figure A-39. Stress-strain curve for dynamic unconfined granite test.

DYNAMIC UNCONFINED GRANITE TEST

DCGU-3, STRAIN RATE = 24/SEC

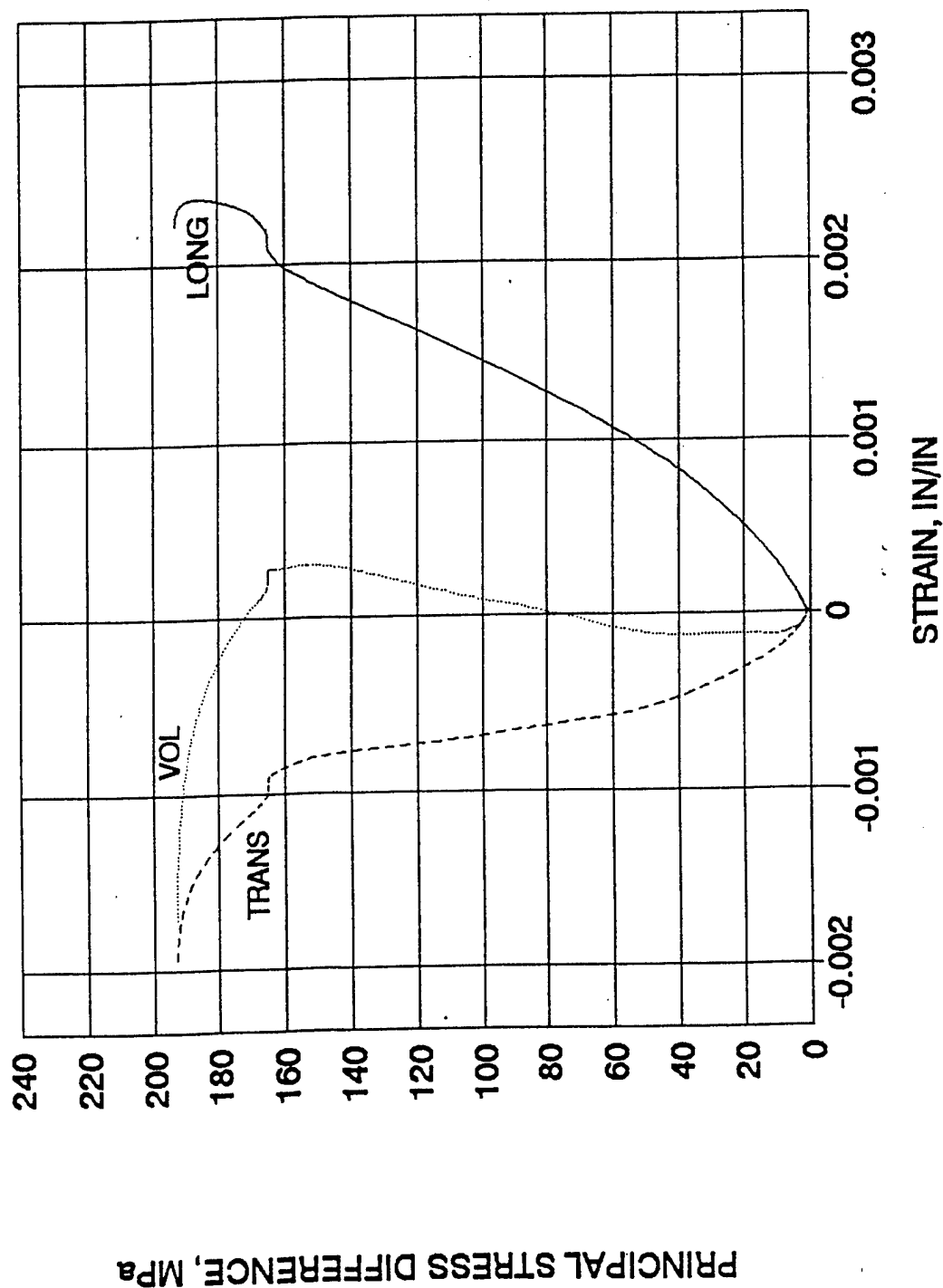


Figure A-40. Longitudinal, transverse and volumetric strain for dynamic unconfined granite test.

DISTRIBUTION LIST
AFRL-MN-EG-TR-2001-7044

Defense Technical Information Center 8725 John J. Kingman Road, Ste 0944 Ft Belvoir, VA 22060-6218	1
AFRL/MN CA-N	1
AFRL/MNOC-1 (STINFO Office)	1
AFRL/MNA	1
MNAC	5
AFRL/MNMI	1
MNMW	1